Fakultät für Medizin

Molekulare Kardiologie

I. Medizinische Klinik und Poliklinik

Klinikum rechts der Isar

Discovery of transcriptional modules in lineage specification

Jessica Kornherr

Vollständiger Abdruck der von der Fakultät für Medizin der Technischen Universität München zur Erlangung des akademischen Grades eines

Doktors der Naturwissenschaften (Dr. rer. nat.)

genehmigten Dissertation.

Vorsitzender:
Prof. Dr. Dirk Busch

Prüfer der Dissertation:
1. Prof. Dr. Karl-Ludwig Laugwitz
2. Priv.-Doz. Dr. Karl Kramer

Die Dissertation wurde am 24.04.2018 bei der Technischen Universität München eingereicht und durch die Fakultät für Medizin am 10.10.2018 angenommen.

Abstract

The mammalian heart is the first organ to form and is composed of a complex set of muscle and non-muscle cells arising from multipotent cardiac progenitors. Complex pathways induce lineage specification leading to formation of various structures and regionalization of the heart tube. Over the past years, genetically modified mouse models and lineage tracing experiments have extensively contributed to better understanding of cardiogenesis; however, a complete view of molecular pathways underlying heart development remains still elusive. Isl1 is the key transcriptional regulator of cardiac development. It is expressed in second heart field (SHF) progenitors and required for maintenance of their proliferative state and survival, before they differentiate and incorporate into the forming heart. Cardiac precursors also express transcription factor Nkx2-5, which is likewise essential for proper heart development.

Making use of a mouse embryonic stem cell (ESC) system with constitutive *Nkx2-5* and *Isl1* overexpression, an opposed effect of Nkx2-5 and Isl1 on specification of cardiac progenitors was demonstrated. Ectopic expression of Nkx2-5 delayed, whereas Isl1 overexpression led to enhanced specification of cardiac precursors. Nkx2-5 repressed *Isl1* and its transcriptional program by direct binding to *Isl1* enhancer. Furthermore, embryos with a conditional knockout of Nkx2-5 in Isl1 expressing cells failed to downregulate Isl1 in cardiomyocytes of the developing heart, confirming negative regulation of *Isl1* by Nkx2-5 *in vivo*. Constitutive overexpression of Isl1 resulted in increased numbers of cardiomyocytes associated with higher beating frequencies. Importantly, molecular characterization combined with functional action potential (AP) imaging of Isl1 overexpressing myocytes revealed an increase of nodal cells at the expense of the ventricular lineage. Together, these findings suggest that Nkx2-5-mediated direct repression of *Isl1* regulates specification of cardiac progenitors into cardiomyocytes of the working myocardium and thus, ensures proper acquisition of myocyte subtype identity.

In addition to the well-established cardiomyocytic differentiation potential of $Isl1^+$ SHF field precursors, Isl1 lineage tracing in mice showed that these progenitors can generate both cardiac muscle cells and epicardial fat *in vivo*. Further fate-mapping experiments and immunohistological analysis demonstrated that $Isl1^+$ precursors, which give rise to both lineages, co-express Wt1 and emerge early and transiently at developmental stages preceding proepicardial organ (PEO) formation. Concomitantly, experiments using an ESC system provided evidence that a single $Isl1^+/Wt1^+$ precursor can differentiate into both cardiomyocytes and adipocytes *in vitro*, suggesting related mechanisms of determination between the two lineages.

Abstract

Taken together, this work reveals an Isl1/Nkx2-5-mediated mechanism of myocyte subtype specification and uncovers a novel role of Isl1 in cardiac fat formation contributing to better understanding of the biology of the heart.

Zusammenfassung

Das Herz eines Säugetieres ist das erste funktionstüchtige Organ und wird aus einem komplexen Zusammenspiel von Muskelzellen mit anderen Zelltypen gebildet. Diese entstehen aus multipotenten Vorläuferzellen. Vielschichtige Signalwege induzieren unterschiedliche Zelllinienspezifizierungen, die sowohl zur Formierung verschiedener Strukturen als auch zur Kompartimentierung des primitiven Herzschlauchs führen. Über die letzten Jahrzehnte trugen unter anderem Experimente mit genetisch veränderten Mäusen maßgeblich zu dem heutigen Verständnis der Entwicklungsbiologie des Herzens bei. Viele darin involvierte molekulare Signalwege sind jedoch immer noch nicht vollständig verstanden. Der Transkriptionsfaktor Isl1 wurde bereits als wichtiger Faktor in der Herzentwicklung identifiziert. Er wird in allen Vorläuferzellen des zweiten Herzfeldes exprimiert und wird für deren Erhalt in einem undifferenzierten Zustand benötigt, bevor diese differenzieren und in das wachsende Herz einwandern. Die kardialen Vorläuferzellen exprimieren zudem den Transkriptionsfaktor Nkx2-5, welcher ebenfalls essentiell für die Herzentwicklung ist.

Durch Experimente mit embryonalen Stammzellen, die *Nkx2-5* oder *Isl1* überexprimieren, konnte ein entgegengesetzter Effekt von Isl1 und Nkx2-5 auf die Spezifizierung von kardialen Vorläuferzellen festgestellt werden. Die ektopische Expression von Nkx2-5 wirkte verzögernd, wohingegen die Überexpression von Isl1 die Wirkung auf deren Spezifizierung verstärkte. Durch eine direkte Bindung von Nkx2-5 an *Isl1* wird dessen Transkription und somit sein transkriptionelles Programm unterbunden. Des Weiteren zeigten Embryos mit konditionellem Nkx2-5 Knockout in Isl1 exprimierenden Zellen während der Entwicklung eine fehlende negative Regulierung von Isl1 in Kardiomyozyten. Eine konstitutive Überexpression von Isl1 führte zu einer größeren Anzahl von Kardiomyozyten, welche zudem auch eine höhere Schlagfrequenz aufzeigten. Die molekulare Charakterisierung in Verbindung mit funktionellen Aktionspotential-Messungen in Isl1 überexprimierenden Myozyten ergab, dass mehr Kardiomyozyten vom nodalen Subtyps auf Kosten des ventrikulären Subtyps gebildet wurden. Diese Erkenntnisse lassen darauf schließen, dass die Nkx2-5 vermittelte, direkte Hemmung von *Isl1* zu einer Spezifizierung von kardialen Vorläuferzellen zu Myozyten des ventrikulären Subtyps führt und somit die richtige Identität der Myozyten Subtypen sicherstellt.

Zu dem bereits bekannten Potential von $Isl1^{+}$-Vorläuferzellen in Kardiomyozyten zu differenzieren, wurde durch unsere Isl1-Zelllinienmarkierung gezeigt, dass diese Progenitoren sowohl Herzzellen als auch epikardiales Fett *in vivo* bilden können.

Zusammenfassung

Immunohistologische Analysen deckten auf, dass Isl1^{+} Vorläuferzellen in einem frühen und transienten Stadium kurz vor der Bildung des proepicardialen Organs Wt1 co-exprimieren.

In dieser Studie wird mittels embryonaler Stammzellen bewiesen, dass eine einzelne Isl1^{+}/ Wt1^{+}-Vorläuferzelle *in vitro* sowohl in Herzzellen als auch in Fettzellen differenzieren kann. Das bringt uns zu der Annahme, dass diese beiden Zelllinien gemeinsame Mechanismen in der Entwicklung teilen.

Zusammengefasst, zeigt diese Arbeit einen Isl1/Nkx2-5 vermittelten Mechanismus zur Myozytensubtyp-Spezifizierung und eine neue Rolle von Isl1 in der Entwicklung von kardialem Fett, was zu einem besseren Verständnis der Biologie des Herzens führt.

Table of contents

Table of contents

List of abbreviations

AF	Alexa Fluor
AP	Action potential
APD	Action potential duration
ARVC	Arrhythmogenic right ventricular cardiomyopathy
AVC	Atrioventricular canal
AVN	Atrioventricular node
Bmp	Bone morphogenetic protein
bp	Base pair
Bry	Brachyury T
BSA	Bovine serum albumin
cDNA	Copy DNA
C/EBPα	CCAAT/enhancer binding protein alpha
ChIP	Chromatin immunoprecipitation
CMC	Cardiac mesenchymal feeder cell
CMV	Cytomegalovirus
CNCCs	Cardiac neural crest cells
cTnT	Cardiac troponin T
CreERT2	Tamoxifen inducible variant of Cre recombinase
DEPC	Diethyl pyrocarbonate
DNA	Desoxyribonucleic acid
Dsp	Desmoplakin
E	Embryonic day
EAT	Epicardial adipose tissue
EB	Embryoid body
EBIO	1-ethyl-2-benzimidazolinone
ESC	Embryonic stem cell
EDTA	Ethylenediaminetetraacetic acid
EGFP	Enhanced green fluorescent protein
EMSA	Electromobility shift assay
EMT	Epithelial-mesenchymal transition
EYFP	Enhanced yellow fluorescent protein
FA	Formaldehyde
FAP	Fibro-adipogenic progenitor
FACS	Fluorescence-activated cell sorting
FBS	Fetal bovine serum

List of abbreviations

Fgf	Fibroblast growth factor
FHF	First heart field
FITC	Fluorescein isothiocyanate
Flk1	Fetal liver kinase 1
Foxa2	Forkhead box A2
Gapdh	Glyceraldehyde-3-phosphat dehydrogenase
Gata1	GATA binding protein 1
Gata4	GATA binding protein 4
g	Gravity
GFP	Green fluorescent protein
GSK3β	Glycogen synthase kinase 3 beta
HEK	Human embryonic kidney cell lines
Hcn4	Hyperpolarization activated cyclic nucleotide gated potassium channel 4
IBMX	3-isobutyl-1-methylxanthine
IgG	Immunoglobulin G
Igfbp5	Insulin-like growth factor binding protein 5
iPSC	Induced pluripotent stem cell
Isl1	Islet 1
IRES	Internal ribosome entry site
LA	Left atrium
LacZ	β-Galactosidase gene
LBD	Ligand-binding domain
LV	Left ventricle
Mef2C	Myocyte enhancer factor 2C
MeOH	Methanol
Mer	Mutated estrogen receptor
Mesp1	Mesoderm posterior 1
Mlc2a	Myosin light chain 2a
Mlc2v	Myosin light chain 2v
mRNA	Messenger RNA
MRTF	Myocardin-related transcription factor
Myh6	Alpha myosin heavy chain
Neo	Neomycin resistance
Nkx2-5	NK2 homeobox 5
NRG-1β	Neuregulin 1 beta
O.C.T.	Optimal cutting temperature
OE	Overexpression

OFT	Outflow tract
P4w	Four-weeks postnatally
PBS+/+	Phosphate-buffered saline with calcium and magnesium
PBS-/-	Phosphate-buffered saline without calcium and magnesium
PCR	Polymerase chain reaction
Pdgfrα	Platelet-derived growth factor receptor alpha
PE	Phycoerythrin
PEO	Proepicardial organ
PFA	Paraformaldehyde
PG	Plakoglobin
PGK	Phosphoglycerate kinase
pH	Potential hydrogen
PH	Phase contrast
Pkp2	Plakophilin-2
Pparγ	Peroxisome proliferator activated receptor-gamma
PSC	Pluripotent stem cell
qRT-PCR	Quantitative RT-PCR
R26mTmG	Rosa26 membrane-localized tomato, membrane-localized GFP
RA	Right atrium
RhoA	Ras homolog gene family, member A
RNA	Ribonucleic acid
ROCK	Rho-associated kinase
RT	Room temperature
RT-PCR	Reverse transcription polymerase chain reaction
RV	Right ventricle
SAN	Sinus atria node
SHF	Second heart field
SM22α	Smooth muscle protein 22-alpha
SRF	Serum response factor
Suppl.	Supplement
Tbx	T-box transcription factor
V	Volt
Vim	Vimentin
Wt1	Wilms tumor protein 1
YFP	Yellow fluorescent protein

1. Introduction

1.1 Heart development

1.1.1 Embryonic heart progenitors building cardiac cell lineages

During embryogenesis gastrulation is a phase allowing the emergence of the three germ layers endo-, meso- and ectoderm by cell ingression through the primitive streak (Tam and Behringer 1997). Fate mapping studies in mouse and chicken showed that time and location determine the fate of the gastrulating cells. One of the first cells migrating through the primitive streak are naive cardiogenic mesoderm progenitors (Brade, Pane et al. 2013). There are three important components of the mesodermal layer, the paraxial, the intermediate, and the lateral plate mesoderm located on either side of the neural tube. Formation of intraembryonic coeloms accompanies with splitting of the lateral plate mesoderm into a dorsal ectoderm-attached (somatic mesoderm) and a ventral endoderm-attached (splanchnic mesoderm) layer (Fig. 1). The cardiogenic mesoderm progenitors migrate into the regions of the splanchnic mesoderm, one on each side of the embryo, which interact with the adjacent endodermal tissue to become specified for heart development (Fig. 1) (Gilbert 2000).

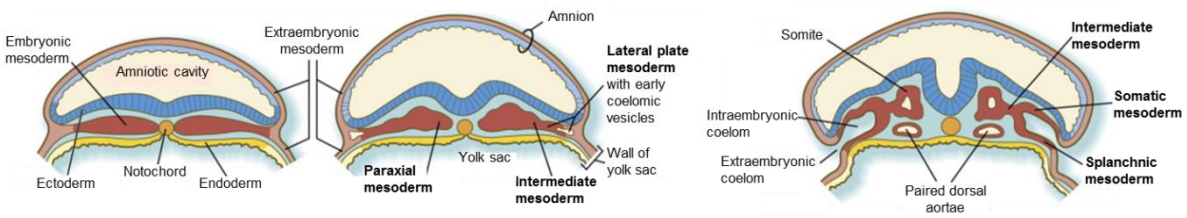

Figure 1: Mesoderm development in a human embryo.
Schematic representation of human mesoderm development. Formation of mesoderm in mammals is similar, driven by the ingression of cells through the primitive streak. Embryonic mesoderm (brown) divides into paraxial, intermediate and lateral plate mesoderm each on both sides of the embryo. Later in development, intraembryonic coeloms divide lateral plate mesoderm further into somatic and splanchnic mesoderm. The latter gives rise to cardiogenic mesoderm progenitors. Adapted from Carlson 2015.

In mouse, at embryonic day (E) 7.5, these precursors form a structure called cardiac crescent, which subsequently fuses at the midline from anterior to posterior and gives rise to the linear heart tube at E8 (Fig. 2). The unfused posterior parts become the openings of the vitelline veins into the heart. These veins carry nutrients from the yolk sac into the sinus venosus, which starts with spontaneous contraction and serves as a pacemaker for the wave-like muscle contraction of the whole heart tube. The blood then flows through a valve into the atrial region of the heart and further through the ventricle and bulbus cordis. At the anterior end of the heart tube the contractions of the truncus arteriosus pump the blood into

the aorta (Gilbert 2000). The early functioning of the embryo heart ensures distribution of the nutrients in the whole developing organism. The heart tube undergoes rightward looping at E8.5 and grows rapidly by two mechanisms: cell proliferation and recruitment of additional cells (Fig. 2). At E10.5, the looped heart tube forms four chambers, which become segregated and connected to the pulmonary trunk and aorta by E14.5 (Fig. 2) (Brade, Pane et al. 2013). By this time the heart is developed as the first functional organ.

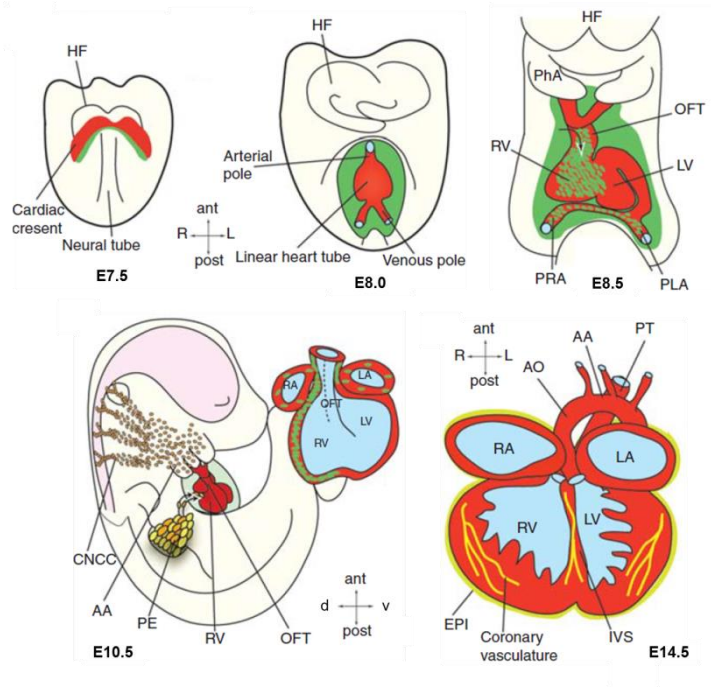

Figure 2: Formation of the heart during mouse embryonic development.
At E7.5, the cardiac crescent forms at the ventral side of the embryo. After fusion from anterior to posterior, the cardiac crescent forms a beating linear heart tube at E8.0, which undergoes rightward looping at E8.5. Two days later, the heart shows defined four-chambered morphology. Those chambers become fully septated and connected to the pulmonary trunk and the dorsal aorta at E14.5. AA = Aortic arch, ant = anterior, AO = dorsal aorta, CNCC = cardiac neural crest cells, d = dorsal, EPI = epicardium, HF = headfolds, IVS = interventricular septum, L = left, LA = left atrium, LV = left ventricle, OFT = outflow tract, PE = proepicardium, PhA = pharyngeal arch, PLA = primitive left atrium, post = posterior, PRA = primitive right atrium, PT = pulmonary trunk, R = right, RA = right atrium, RV = right ventricle, v = ventral. Adapted from Brade, Pane et al. 2013.

Additional to the cardiogenic mesoderm, which arises as earliest precursor population at E6.5, there are two more spatially and temporally distinct sources of precursors contributing to the heart formation during cardiogenesis, including the PEO present at E9.0-E10.5 and the cardiac neural crest cells emerging at E10.5 (Fig. 2). The cardiogenic mesoderm cells build major proportion of the ventricular, atrial, and outflow tract (OFT) myocardium and contribute cells to the endocardium, the conduction system, and the aortic and pulmonary cushions (Fig. 3a). PEO precursors form the epicardium, which differentiates into interstitial fibroblasts residing in the myocardium, smooth muscle and endothelial cells of the coronary vessels, some cardiomyocytes and epicardial adipocytes (Fig. 3c) (Brade, Pane et al. 2013). Intramyocardial adipocytes have been shown to derive from the endocardium (Zhang, Pu et al. 2016). Cross-talk of the epicardium and myocardium influences chamber maturation and ventricular muscle growth. The cardiac neural crest progenitors give rise to the distal smooth muscle cells of the OFT and the aorticopulmonary septum as well as to the autonomous nervous system of the heart (Fig. 3b). Proper cardiac neural crest development is important for correct cardiac valve formation and septation of the heart. (Brade, Pane et al. 2013).

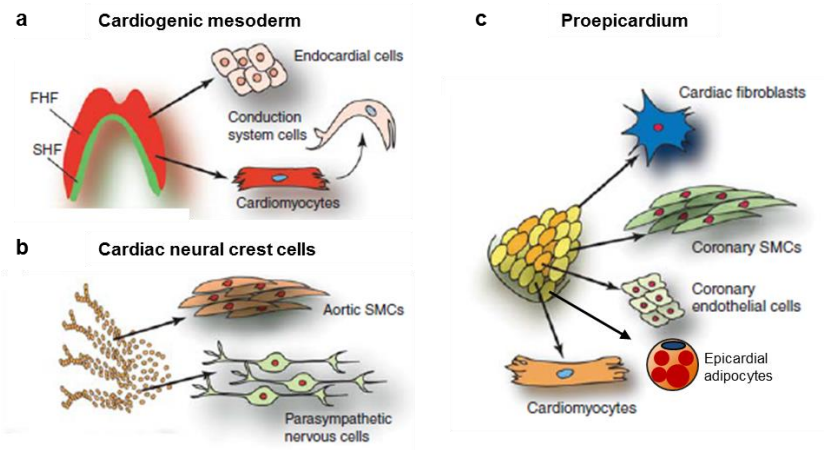

Figure 3: Three sources of precursor populations building the mouse heart. Progenitors of the cardiogenic mesoderm (a), cardiac neural crest cells (CNCC) (b) and proepicardium (c) contribute to the developing heart. FHF = first heart field, SHF = second heart field, SMCs = smooth muscle cells. Adapted from Brade, Pane et al. 2013.

1.1.2 Structures building the heart

Cardiogenic mesoderm

Cardiogenic mesoderm progenitors are located in the splanchnic mesoderm. The bilateral zones of the splanchnic mesoderm are therefore referred to as heart-forming regions. As soon as the cardiac crescent forms, two spatially and temporally different sources of precursors arise within those regions, the so-called first and second heart field (Fig. 3a+4) (Buckingham, Meilhac et al. 2005).

Cells of the first heart field (FHF) are difficult to locate precisely due to the lack of markers. Those precursors form the cardiac crescent. Because of their position in the crescent, they are exposed to factors, which initiate cardiac differentiation process (Brade, Pane et al. 2013). From the temporal point of view, FHF progenitors differentiate before the SHF cells and give rise to the primary heart tube, by folding its outer edges together (Fig. 4) (van Wijk and van den Hoff 2010). The center of the primary heart tube becomes the left ventricle of the myocardium. Additionally, some FHF precursors participate in forming the right ventricle and the atria (Fig. 4) (Zaffran, Kelly et al. 2004).

The cardiogenic progenitors located medially and caudally within the heart-forming region are referred to as the SHF precursors. In contrast to FHF cells, progenitors of the SHF can be clearly identified by the expression of *Isl1*, which maintains the cells in a proliferative state (Cai, Liang et al. 2003). After the formation of the primary heart tube they are gradually added to its both ends, the caudally located inflow and the cranially located outflow regions of the heart (van Wijk and van den Hoff 2010). The atria, which are formed by the inflow region, are thus derived from the SHF progenitors. In addition, SHF progenitors generate most of the cells of the right ventricle and OFT. In summary, the heart tube grows in size as a result of the growing amount of cells added and subsequently undergoes looping (Fig. 4).

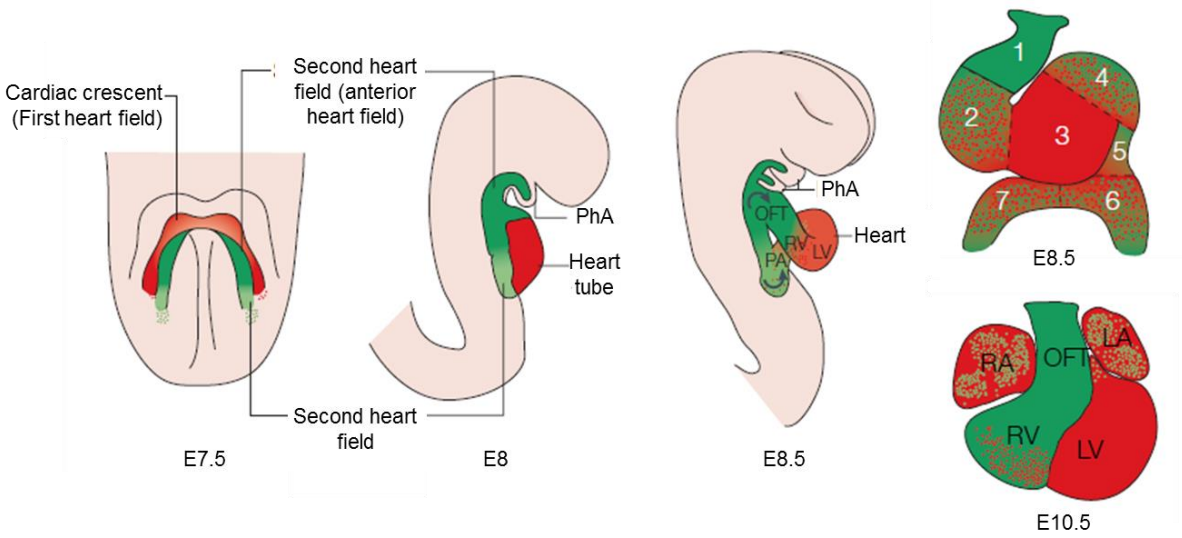

Figure 4: Heart field contribution to the developing mouse heart.
Location and contribution of first (red) and second (green) heart field to the mouse embryo (three left panels) and in the embryo heart (right panels). Frontal views are shown for E7.5 and E10.5, and lateral views for stages E8 and E8.5. LA = left atria, LV = left ventricle, OFT = outflow tract, PA = primitive atria, PhA = pharyngeal arches, RA = right atrium, RV = right ventricle, 1 = outflow region, 2 = primitive right ventricle, 3 = primitive left ventricle, 4/5 = atrioventricular region, 6/7 = primitive left and right atria. Adapted from Buckingham, Meilhac et al 2005.

Proepicardium

SHF progenitors give rise to both myocardial and non-myocardial cells. In a region next to the inflow tract SHF progenitors decide to differentiate into either cardiomyocytes contributing directly to the growing myocardium or into cells of the non-myocardial component of the heart, which is largely derived from a structure called PEO (van Wijk and van den Hoff 2010). The PEO itself arises as a cauliflower-shaped structure in the atrioventricular canal at E9.5 (Fig. 5). It grows by addition of progenitors and starts to spread over the heart within the next day forming the epicardium (Fig. 5) (van Wijk, van den Berg et al. 2009).

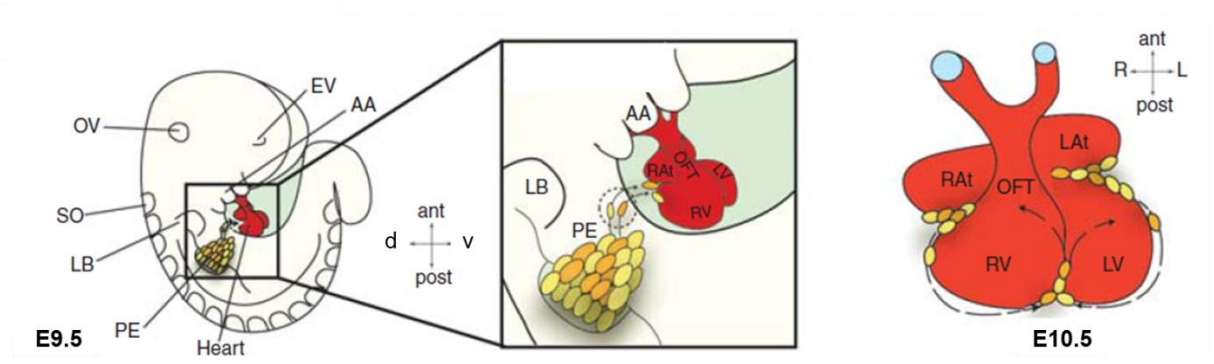

Figure 5: Proepicardial progenitor contribution to the forming mouse heart.
Formation of the PEO at E9.5 during mouse embryonic development. Proepicardial progenitors migrate over the forming heart starting from the atrioventricular canal region. The whole heart will be covered by an epicardial epithelial sheet within the next day. AA = Aortic arch, ant = anterior, d = dorsal, EV = Eye vesicle, L = left, LAt = left atrium, LB = limb bud, LV = left ventricle, OFT = outflow tract, OV = Optic vesicle, PE = proepicardium, post = posterior, R = right, RAt = right atrium, RV = right ventricle, SO = somites, v = ventral. Adapted from Brade, Pane et al. 2013.

One important function of the epicardium is to serve as a source of secreted factors, which regulate mitogenic expansion of the myocardium and assembly of blood vessels. Furthermore, the epicardium acts as a multipotent progenitor pool, not only during cardiogenesis but also in adulthood in response to injury (Masters and Riley 2014). Epicardial progenitors undergo epithelial-mesenchymal transition (EMT) to provide mesenchymal cells, which reside in the subepicardial space between epicardium and myocardium. One part of the cells migrates into the myocardium and becomes the predominant source of cardiac fibroblasts. The extracellular matrix produced by the cardiac fibroblasts is important for the mature heart structure. Another part gives rise to endothelial cells, which build nascent coronary endothelial tubes. A further subset of epicardial cells assembles around those tubes forming the smooth muscle layer around the vessels in the adult heart (Fig. 6).

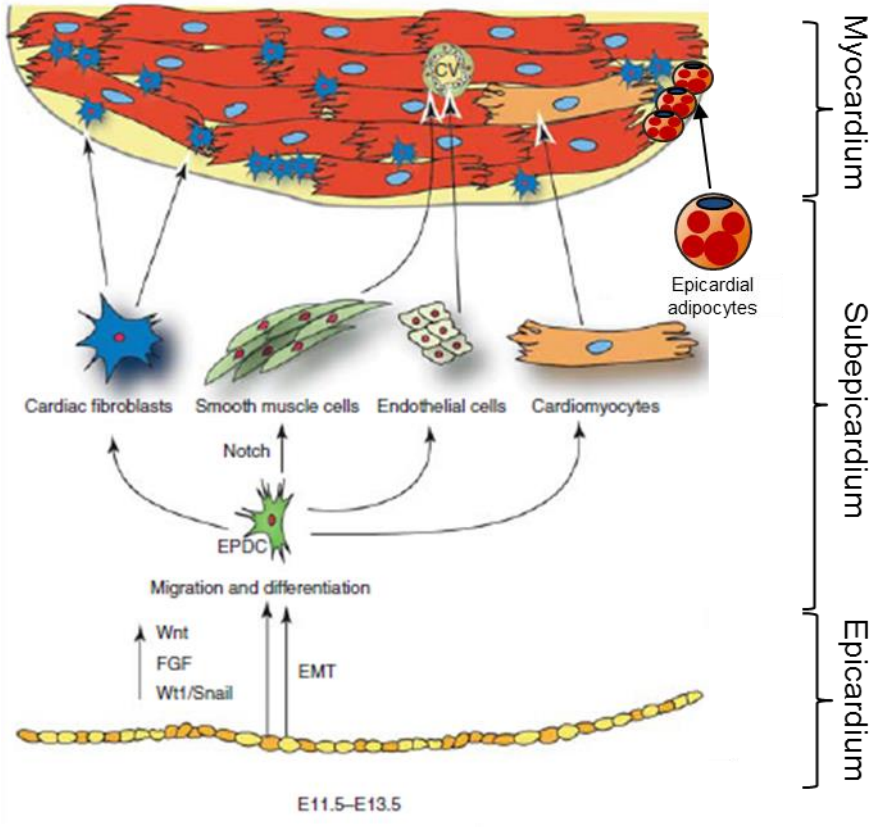

Figure 6: EMT of epicardial progenitors provides mesenchymal cells.
At E11.5–13.5, epicardial cells undergo an EMT (mediated by Wnt, FGF, and Wt1/Snail signals) and epicardium-derived cells (EPDCs) migrate and differentiate in the subepicardial space. EPDCs differentiate then towards various cell types, as indicated. CV = coronary vessels. Adapted from Brade, Pane et al. 2013.

A recent study using genetic fate mapping approaches showed that epicardial adipose tissue (EAT) is also derived by mesenchymal transformation of the epicardium (Liu, Huang et al. 2014, Yamaguchi, Cavallero et al. 2015). Its developmental origin was long time unclear,

since mice and other experimentally traceable animals were thought not to have that tissue. EAT in adult rodents is very little in size and located in the atrioventricular groove and underneath the atria next to the coronary vessels only. In the human heart, the EAT is also located in the atrioventricular groove and around the coronary vessels, but it increases with age and starts to spread across mainly the right ventricle towards the apex. The biological function of EAT lies in mechanical support of the heart and absorption of free fatty acids out of the circulation, thus protecting the sensitive cardiomyocytes (Yamaguchi, Cavallero et al. 2015).

Neural Crest

Beside the two heart fields representing the major sources of the heart-forming cells, there is a third population contributing to the heart, the cardiac neural crest. These cells are of the ectodermal lineage and arise from the dorsal neural tube. They migrate through the pharyngeal arches towards the heart. Derivatives of the cardiac neural crest cells form the parasympathetic innervation of the heart and contribute smooth muscle cells within the aortic and pulmonary arteries (Spater, Hansson et al. 2014).

In summary, the FHF builds the center of the primitive heart tube, while the SHF contributes to both ends of the primitive heart tube. The caudal end of the heart forms the inflow region, which builds the venous poles and later the base of the superior and inferior vena cava. Cells of the PEO migrate over the heart tube and contribute to the epicardium and a large number of non-myocardial cells within the myocardium. The cranial end of the heart forms the right ventricle and the OFT, which later builds the base of the aorta and pulmonary trunk. The ectoderm-derivative cardiac neural crest cells migrate into the OFT region and differentiate into smooth muscle cells within the aortic and pulmonary arteries and form the nervous system of the heart (Spater, Hansson et al. 2014).

1.1.3 Molecular aspects of early heart development

Mesoderm induction is crucial for cardiogenesis and its transcriptional regulation is evolutionary conserved. Its key signaling networks include Nodal, bone morphogenic protein (BMP), fibroblast growth factor (FGF) and the canonical Wnt pathway (Kimelman 2006, Noseda, Peterkin et al. 2011). As soon as the mesodermal precursors ingress through the primitive streak, they initiate expression of the T-box transription factor Brachyury/T (Bry) upon activation of Wnt/ß-catenin signaling pathway (Showell, Binder et al. 2004). Bry^{+} progenitors upregulate Flk1 expression and specify into hemangioblasts, which differentiate

into cells of the blood and endothelial lineage. A second Bry expressing population turns on Flk1 later and specifies further into cardiogenic mesoderm progenitors. The commitment of those cells requires both inhibition of the initial canonical Wnt pathway and activation of the non-canonical Wnt signaling (Gessert and Kuhl 2010). At the time point, when those progenitors migrate into the endoderm-adjacent splanchnic mesoderm, they become influenced by endodermal factors, such as T-box transcription factor eomesodermin, and downregulate Bry, while inducing *mesoderm posterior 1* (*Mesp1*) gene expression (Fig. 7a). Studies in the past have suggested that a population of $Mesp1^+$ cells precedes the establishment of the anatomically and molecularly distinct “heart fields” (Saga, Hata et al. 1996, Saga, Miyagawa-Tomita et al. 1999, Bondue, Lapouge et al. 2008, Lindsley, Gill et al. 2008). Additionally, $Mesp1^+$ cells can also contribute to a broad range of mesodermal derivatives, such as paraxial mesoderm and skeletal muscle of the head (Yoshida, Vivatbutsiri et al. 2008, Chan, Shi et al. 2013).

Clonal analysis showed that temporally distinct Mesp1 expressing populations exist, which are already committed to specify into either the FHF or SHF lineage, indicating a very rapid and precise patterning of progenitor populations during gastrulation (Devine, Wythe et al. 2014, Lescroart, Chabab et al. 2014). The first $Mesp1^+$ cells form the cardiac crescent and are exposed both to cytokines of the BMP and FGF families and to inhibitors of Wnt/ß-catenin signaling pathway, which initiates cardiac differentiation program by induction of the key FHF markers Nkx2-5, Gata-4 and Tbx5. These molecules drive expression of contractile proteins, such as myosin light chain-2a (Mlc2a) and sarcomeric myosin heavy chains (MHCs). Cardiomyocytic differentiation of FHF progenitors starts in the cardiac crescent and continues throughout the primitive heart tube.

The second Mesp1 expressing cells reside in the pharyngeal mesoderm, where they are exposed to canonical Wnt signaling. This activates the expression of the SHF key molecule LIM-homeodomain transcription factor Isl1 (Lin, Cui et al. 2007). Isl1 expression is required for survival, proliferation and migration of SHF progenitors into the primitive heart tube (Cai, Liang et al. 2003). As soon as they reach the developing heart and differentiate, its expression is downregulated and Nkx2-5 is upregulated (Moretti, Caron et al. 2006). The interplay of signals during SHF progenitor cell proliferation (FGF, Shh, canonical Wnt) and differentiation (BMP, Notch, non-canonical Wnt) defines the fate of the SHF precursors (Fig. 7b). Furthermore, epigenetic mechanisms contribute to the progression of progenitors into terminally differentiated muscle and non-muscle lineages (Liu and Olson 2010).

Different Isl1 expressing progenitor populations have been identified. Multipotent $Isl1^+$/$Nkx2\text{-}5^+$/$Flk\text{-}1^+$ cells are able to give rise to both myocardial and vascular lineages. After downregulation of Nkx2-5, $Isl1^+$/$Flk\text{-}1^+$ progenitors differentiate into endothelial cells and

smooth muscle cells. Flk-1^{-}/Isl1^{+}/Nkx2-5^{+} progenitors are committed to form cardiomyocytes, smooth muscle cells and contribute to the proepicardium (Fig. 7c) (Moretti, Caron et al. 2006, Cai, Martin et al. 2008, Zhou, Ma et al. 2008, Zhou, von Gise et al. 2008).

Two genetically distinct proepicardial populations have been identified, including the Scx/Sema3D expressing population, which gives rise to coronary vascular endothelial cells (Katz, Singh et al. 2012) and the Wt1^{+}/Tbx18^{+} group of cells, which differentiate into cardiac fibroblasts, smooth muscle cells (Yamaguchi, Cavallero et al. 2015), and as controversially discussed, cardiomyocytes (Fig. 7c) (Cai, Martin et al. 2008, Christoffels, Grieskamp et al. 2009, Rudat and Kispert 2012). Epicardial adipocytes have been shown to derive from Wt1^{+}/Tbx18^{+} epicardial cells as well, suggesting its origin from the latter proepicardial progenitor population.

Nkx2-5 and Isl1

Nkx2-5 and Isl1 are critical transcription factors during early cardiogenesis. Global knockout of Nkx2-5 in mice leads to embryonic lethality at E9-10, due to defects in cardiac development. Nkx2-5 mutant embryos remain in a linear heart tube-conformation: they show a bulbous ventricle, which does not get delimited from the atrium. In addition, Nkx2-5 deficient embryos display a grossly truncated OFT. Around E9 they develop pericardial edema, which leads to severe growth retardation and lethality one day later (Lyons, Parsons et al. 1995). Interestingly, in Nkx2-5 mutant embryos, expression of cardiac progenitor genes including *Isl1* is not restricted to progenitors, but persists in the myocardium (Prall, Menon et al. 2007), suggesting Nkx2-5 to be a negative regulator of Isl1.

Isl1 is a LIM-homeodomain transcription factor and is expressed in all cells of the SHF, which is a major source of the cardiac progenitors that contribute to the OFT, the right ventricle and parts of the left ventricle and the atria (Moretti, Caron et al. 2006). Isl1 knockout mice demonstrate a severe cardiac phenotype as well: they fail to loop the heart tube, lack completely the OFT and do not show any chamber separation. Growth retardation begins at around E9.5 and the mutant embryos die approximately at E10.5 (Cai, Liang et al. 2003). Heterozygous mice of both lineages do not show any apparent phenotype.

Wt1

The Wilms' tumor-1 (Wt1) is expressed in multiple organs during development including kidneys, gonads (Kreidberg, Sariola et al. 1993), the PEO and epicardium and is required for EMT (Duim, Goumans et al. 2016). In the heart, EMT is essential for the generation of epicardial-derived cells that will contribute to the formation of coronary vessels and interstitial fibroblasts (Duim, Goumans et al. 2016). Epicardial-specific knockout of Wt1 in mice prevents formation of the vasculature of the heart, which results in prenatal death around E16.5 and E18.5 (Martinez-Estrada, Lettice et al. 2010). Moreover, this study provides first evidence that Wt1 is required for cardiomyocyte formation through EMT by Snai1-rescue experiments (Martinez-Estrada, Lettice et al. 2010).

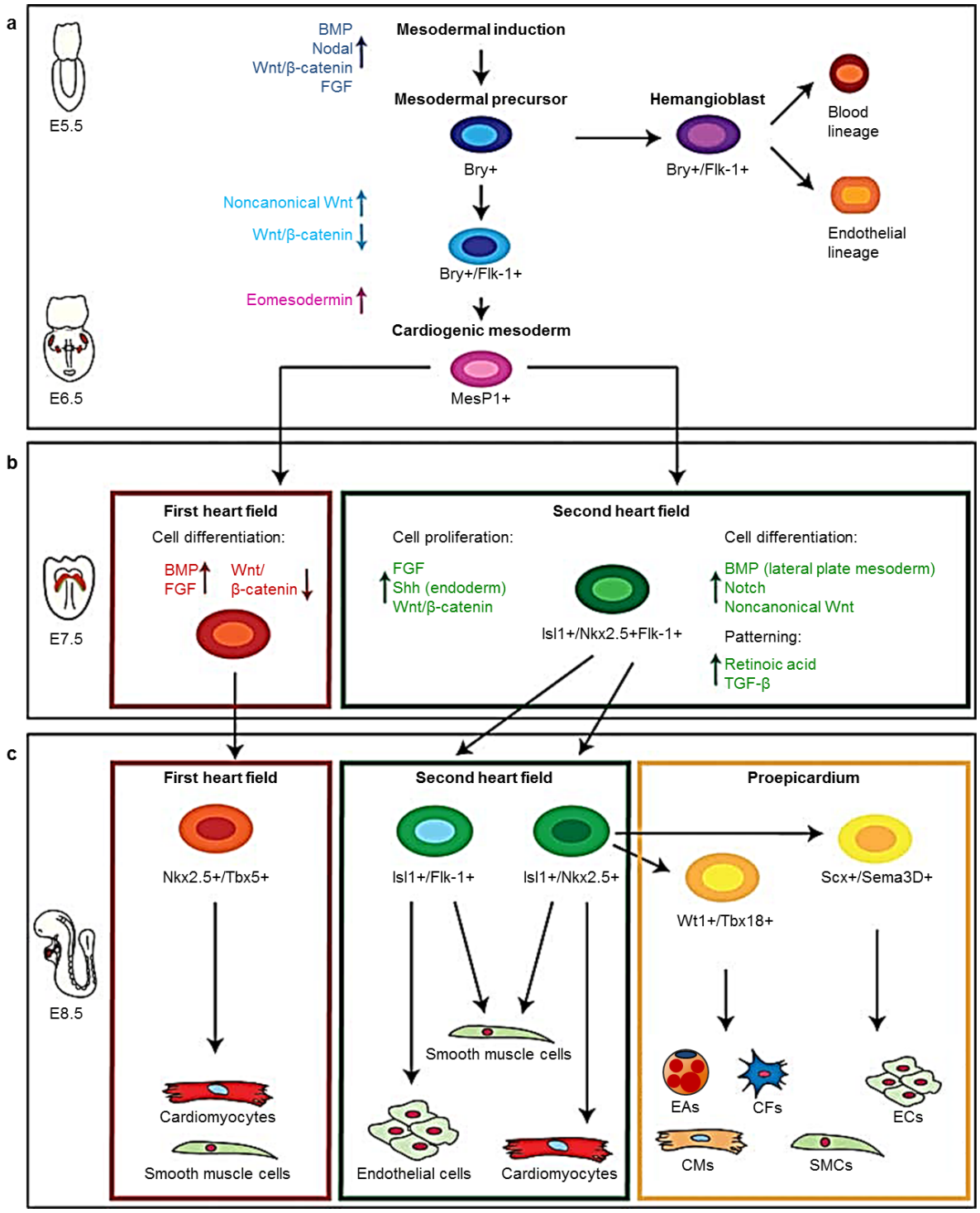

Figure 7: Molecular aspects of early mouse cardiogenesis.
Cellular hierarchy of cardiac progenitor cells and their lineage specification. a) Stepwise mesodermal induction towards Mesp1^{+} cardiogenic mesoderm precursors from E5.5 to E6.5 during mouse development. b) Specification of Mesp1^{+} cardiogenic mesoderm precursors into progenitors of the two heart fields at the cardiac crescent stage at E7.5 c) Further differentiation of the first and second heart field progenitors into cardiomyocytes (CMs), smooth muscle cells (SMCs), endothelial cells (ECs), and the proepicardium. Proepicarium gives rise to epicardial adipocytes (EAs), cardiac fibroblasts (CFs), ECs, CMs and SMCs. Involved signaling pathways are written in different colors and colored arrows indicate up- or downregulation of the corresponding pathway. Adapted from Brade, Pane et al. 2013.

1.2 Tools for investigation of cell lineage specification and differentiation

Cellular specification and differentiation is a requirement for the formation of multicellular organisms, in which differently specialized cells complement each other. The same process enables the building of complex structures of cell types and tissues. Although many of pathways controlling cell fate decisions have been a matter of investigation, much is still unknown. Several tools have been developed to shed more light into the complexity of heart development.

1.2.1 Studying cardiogenesis *in vivo* in mice

The mouse shares 99% of the human genome and exhibits vast similarities in development, anatomy and physiology to humans and therefore can serve as a model organism. Many powerful tools are available to investigate biological processes during development in mice, such as various lineage-tracing models allowing irreversible marking of the cells and their derivatives (Kretzschmar and Watt 2012), reporter mouse lines, which enable visualization of endogenous genes expression (Hadjantonakis, Dickinson et al. 2003), and mouse mutants generated to study gene function (Capecchi 2005). In addition to global gene knockout, conditional knockout models offer the possibility to delete a gene of interest in specific cells only. Therefore, the Cre-lox system has become an important tool (Feil 2007) and has been also widely used for lineage tracing of cells during embryonic development and in adult mice (Joyner and Zervas 2006). These studies typically require crossing of two mouse lines: a mouse, in which the Cre recombinase is expressed under a tissue/cell-specific promoter, and the target or reporter mouse, in which the gene of interest is flanked by two loxP sites for Cre-mediated recombination (Feil 2007). In the offspring, the bacteriophage P1 Cre recombinase catalyzes site-specific recombination between two loxP sites and efficiently excises DNA flanked by two loxP sites in the same orientation (Sauer and Henderson 1989). Moreover, an inducible form of Cre recombinase enables temporal resolution, by fusing it with the ligand-binding domain (LBD) of a mutated estrogen receptor (Mer) (Metzger, Clifford et al. 1995). The mutation prevents binding of endogenous estrogen but allows binding to the synthetic ligand 4-hydroxytamoxifen (4-OHT), which is the major active metabolite of the drug tamoxifen. In the absence of its ligand, CreMer is inactive in the cytoplasm as it is bound to heat shock protein 90, which prevents its delivery to the nucleus. 4-OHT disrupts this binding and CreMer is free to move into the nucleus where it acts on the loxP sites. In this study two improved versions of CreMer have been used: MerCreMer, a double fusion of

Cre with two mutated (G525R) murine ER-LBDs (Sohal, Nghiem et al. 2001) and CreERT2, a Cre fusion protein to a triple mutated (G400V, M543A, L544A) ER-LBD of human origin (Indra, Warot et al. 1999). Those improved versions decrease their nuclear translocation in the absence of the inducer, and at the same time increase their sensitivity to tamoxifen and recombination efficiency. Since the recombination event is irreversible and passed to every descendant cell, it is crucial for lineage tracing that there is no CreMer translocation to the nucleus in the absence of tamoxifen (Liu, Suckale et al. 2010).

1.2.2 Studying cardiogenesis *in vitro* using pluripotent stem cells

Pluripotent stem cells (PSCs), including ESCs and induced pluripotent stem cells (iPSCs), can self-renew (symmetrical cell division) indefinitely in culture, while maintaining the ability to differentiate in any cell type (asymmetrical cell division) (Takahashi et al., 2007; Thomson et al., 1998; Yu et al., 2007). Mouse and human ESCs can be isolated from blastocysts. To overcome the challenge of obtaining ESCs from human embryos, the iPSCs system can be used, which offers a great possibility to generate pluripotent cells with desired patient genetic background.

Convincing evidence suggests that *in vitro* differentiation of PSCs recapitulate aspects of embryonic development, and may be used as a model system for developmental studies (Zhu and Huangfu 2013). When cultured in suspension, pluripotent cells spontaneously form aggregates, referred to as embryoid bodies (EBs) (Itskovitz-Eldor, Schuldiner et al. 2000). Differentiation of EBs can be directed into various cell lineages by treatment with growth factors and small molecules, which activate or inhibit various signaling pathways mimicking embryonic development. Cardiogenesis for example can be induced by addition of fetal bovine serum and ascorbic acid in human PSCs or by withdrawal of leukemia inhibitory factor in mouse PSCs. Differentiation protocols get continuously improved for higher yield and better maturation state of the desired cell type.

Furthermore, pluripotent stem cells offer the possibility to be genetically manipulated. Deletion of a gene of interest or insertion of transgenes allows for modifying gene expression of the PSCs and all its progeny. In addition, introduction of reporter genes into PSCs represent another useful tool, which can be used for lineage tracing by marking of progenitors throughout the differentiation process. Thus, PSC culture offers the great opportunity to look inside embryogenesis in a dish.

1.3 Aberrations in the lineage specification program

Lineage specification of progenitors is tightly controlled, since aberrations can lead to severe diseases. Once they have differentiated, functional cells usually maintain their cellular specificities in the multicellular organizations of animals, which is crucial for proper function of complex tissues. It is still largely unexplored how mature cells retain their identity. In some pathological conditions, such as reparative regeneration (Park, Wells et al. 2006, El Agha, Moiseenko et al. 2017, Plikus, Guerrero-Juarez et al. 2017), tumorigenesis and carcinogenesis (Gestblom, Hoehner et al. 1997), conversion of cellular specificities can frequently be observed (Eguchi and Kodama 1993). In arrhythmogenic right ventricular cardiomyopathy (ARVC) it is still not completely understood whether aberrant lineage specification program of progenitors or alterations in cellular identity of mature cells leads to the disease phenotype.

1.3.1 In diseased setting: ARVC

ARVC is a heritable disease characterized by fibro-fatty replacement of cardiomyocytes. The fibro-fatty tissue progresses from the epicardium toward the endocardium and predominantly involves the right ventricle, resulting in wall thinning and aneurysmal dilatation, which are typically localized in the inflow tract (subtricuspid region), OFT (infundibular region), and apex, referred to as “triangle of dysplasia” (Marcus, Fontaine et al. 1982, Basso, Thiene et al. 1996). In advanced stages of the disease the left ventricle can also get affected or is in few cases the predominant site of involvement (Corrado, Basso et al. 1997, Corrado, Link et al. 2017). The resulting disruption of normal myocardial architecture in ARVC can lead to severe right ventricular dysfunction, life-threatening arrhythmias and sudden cardiac death. A number of genetic studies have identified disease causing mutations in components of the desmosome accounting for approximately 50% of ARVC cases (Awad, Calkins et al. 2008). Desmosomes are cell structures specialized for cell-cell adhesion helping to resist intense shearing forces, known to be expressed in epithelial cells, keratinocytes and cardiomyocytes. They also play an important role in cell signaling (Jamora and Fuchs 2002). Causative mutations for ARVC phenotype were identified in the desmosomal proteins plakoglobin (PG) (McKoy, Protonotarios et al. 2000), desmoplakin (DSP) (Rampazzo, Nava et al. 2002), plakophilin-2 (PKP2) (Gerull, Heuser et al. 2004), desmoglein-2 (DSG2) (Pilichou, Nava et al. 2006), and desmocollin-2 (DSC2) (Syrris, Ward et al. 2006). In ARVC, the most affected gene is *PKP2*, which is responsible for approximately 20 to 30% of ARVC cases (Gerull, Heuser et al. 2004, Fressart, Duthoit et al. 2010). Plakophilin-2 links desmosomal cadherins with desmoplakin to the intermediate filament system (Mertens, Kuhn et al. 1996).

Furthermore, it has been reported to directly act on the canonical Wnt/β-catenin pathway, which could, when disrupted, play a role in the pathogenesis of ARVC. PKP2 binds to the desmosome components PG and DSP (Chen, Bonne et al. 2002). It has been shown that in Dsp deficient mice, PG failed to be anchored at the plasma membrane and translocated into the nucleus (Garcia-Gras, Lombardi et al. 2006). In the nucleus, PG could possibly compete with β-catenin and downregulate β-catenin signaling pathway, which plays an important role in maintaining myogenic transcriptional program, when it is active. Suppression of Wnt/β-catenin pathway activates adipogenic transcription factors C/EBPα and PPARγ, and promotes differentiation of preadipocytes into adipocytes (Fig. 8) (Ross, Hemati et al. 2000, Garcia-Gras, Lombardi et al. 2006). The process of inhibiting myogenic program and simultaneously promoting adipogenic program by the Wnt/β-catenin pathway could thus represent one possible disease mechanism. Another pathway leading to the disease phenotype is the Hippo pathway (Chen, Gurha et al. 2014). Interestingly, this pathway is interwoven with Wnt/β-catenin signaling; strengthening the hypothesis of the role of Wnt/β-catenin in ARVC.

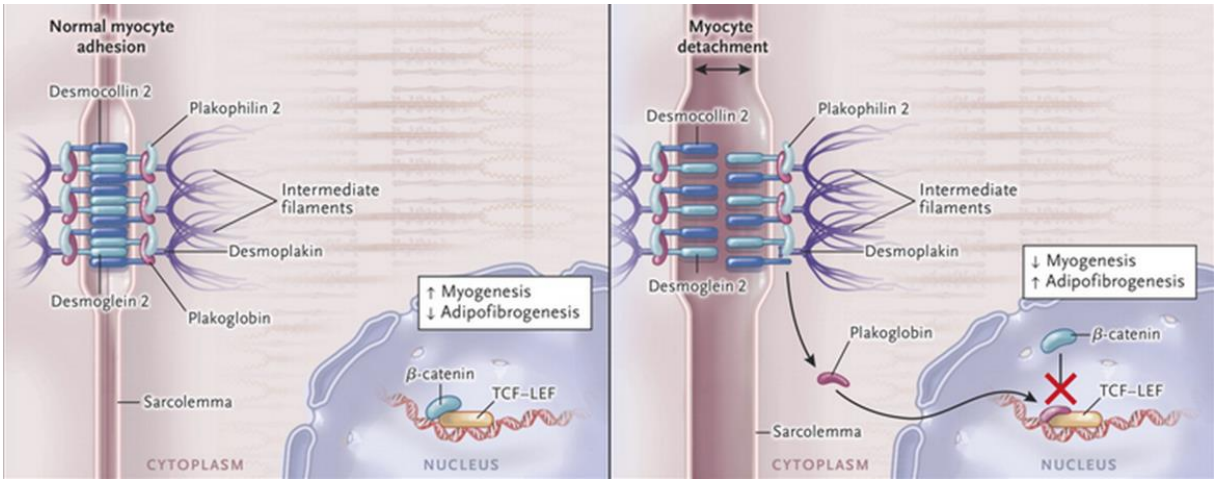

Figure 8: Pathogenesis of Arrhythmogenic Right Ventricular Cardiomyopathy.
Mutations in desmosomal genes have been identified as causative for ARVC. Desmosomes consist of desmoplakin (which binds to intermediate filaments), desmoplakin/cell adhesion protein linking (plakophilin-2 and plakoglobin) and cell adhesion (desmocollin-2 and desmoglein-2) proteins. In cardiomyocytes myogenic transcriptional program is active and adipo-fibrogenesis is inhibited through canonical Wnt/β-catenin signaling pathway (left panel). Abnormal desmosomes fail in anchoring plakoglobin into the membrane. Nuclear translocation of plakoglobin leads to suppressed Wnt/β-catenin signaling and a switch of the myogenic to adipogenic transcriptional program (right panel). Adapted from Corrado, Link et al. 2017.

The origin of excess adipocytes in ARVC is still not completely clear and several hypotheses exist. Lineage tracing experiments using *Nkx2-5*$^{Cre/+}$;*Dsp*$^{fl/+}$;*R26*$^{EYFP/EYFP}$ and *Mef2c*$^{Cre/+}$;*Dsp*$^{fl/+}$;*R26*$^{EYFP/EYFP}$ mouse lines suggested a SHF progenitor as a possible origin of adipocytes in the heart (Lombardi, Dong et al. 2009). In line with this, very recently, enhanced adipocyte differentiation from desmoplakin-deficient fibro-adipogenic progenitors (FAPs) has been reported (Lombardi, Chen et al. 2016), which derive from SHF derivatives.

FAPs sit in the epicardium and serve as a regenerative progenitor pool upon activation through injury. On the other hand, direct myocyte-to-adipocyte transdifferentiation has been proposed as another possible mechanism for the simultaneously occurring myocyte loss and adipocyte infiltration. This assumption was made based on the analysis of ARVC hearts displaying cardiomyocytes with progressive replacement of myofibrils and accumulation of fat droplets and expression of both myocyte-specific marker desmin and adipocyte-specific marker vimentin (d'Amati, di Gioia et al. 2000) as well as iPSC-derived ARVC disease models (Caspi, Huber et al. 2013, Kim, Wong et al. 2013, Ma, Wei et al. 2013, Dorn, Kornherr et al. 2018). Nevertheless, it cannot be excluded that an interplay of both mechanisms could lead to the ARVC phenotype.

1.4 Aims of the study

The heart is a multicellular organ and composed of diverse muscle and non-muscle cell types originating from multipotent cardiac progenitors. Despite the tremendous progress made during the last years in delineating the processes of cardiac differentiation, the exact programs determining progenitor cell fate decisions are still not completely understood.

The aims of the project were to investigate the molecular mechanisms regulating lineage specification of the cardiac progenitors into differentiated cell types during heart development.

One aim of this study was to analyze the interplay of Isl1 and Nkx2-5 during cardiac progenitor differentiation. Isl1 and Nkx2-5 are key transcription factors that are essential for proper heart development. Both proteins are co-expressed in SHF precursors. As soon as they reach the primitive heart tube and differentiate, Isl1 is switched off, while Nkx2-5 expression is maintained and even increases. In Nkx2-5 knockout mutants, genes expressed in SHF that are normally downregulated in the process of differentiation, demonstrate ectopic activation in differentiating myocytes, including Isl1, suggesting a repressive role for Nkx2-5 in cardiac differentiation. In this respect, specific questions were: Can Nkx2-5 repress Isl1 and is this repression direct? If Nkx2-5 switches off Isl1, what is the biological significance of this regulation? Is downregulation of Isl1 essential for differentiation of progenitors into cardiomyocytes and what are the consequences of maintained Isl1 expression for cardiac differentiation?

Isl1 expressing cardiac progenitors are multipotent and give rise to the three major cell lineages of the heart: cardiac muscle, smooth muscle and endothelial cells. Epicardial fat is another lineage contributing to the forming heart and is critical for its function. Recent lineage mapping studies have suggested an epicardial origin of this tissue. It is not known whether $Isl1^{+}$ progenitors can also give rise to epicardial adipocytes. Therefore, the second aim of this project was to determine if Isl1 expressing multipotent cardiac progenitors can differentiate into cardiac adipocytes and if there is a common progenitor for both cardiac fat and muscle, thus, defining a developmental relationship between both lineages. Furthermore, if such a precursor exists, what is the molecular signature of this progenitor?

2. Material & Methods

2.1 *In vivo* methods

2.1.1 Transgenic mice

Isl1$^{Cre/+}$ and *Isl1*$^{MerCreMer/+}$ mice were generously provided by Sylvia Evans (University of California-San Diego, La Jolla, CA) (Laugwitz, Moretti et al. 2005, Yang, Cai et al. 2006). *Wt1*$^{CreERT2/+}$, *Rosa26*$^{EYFP/EYFP}$ (*R26*$^{YFP/YFP}$) and *Rosa26*$^{mTmG/mTmG}$ (*R26*$^{mTmG/mTmG}$) were purchased from Jackson Laboratory. *Nkx2-5*$^{fl/fl}$ mice were obtained from Kenneth R. Chien (Karolinska Institute, Solna, Sweden) (Pashmforoush, Lu et al. 2004). Mice are in a mixed 129 x C57Bl/6 background. *Isl1*$^{Cre/+}$ mice were crossed with *Nkx2-5*$^{fl/fl}$ in two rounds of breeding to generate *Isl1*$^{Cre/+}$*;Nkx2-5*$^{fl/fl}$ mice to conditionally remove Nkx2-5 in Isl1 expressing cells. *Isl1*$^{Cre/+}$, *Isl1*$^{MerCreMer/+}$, and *Wt1*$^{CreERT2/+}$ were crossed with the *R26*$^{mTmG/mTmG}$ or *R26*$^{YFP/YFP}$ reporters for fate mapping studies.

2.1.2 Timed matings

Isl1$^{Cre/+}$*;Nkx2-5*$^{fl/+}$ female mice were mated with *Nkx2-5*$^{fl/fl}$ male mice; *Isl1*$^{Cre/+}$, *Isl1*$^{MerCreMer/+}$ or *Wt1*$^{CreERT2/+}$ female mice were mated with *R26*$^{mTmG/mTmG}$ male mice and the next morning checked for vaginal plug. The noon of the day the plug was detected was referred as embryonic day (E) 0.5.

2.1.3 Tamoxifen injection

For induced lineage tracing in *Isl1*$^{MerCreMer/+}$ and *Wt1*$^{CreERT2/+}$ mice, tamoxifen (Cat. N° T5648, Sigma Aldrich) was administered into pregnant females at a certain time point of gestation. Therefore 20 mg per ml tamoxifen was dissolved in corn oil (Cat. N° C8267, Sigma Aldrich) for 1 h at 65°C in the dark. Pregnant mice received a single dose injection of 75 µg per gram bodyweight intraperitoneally with a 27G-needle (Cat. N° 4665406, Braun Melsungen AG).

2.1.4 Freezing of mouse embryos and hearts

Depending on the stage of development to be examined the pregnant mother was sacrificed by cervical dislocation and embryos were sectioned out of the uterus. Under microscopic

observation the yolk sack was removed. Tail biopsies were taken for genotyping. After fixation in 4% phosphate-buffered PFA for 2 h shaking on ice, embryos were washed twice for 5 min in PBS without calcium and magnesium (Cat. N° 14190-250, Invitrogen). To protect the structure of the samples during freezing, water was substituted through sucrose gradient by letting embryos sink in 5%, 10% and finally 20% sucrose (Cat. N°S9378, Sigma Aldrich) in PBS-/- overnight. The next morning, the samples were incubated in freezing medium (1:1 O.C.T. (Cat. N° 4583, Sakura): 20% sucrose) for few minutes and adjusted in the right position in a cryomold (Cat. N° 4566, Sakura) filled with freezing medium under microscopic observation and frozen in liquid nitrogen using a glass jar filled with approx. 1 cm high pre-chilled 2-methylbutane. Samples were stored at -80°C immediately.

After sacrificing adult mice by cervical dislocation the heart was removed immediately and washed in PBS with calcium and magnesium (Cat. N° 14190-250, Life Technologies) and 10 U/ml Heparin (Cat. N° H3149, Sigma Aldrich) until remaining blood was pumped out of the heart. After removal of calcium and magnesium by washing in PBS-/- the heart was relaxed in 0.3 M KCl for 5 min. The adult hearts were fixed and cryopreserved as described above.

2.1.5 Cryosectioning

Embryos were cut in transverse or sagittal sections at 6 µm thickness using a Cryostat (Microm HM 560, Thermo Scientific). Adult hearts were cut in 8 µm sagittal sections and adipose tissue in 10-16 µm thickness. Polysine-coated slides (Cat. N° J2800AMNZ, Thermo Scientific) were used for better attachment of the samples. Slides were stored at -80°C or processed immediately.

2.2 Cell culture methods

2.2.1 Cell lines

To investigate the role of Isl1 and Nkx2-5 during early mesoderm development an Isl1^{nlacZ} knock-in mouse ESC line (Moretti, Caron et al. 2006) overexpressing Nkx2-5 or Isl1 was generated. Isl1^{nlacZ} cells were infected with a lentivirus coding for Nkx2-5 or Isl1 (Nkx2-5 OE ESCs or Isl1 OE ESCs). A corresponding control was generated by infecting the Isl1^{nlacZ} ECSs with the control GFP lentivirus (GFP ESCs). Lentiviruses were produced in HEK293T cells by transient co-transfection of the lentiviral transfer vector, packaging CMVΔR8.74

plasmid and envelope VGV.G plasmid using Fugine HD (Promega GmbH). Additionally, a second line stably overexpressing Isl1 was generated by Michael Kühl (Ulm University/ Institute for Biochemistry and Molecular Biology) using a plasmid-based approach in E14 ESCs, as previously described (Herrmann, Bundschu et al. 2011), which produced identical results to the lentiviral approach. Moreover, an ESC line was generated from *Isl1*$^{Cre/+}$*;R26*$^{YFP/+}$ mouse blastocysts as previously described (Nichols, Jones et al. 2009).

2.2.2 Mouse ESC maintenance and differentiation

ESCs were maintained in 2i medium supplemented with Leukemia inhibitory factor (0.1 mg/ml, Cat. N° LIF2005, Merck Millipore), MEK-inhibitor (1 µM, Cat. N° PD0325901, Axon Medchem) and GSK3β-inhibitor (3 µM, Cat. N° CHIR99021, Axon Medchem) on 0.1% gelatin-coated cell culture dishes. For passaging, cells were trypsinized with 0.05% trypsin (Cat. N° 25300-096, Invitrogen) for 5 min at 37°C, neutralized in mouse ESC medium, centrifuged at 200x g for 5 min (Hettich centrifuge Rotina 420R) and re-suspended in 2i medium with supplements and seeded at a density of 1.4 x 10^3 per cm^2. Spontaneous differentiation was induced by seeding 1.1 x 10^4 cells per cm^2 on 5% poly-2-hydroxyethyl methacrylate (polyHEMA)-coated petri dishes to avoid attachment and allow forming of EBs in mouse ESC medium. Medium was changed on day 4 and then every other day.

2.2.3 Analysis of beating frequency

For the analysis of beating activity, EBs at 4 days of differentiation were plated onto 0.1% gelatin-coated 24- or 6-well plates. For quantification of beating the number of wells containing beating EBs was divided by the total number of wells after 7 and 14 days of EB differentiation. Beating frequency was measured at day 14 of EB differentiation as the number of beats per minute and statistically evaluated with Prism 5 (GraphPad Software).

2.2.4 Single cell dissociation of EBs

At day four of spontaneous differentiation EBs were collected by sedimentation and washed twice with PBS-/-. EBs were trypsinized by incubation with 5 ml 0.25% trypsin (Cat. N° 25200056, Invitrogen) for 5 min shaking in a 37°C water bath. The dissociation process was immediately stopped by diluting trypsin in 20 ml mouse ESC medium. Cell suspension was filtered through 100 µm for removal of remaining cell clusters. After a first centrifugation step

for 5 min at 200x g single cells were re-suspended in PBS-/- for washing. After a second round cells were re-suspended in ice cold 1% BSA (Cat. N° 15260037, Life Technologies) in PBS-/- supplemented 2 mM EDTA (Cat. N° AM9260G, Life technologies) for flow cytometry analysis.

2.2.5 Fluorescence-Activated Cell Sorting

Cells were sorted based on either β-galactosidase (β-gal) or YFP expression. EBs were dissociated with 0.25% trypsin for 5 min at 37°C. For β-gal-based flow cytometry sorting, cells were incubated with 1 mM C_{12}FDG (Cat. N° D2893, Molecular Probes) for 2 min at 37°C. Isolation of $C_{12}FDG^+$ cells was performed using FACSAria (BD) and data were analyzed with FACSDiva software (BD). For Ki67 proliferation flow cytometry analysis, FDG^+ sorted cells from 5-day-old EBs were fixed with 3.7% formaldehyde, blocked and incubated with primary Ki67 antibody. Subsequently, anti-rabbit AlexaFluor-647-conjugated secondary antibody was used. Flow cytometry was performed on a MoFlo XDP (Beckman-Coulter) and data were analyzed using Kaluza software (Beckman-Coulter). For cTnT flow cytometry analysis, day 14 EBs were dissociated with 1.5 mg/ml collagenase type II (Worthington), fixed with 3.7% formaldehyde, blocked and incubated with primary cTnT antibody. For detection, anti-mouse AlexaFluor-647-conjugated secondary antibody was used. Samples were measured on the FACSCalibur (BD). Data were analyzed using CellQuest software (BD).

For YFP-based flow cytometry sorting, sorted cells were collected in 1% bovine serum albumin supplemented with 2 mM EDTA.

2.2.6 Clonal growth and differentiation of cardiac progenitors

Cardiac progenitors were grown on mitomycin-treated cardiac mesenchymal feeder cells (CMCs) (Laugwitz, Moretti et al. 2005). CMCs were incubated with 1 mg/ml mitomycin C (Cat. N° M4287, Sigma Aldrich) for 2 h, washed three times with EB20 medium and then used immediately or trypsinized and frozen for later usage. Cardiac progenitors sorted from d4 EBs were seeded on top of the CMCs in EB20 medium at a very low density of 2.3 x 10^3 cells per cm^2. Resulting clones were picked after 6 days co-culture, dissociated into single cells with 0.05% trypsin for 5 min at 37°C and then divided into three parts. One part of each clone was plated in a 384-well coated with 0.1% gelatin in mouse ESC medium with insulin (5 µM, Cat. N° I-5500, Sigma Aldrich) and dexamethasone (0.1 µM, Cat. N° D4902, Sigma

Aldrich) and differentiated into the adipogenic cell lineage. Another part was plated in a 384-well coated with fibronectin in myogenic medium and differentiated into the myogenic lineage. Medium was changed every other day for four weeks until the analysis. The third part was used for RNA extraction and gene expression analysis.

2.2.7 List of media and supplements

2i medium

Neurobasal medium DMEM/F12	1:1
L-Glutamine	2.0 mM
NDiff Neuro 2 Medium Suppl.	1x
(Cat. N° SCM012, Merck Millipore)	
B-27 Serum free Suppl.	1x
(Cat. N° 17504044, Thermo Scientific)	
β-Mercaptoethanol	0.1 mM

Supplemented factors:

MEK-Inhibitor	1.0 µM
(Cat. N° PD0325901, Axon Medchem)	
GSK3β-Inhibitor	3.0 µM
(Cat. N° CHIR99021, Axon Medchem)	
Leukemia inhibitory factor	0.1 mg/ml
(Cat. N° LIF2005, Merck Millipore)	

mouse ESC medium

DMEM high glucose	1x
L-Glutamine	2.0 mM
Penicillin	50 U/ml
Streptomycin	50 µg/ml
Non-essential amino acids	0.1 mM
Sodium Pyruvat	1.0 mM
β-Mercaptoethanol	0.2 mM
FBS (Lot N° 9SB023, Lonza)	15%

Material & Methods

EB20 medium

DMEM/F12	1 x
L-Glutamine	2.0 mM
Penicillin	50 U/ml
Streptomycin	50 µg/ml
Non-essential amino acids	0.1 mM
β-Mercaptoethanol	0.1 mM
FBS	20%

Adipogenic medium (mouse ESC medium + 2F)

mouse ESC Medium	1x
Insulin	5.0 µM
(Cat. N° I-5500, Sigma Aldrich)	
Dexamethasone	0.1 µM
(Cat. N° D4902, Sigma Aldrich)	

Myogenic medium

DMEM:M199	4:1
FBS	15%
L-Glutamine	2.0 mM
Penicillin	50 U/ml
Streptomycin	50 µg/ml
Non-essential amino acids	0.1 mM
β-Mercaptoethanol	0.1 mM

Plate-coating agents

Poly(2-hydroxyethyl methacrylate) (Cat. N° P3932, Sigma Aldrich)
Gelatin (Cat. N° G1393, Sigma Aldrich)
Fibronectin from bovine plasma (Cat. N° F1141, Sigma Aldrich)

All Media were sterile filtered. Cell culture reagents were purchased from Life Technologies if not stated otherwise.

2.3 Molecular biology and imaging methods

2.3.1 Chromatin immunoprecipitation assay

EBs at 4 days of differentiation were dissociated with 0.25% trypsin, fixed in 1% final concentration of FA for 10 min at RT and quenched with 125 mM Tris pH=7.5. Lysis of cells was performed using L1 lysis buffer (50 mM Tris pH=8, 2 mM EDTA pH=8, 0.1% NP40, 10% glycerol, 2 mM DTT, protease and phosphatase inhibitors) for 5 min on ice. Nuclei were pelleted by centrifugation at 3000 rpm for 5 min at 4°C and re-suspended in L2 buffer (1% SDS, 5 mM EDTA pH=8.5, 50 mM Tris pH=8, 2 mM DTT, protease and phosphatase inhibitors). DNA fragments of 500-1000 bp were produced by sonification of the cell nuclei. Subsequently, the samples were treated with protein G and pre-saturated with salmon sperm DNA for 2 h at 4°C. Extracts were incubated with 1 µg Isl1 antibody at 4°C overnight on a rotator. DNA-Protein-antibody complexes were precipitated with pre-saturated protein A at 4°C for 30 min, washed 4x with NaCl-washing buffer (0.1% SDS, 1%NP40, 2 mM EDTA, 500 mM NaCl, 20 mM Tris pH=8, 1 mM PMSF), three times with LiCl-washing buffer (0.1% SDS, 1% NP40, 2 mM EDTA, 500 mM LiCl, 20 mM Tris pH=8, 1 mM PMSF) and three times with TE-buffer (10 mM Tris, 1 mM EDTA pH=8). These complexes were eluted in elution buffer (TE-buffer, 2% SDS). Crosslinking of DNA was reverted overnight at 65°C and subsequently proteins were digested by 100 µg Proteinase K (Cat. N° P2308, Sigma Aldrich) treatment for 1 h at 50°C. Following, ChiPed DNA was precipitated, digested with RNAse A and ligated to linker primers. After PCR amplification DNA fragments were subcloned into TOPO vector (pCR-Blunt II-TOPO vector, Life Technologies) and 1000 clones were sequenced (MWG).

Quantitative PCR analysis for selected genes revealed measurement of enrichment of precipitated DNA fragments relative to input DNA (Dorn, Goedel et al. 2015). Chromatin immunoprecipitation assay was performed by Gergana Dobreva.

2.3.2 Reverse transcription and real-time quantitative PCR

RNA isolation was performed using, depending on the amount of starting material, the Absolutely RNA Mini-, Micro- or Nanoprep Kit (Cat. N° 400800, 400805 or 400753, Agilent) according to the manufacturer's instructions. RNA was quantified using Nanodrop 1000 Spectrophotometer (Thermo Fisher Scientific) and analyzed with ND1000 software. 0.5 µg mRNA was reverse transcribed into cDNA using the High-Capacity cDNA Reverse Transcription Kit (Cat. N° 4368813, Applied Biosystems) following the manufacturer's

protocol described below. PCR was performed in a Thermocycler DNA Engine PCR machine (Peltier Thermal Cycler, Biorad).

Reverse transcription reaction:

10x RT buffer	2.0 µl
Nuclease-free H_2O	3.2 µl
25x dNTP Mix (100 mM)	0.8 µl
10x RT random primers	2.0 µl
RNA (0.05 µg/µl)	10.0 µl
RNase inhibitor	1.0 µl
MultiScribeTM reverse transcriptase	1.0 µl

Reverse transcription program:

10 min	25°C	Step 1
120 min	37°C	Step 2
5 sec	85°C	Step 3
Endless	4°C	Step 4

PCR products were mixed with 5x DNA loading dye (Cat. N° 239901, Qiagen) and loaded on a 2% ethidium bromide-agarose gel together with a 2-log DNA ladder (Cat. N° N3200S, New England Biolabs). The gel electrophoresis was performed for 30 min at 100 V. Separated bands were monitored and documented with a UV-light Biovision 3000WL documentation system from PeqLab.

For qRT-PCR cDNA was diluted 1:3 with water and immediately used or stored at -20°C. To determine relative expression of genes, qRT-PCR was performed using the Power SYBR™ Green PCR Master Mix (Cat. N° 4367659, Applied Biosystems) or TaqMan gene expression assays according to the manufacturer's instructions. *GAPDH* was used to normalize gene expression. For qRT-PCR a 7300 Real Time PCR System (Applied Biosystems) and the following protocol was used:

SYBR Green-qRT-PCR reaction:

2x SYBR Green Master Mix	5.0 µl
Primer forward	0.3 µl
Primer reverse	0.3 µl
H_2O	3.4 µl
cDNA	1.0 µl

TaqMan-qRT-PCR reaction:

2x TaqMan Master Mix	5.0 µl
20x TaqMan assay	0.5 µl
H_2O	3.5 µl
cDNA	1.0 µl

qRT-PCR-program:

10 min	95°C	Enzyme activation
15 sec	95°C	Denaturation
1 min	60°C	Annealing/Elongation

Gene expression values were normalized to *GAPDH* and corresponding control was used as a reference.

2.3.3 List of oligonucleotides used in this study

qRT-PCR

Gene	**TaqMan assay**
Fgf10	Mm004 33275_m1
Gapdh	Mm999 999 15_g1
Gata4	Mm004 846 89_m1
Hcn4	Mm011 76086_m1
Isl1	Mm006 278 60_m1
Kdr	Mm012 22419_m1
Nkx2-5	Mm006 577 83_m1
Tbx5	Mm008 03521_m1
Tbx20	Mm004 51515_m1
Tnnt2	Mm004 41992_m1

Gene	**Forward primer 5'->3'**	**Reverse primer 5'->3'**
Acta2	TCTCTTCCAGCCATCTTTCATT	TGCTGTTATAGGTGGTTTCGTG
Cacna1c	CAATCTCCGAAGAGGGGTTT	TCGCTTCAGACATTCCAGGT
Cacna1d	CTGGTGTCCTTTGGGATTCA	ACGTGCTTAAGTCCCTTTGCT
Cacna1g	CTGTGCTGAGGCCAGTTACC	TGTCAACCCAGCCATCCTTG
Cacna2d2	CTCCCACCCTACAGCACCTA	GCTGGGAAGCAGGAACTCAA
Cd34	CGCAGTTGGAGCCCTACAG	CCTCCACCATTCTCCGTGTAAT

Gene	Forward primer 5'->3'	Reverse primer 5'->3'
Cdh5	TCAACGCATCTGTGCCAGAGAT	CACGATTTGGTACAAGACAGTG
Gata1	CCTGCGGCCTCTATTTCAAG	TCCATCTTTCCTCATGGTCAG
Gja1	GAAGTACCCAACAGCAGCAGA	TGGAGTAGGCTTGGACCTTG
Gja5	GGAAGACGGGCTGTTCCA	CCCATTTCAGAAAACAAACACA
Gjc1	TCTGGTGAACAGGGCAAA	CTAGCAGGCGAGTCAGGAAG
Gjd3	GCTGTCGCCAGACCTGCTA	CTGGTGCATGGAGTAGATGAC
Hcn1	CAATGATGAGAAGAGCCTTTGAG	CACCAGTGTTTAGATCCTTCTGG
Hcn4	GAGGGTTAAGTCAGCAGGGTTT	ATCAGCAACAGCATCGTCAG
Hey1	GCGGACGAGAATGGAAACT	AGCAGATCCCTGCTTCTCAA
Hey2	TTGAAGATGCTCCAGGCTACA	CACTCTCGGAATCCAATGCT
Irx4	AGGGCTATGGCAACTACGTG	TCCTTGGACTCGAAGCTGTT
Kcnd2	CAGACAAACGAAGGGCACA	TGCAGCTGGTTGCTCAGTAG
Kcnj2	TCGGCTCATTCTCTTTCACA	AACTCAGCTGACATCCAGAGAAC
Kcnj3	CAACAGCCACATGGTCTCC	GGGAAGGAACTCACCCTCA
Mlc2a	AAGGGAAGGGTCCCATCAACTTCA	AACAGTTGCTCTACCTCAGCAGGA
Mlc2v	ACTTCACCGTGTTCCTCACGATGT	TCCGTGGGTAATGATGTGGACCAA
Nppa	ATGGGCTCCTTCTCCATCAC	TCTACCGGCATCTTCTCCTC
Pecam-1	CCAAGGCCAAACAGAAACC	TGGAGTTCAGAAGTGGAGCAG
Scn5a	GCCGAGTTTGAGGAGATGCT	TGGGTCAAGGGCGATGATCT
Tbx2	GAACGGCCGTCGGGAGAAAAG	TGGGGGAGGGCGGTGGTT
Tbx3	AGACCATGGAACCCGAAGA	ATCCAGTCCAGAGCACCTCA
Tie2	CGGCCAGGTACATAGGAGGAA	TCACATCTCCGAACAATCAGC

RT-PCR

Gene	Forward primer 5'->3'	Reverse primer 5'->3'	bp
Isl1	GCTATTCACCAATTGTCCAACC	AACCAACACACAGGGAAATCA	116
Wt1	AGT TCC CCA ACC ATT CCT TC	TTC AAG CTG GGA GGT CAT TT	194
Nkx2-5	CAA GTG CTC TCC TGC TTT CC	GTC CAG CTC CAC TGC CTT C	130
Gapdh	GCA GTG GCA AAG TGG AGA TTG	AGA GAT GAT GAC CCT TTT GGC TCC	296

EMSA oligonucleotide	Sequence of EMSA oligonucleotide
Nkx2-5 binding site 1 sense	GAGGGGAAAAAAAAA**TCAAGTG**CTCCTTC
Nkx2-5 binding site 1 antisense	GAAGGAGCACTTGATTTTTTTTTCCCCTC
Nkx2-5 binding site 1 mutated sense	GAGGGGAAAAAAAAA**TCGCTTG**CTCCTTC
Nkx2-5 binding site 1 mutated antisense	GAAGGAGCAAGCGATTTTTTTTTCCCCTC
Nkx2-5 binding site 2 sense	GCAGCATTTCCT**TTAAGTG**TAATTATG

EMSA oligonucleotide	Sequence of EMSA oligonucleotide
Nkx2-5 binding site 2 antisense	CATAATTACACTTAAAGGAAATGCTGC
Nkx2-5 binding site 2 mutated sense	GCAGCATTTCCT**TTCGATG**TAATTATG
Nkx2-5 binding site 2 mutated antisense	CATAATTACATCGAAAGGAAATGCTGC
Nkx2-5 binding site 3 sense	GAGGAGCTGGG**TCAAGTG**AGGACAGAG
Nkx2-5 binding site 3 antisense	CTCTGTCCTCACTTGACCCAGCTCCTC
Nkx2-5 binding site 3 mutated sense	GAGGAGCTGGG**TCTACAG**AGGACAGAG
Nkx2-5 binding site 3 mutated antisense	CTCTGTCCTCTGTAGACCCAGCTCCTC

2.3.4 Luciferase assay

A -4.5 to 8.0 kb *Isl1* enhancer region comprising three Nkx2-5 binding sites was inserted into a minimal-promoter containing luciferase reporter plasmid pgl4.24 (Promega). Luciferase assays were performed in C3H 10 T1/2 cells as described (Witzel, Jungblut et al. 2012, Dorn, Goedel et al. 2015). The day before the assay, C3H 10 T1/2 cells were seeded to reach 80% confluency on the next day. Cells were co-transfected with an empty vector (basal) or with vectors encoding Nkx2-5 or GFP. The plasmid pRSV-ßGal served as control in each experiment to normalize the luciferase activity to the transfection efficiency. The culture medium was replaced 24 h later and the cells were lysed in 100 µl reporter lysis buffer (Promega GmbH) 48 h after transfection. Subsequently, the cells were incubated for 30 min at -80°C, followed by 30 min incubation at RT. The cell lysate was transferred into PCR tubes and spun down. 10 µl of the lysate was placed into a lumi-vial and the measurement was carried out using 50 µl luciferase assay reagent (Promega GmbH). For normalization, relative light unit (RLU) values were divided by the corresponding values of the ß-galactosidase assay. The means were calculated and the x-fold change of the inactivation of luciferase by Nkx2-5 compared to the control was determined. Those values were divided by the x-fold activation of the control vector to eliminate unspecific effects of the vector. Luciferase Assay was performed by Alexander Goedel and Jason T. Lam.

2.3.5 Electrophoretic mobility shift assay (EMSA)

Oligonucleotides were ordered at Eurofins MWG Operon and double stranded DNA probes, generated by annealing of sense and antisense oligonucleotides, were biotin-labeled using Biotin 3' End DNA Labeling Kit (Cat. N° 89818, Thermo Scientific). Nkx2-5 DNA-binding activity was determined by the non-radioactive LightShift Chemiluminescent EMSA (Cat. N° 20158, Thermo Scientific). Nkx2-5 protein extract was yielded by transient transfection of

HEK293T cells with pcDNA-Nkx2-5 plasmid using SuperFect Transfection Reagent (Cat. N° 301305, Qiagen) and extracting nuclear protein 48 h later with NE-PER Nuclear and Cytoplasmic Extraction Reagent Kit (Cat. N° 78833, Thermo Scientific). For blotting, a Biodyne B nylon membrane (Cat. N° 77016, Thermo Scientific) was used. Signals were detected by applying stabilized Streptavidin Horseradish Peroxidase Conjugate and luminol solution (Thermo Scientific). The sequences of EMSA oligonucleotides are listed above (Dorn, Goedel et al. 2015). EMSA was performed by Alexander Goedel and Jason T. Lam.

2.3.6 Optical recording and analysis of APs

Optical recordings and analysis of APs were performed by Qinghai Tian and Peter Lipp at the Institute for Molecular Cell Biology of the Universitätsklinikum Homburg/Saar.

2.3.7 *In Situ* Hybridization

Isl1- and Nkx2-5-cDNA-pCR-BluntII-TOPO clones were used to synthesize antisense and sense RNA probes. *Tbx5 in situ* probe was kindly provided by Sylvia Evans (University of California-San Diego, La Jolla, CA) (Cai, Liang et al. 2003). Wnt11 *in situ* probe was kindly provided by Andreas Kispert (Hannover Medical School, Hannover, Germany) (Kispert, Vainio et al. 1996). Probes were prepared by incubating 10 µl of 5 µg linearized cDNA construct with 4 µl 5x transcription buffer, 2 µl DTT, 2 µl DIG RNA labeling mix, 1 µl RNAse inhibitor and 1 µl RNA T7 polymerase in DEPC treated water for 2 h at 37°C. Purification was performed using RNeasy minElute Cleanup Kit (Cat. N° 74204, Qiagen) and the probe was eluted in 50 µl DEPC-H_2O and 2 µl of the probe was run on a 2% agarose gel. The dissected embryos were fixed in precooled DEPC-PBS and 4% PFA at 4°C overnight. Dehydration row was performed by 5 min steps each in DEPC-PBT (PBS-/- + 0.1% Tween-20) twice, 25% MeOH in DEPC-PBT, 50% MeOH in DEPC-PBT, 75% MeOH in DEPC-PBT and 100% MeOH in DEPC-PBT twice. Embryos were stored at -20°C or processed for *in situ* hybridization. Re-hydrated embryos were bleached in 6% H_2O_2 in DEPC-PBT, washed and treated with 10 µg/ml proteinase K for 5-15min depending on embryo size. 2 mg/ml glycine in DEPC-PBT was applied for 5 min to inactivate proteinase K and samples were washed 3 times in DEPC-PBT. Embryos were re-fixed in 0.2% glutaraldehyde and 4% PFA in DEPC-PBT for 20-30 min and washed 3 times in DEPC-PBT. Embryos were saturated in Hybridization buffer (50% formamide, 5x SSC, 1% SDS, 50 µg/ml heparin and 50 µg/ml yeast transfer RNA in DEPC-H_2O) for 3 h and 2 µl of probe was added and incubated at 68°C overnight in a shaking water bath. On the next day embryos were washed in

Hybridization buffer three times at 68°C for 30 min and in TNT (10 mM Tris-HCl pH=7.5, 0.5 M NaCl, 0.1% Tween-20) at RT for three times 5 min. Samples were treated with 100 µg/ml RNAse A in TNT for 1 h at RT and washed with 5x SSC for 5 min, twice with 2x SSC/50% formamide 20 min each, twice with 2x SSC 15 min each, twice with 0.2x SSC for 15 min each, all at 68°C. Three washes with MAB-TW (0.1 M maleic acid pH=7.5 adjusted with NaOH, 0.15 M NaCl, 0.1% Tween-20, 2 mM levamisole) were performed for 10 min each at RT. The samples were blocked using 2% blocking reagent (Roche) in 1x MAB-TW for 1-2 h at RT. Anti-DIG antibody (Roche) was incubated overnight at 4°C 1:2000 diluted in blocking solution. On the third day three washes in MAB-TW 5 min each followed by three to five washes 1 h each and one wash overnight at 4°C were performed. On the last day three washing steps in NTMT (100 mM NaCl, 100 mM Tris-HCl [pH 9.5], 50 mM $MgCl_2$, 0.1% Tween-20, 2 mM levamisole) for 10-15 min each at RT were made and BM purple staining solution was applied until the signal reached the desired intensity. Another three times washing with NTMT for 5 min each at RT was performed followed by three times washing with DEPC-PBT pH=5.5 for 10-15 min each at RT. Embryos were fixed in 4% for 15 min at RT and washed three times in DEPC-PBT for 10-15 min each at RT. The samples were stored at 4°C. Pictures were taken using a MZ 16 F stereomicroscope, with a DFC425C camera and Leica Application Suite software from Leica Microsystems.

2.3.8 LacZ staining

Plated EBs at day 2 of differentiation were subjected to Lacz staining after fixation with 0.2% glutaraldehyde, incubation in X-Gal solution containing 1.25 mM $K_3(Fe(CN)_6)$, 1.25 mM $K_4(Fe(CN)_6)$, 2 mM $MgCl_2$, 0.02% Nonidet P-40, and 0.25 mg/ml X-Gal in PBS. For each differentiation experiment and time point, nuclear $lacZ^+$ cells were counted blinded to the genotype in 20 EBs from each of the transgenic mouse ESC lines using a 40x objective in bright field. Proliferation was inhibited by treatment of plated EBs with 2 µg/ml mitomycin C at day 3 of differentiation and $lacZ^+$ cells were counted on the two following days. Samples were imaged using a DMI6000B microscope and Leica Application Suite software from Leica Microsystems.

2.3.9 Immunofluorescence staining

Samples were fixed in 3.7% FA (in PBS+/+) for 10 min at RT and subsequently washed 3x for few minutes with PBS+/+. Permeabilization and blocking was performed with 10% FBS in 0.1% Triton (in PBS+/+) for at least 1 h at 37°C. Primary antibodies were diluted in 1% FBS

in 0.1% Triton (in PBS+/+) and samples were incubated for 1-2 h at 37°C. After five times washing 5 min each in PBS+/+ samples were incubated with secondary antibodies and Hoechst Dye 33258 in 1% FBS in 0.1% Triton (in PBS+/+) for 1 h at 37°C. For better performance of immunofluorescence probes were mounted with DAKO mounting media. Microscopy was performed using a DMI6000B epifluorescence microscope or SP8 confocal microscope and Leica Application Suite software from Leica Microsystems.

2.3.10 Statistical analysis

Data are presented as means ± SEM. Data that passed evaluation for normality and equal variance were analyzed using two-tailed Student's t test. Data not fulfilling these criteria were analyzed using the Mann-Whitney test. P-values less than 0.05 were considered statistically significant.

2.3.11 List of antibodies and staining agents used in this study

Designation	Antibody	Species	Company	Cat#	Dilution
α-actinin	α-actinin	Mouse	Sigma Aldrich	A7811	1/300
α-sma	α-smooth muscle actin	Mouse	Sigma Aldrich	A2547	1/400
β-actin	β-actin	Rabbit	Abcam	ab8227	1/1000
cTnT	cardiac Troponin T	Mouse	Thermo Scientific	MS-295-P1	1/500
cTnT	cardiac Troponin T	Rabbit	Abcam	ab92546	1/500-1/300
Hcn4	Potassium/sodium hyperpolarization-activated cyclic nucleotide-gated channel 4	Rabbit	Abcam	ab69054	1/100
Isl1	Islet-1	Mouse	Developmental Hybridoma Bank	39.4D5	1/100
Ki67	Ki67	Rabbit	Abcam	ab15580	1/100
mG	Green fluorescent protein	Rabbit	Acris	SP3005P	1/100
mG	Green fluorescent protein	Chicken	Aves lab	1020	1/250

Designation	Antibody	Species	Company	Cat#	Dilution
Mlc2a	Myosin regulatory light chain 2, atrial isoform	Mouse	Synaptic Systems	311 011	1/200
Mlc2v	Myosin regulatory light chain 2, ventricular/cardiac muscle isoform	Rabbit	Proteintech	10906-1-AP	1/100
mT	Red fluorescent protein	Rat	ChromoTek	5f8	1/1000
Nkx2-5	Homeobox protein Nkx-2.5 (N-19)	Goat	Santa Cruz	sc-8697	1/500
PHH3	Phospho-Histone H3 (Ser10) Antibody Alexa Fluor® 647 Conjugate	Rabbit	Cell Signaling Technology	9716	1/100
Plin1	Perilipin A	Rabbit	Sigma Aldrich	P1998	1/500
Pparγ	Ppar gamma	Rabbit	Cell Signaling Technology	2443S	1/200
Vim	Vimentin	Chicken	Abcam	ab24525	1/500
Wt1	Wilms tumor 1	Rabbit	Merck Millipore	CA1026	1/100
Secondary antibodies	AlexaFluor-488,594,647-conjugates	donkey/goat	Life Technologies		1/500

Designation	Staining agent	Company	Cat#	Dilution
DNA	Hoechst 33258	Sigma Aldrich	861405	1/1000
BODIPY® 493/503	Lipid droplets	Thermo Scientific	D3922	1/100
Phalloidin	AlexaFluor-594-conjugate, F-actin visualization	Life Technologies	A12381	1/100

3. Results

3.1 Role of Isl1 & Nkx2-5 in cardiac lineage specification and differentiation

3.1.1 Nkx2-5 overexpression in mouse ESCs suppresses Isl1 progenitor program during early mesoderm development

An *Isl1-nlacZ* knock-in mouse ESC line with transgenic overexpression of Nkx2-5 was used to investigate the role of Isl1 and Nkx2-5 during early mesoderm development. In this line nuclear *lacZ* gene is inserted into the *Isl1* locus. When Isl1 promoter is active, nuclear *LacZ* gene drives ß-galactosidase (ß-gal) expression, which can be detected by x-Gal staining, thus allowing for monitoring *Isl1* gene expression. Using a lentiviral approach an Nkx2-5 transgene was introduced into this line (Nkx2-5 OE ESCs). As a corresponding control, the *Isl1-nlacZ* knock-in line was transduced with the empty PKG-IRES-eGFP lentiviral vector (GFP ESCs) (Fig. 9). The GFP (green fluorescent protein) expression in all the lines served for separation of transduced cells.

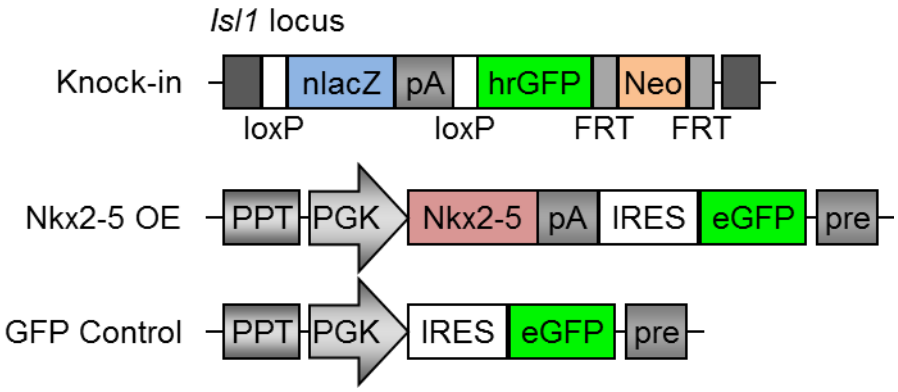

Figure 9: *Isl1-nlacZ* knock-in ESCs overexpressing Nkx2-5 or GFP.
Knock-in of floxed nlacZ with a polyadenylation sequence followed by *hrGFP* and a *FRT*-flanked neo cassette in the *Isl1* locus of embryonic stem cells. Nkx2-5 OE cells were generated by lentiviral-mediated expression of Nkx2-5 in the *Isl1-nlacZ* ESC line. GFP control cells were generated by infection of an empty lentiviral PGK-IRES-eGFP vector. eGFP = enhanced green fluorescent protein, FRT = flippase recognition target, hrGFP = humanized renilla reniformis green fluorescent protein, IRES = internal ribosome entry site, Neo = neomycin cassette, nlacZ = nuclear location signal lacZ, pA = polyadenylation sequence, PGK = phosphoglycerate kinase, PPT = polypurine tract, pre = posttranscriptional regulatory element. Adapted from Dorn, Goedel et al. 2015.

Overexpression of Nkx2-5 at the protein level was confirmed by Western blot analysis in undifferentiated Nkx2-5 OE ESCs. In undifferentiated *Isl1-nLacZ* ESCs and GFP ESCs Nkx2-5 protein was absent (Fig. 10). In this experiment, ß-actin was used as a loading control.

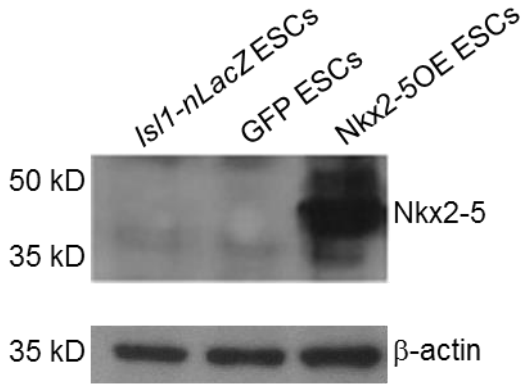

Figure 10: Nkx2-5 overexpression in Nkx2-5 OE undifferentiated ESCs.
Western blot analysis of Nkx2-5 protein expression in undifferentiated embryonic stem cells of *Isl1-nlacZ*, GFP and Nkx2-5 OE line. ß-actin served as loading control. Adapted from Dorn, Goedel et al. 2015.

Under control conditions, Isl1$^+$ progenitors arose starting at day 4 of spontaneous EB differentiation. Quantification of ß-gal$^+$ cells showed that Isl1$^+$ progenitors exponentially increased until 5 days of differentiation. In contrast, Nkx2-5 overexpression resulted in a delayed and reduced appearance of Isl1 expressing cells (Fig. 11).

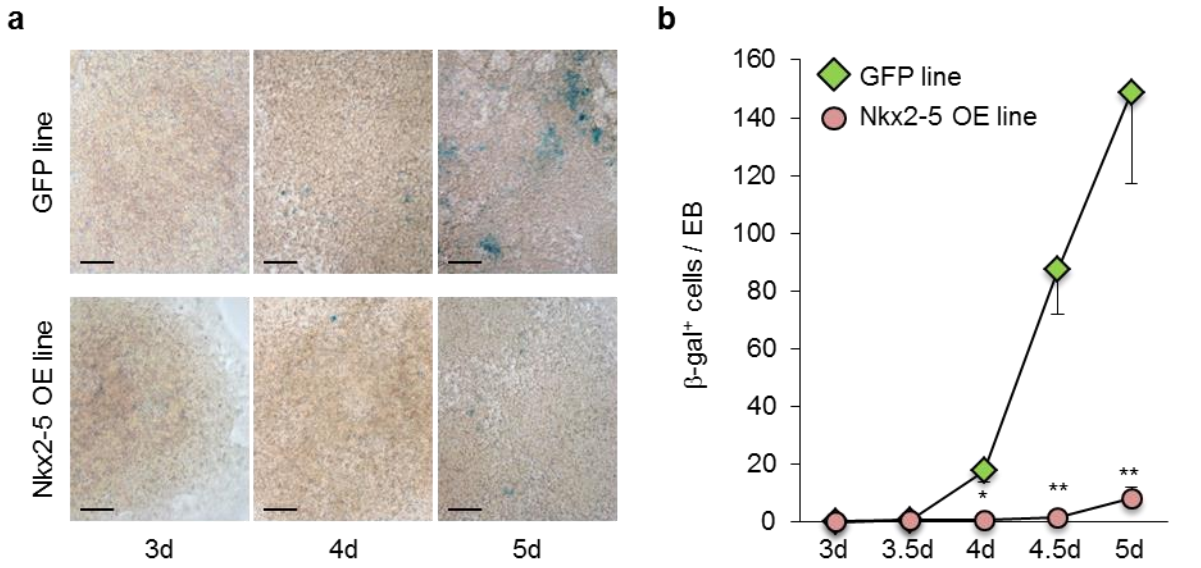

Figure 11: Delayed and reduced Isl1 progenitor specification in Nkx2-5 OE line.
a) X-Gal staining of GFP control (upper panels) and Nkx2-5 OE cells (lower panels) at 3, 4 and 5 days of spontaneous EB differentiation. Scale bars = 150 µm. b) Quantification of ß-gal expressing cells per EB in GFP control (green diamonds) and Nkx2-5 OE (red circles) cell line at indicated time points of spontaneous EB differentiation. Data are mean values ± SEM from three different experiments. * = p-value <0.05 and ** = p-value <0.01 vs. GFP at the same time point. Adapted from Dorn, Goedel et al. 2015.

Gene expression analysis confirmed significantly increased Nkx2-5 expression in the Nkx2-5 OE differentiated cells compared to the GFP control (Fig. 12). Several early key transcription factors of the SHF (*Isl1*, *Tbx20*, *Gata4*, *Fgf10* and *Kdr*) showed a delayed expression during early EB differentiation, suggesting an inhibitory effect of Nkx2-5 on cardiac specification. In addition, Nkx2-5 OE line displayed reduced expression of *Hcn4* and *Tbx5*, the markers of the FHF, as well as *cTnT*, the early cardiac differentiation marker. These results indicate a suppressive effect of Nkx2-5 on *Isl1* expression and general early cardiac specification program (Fig. 12).

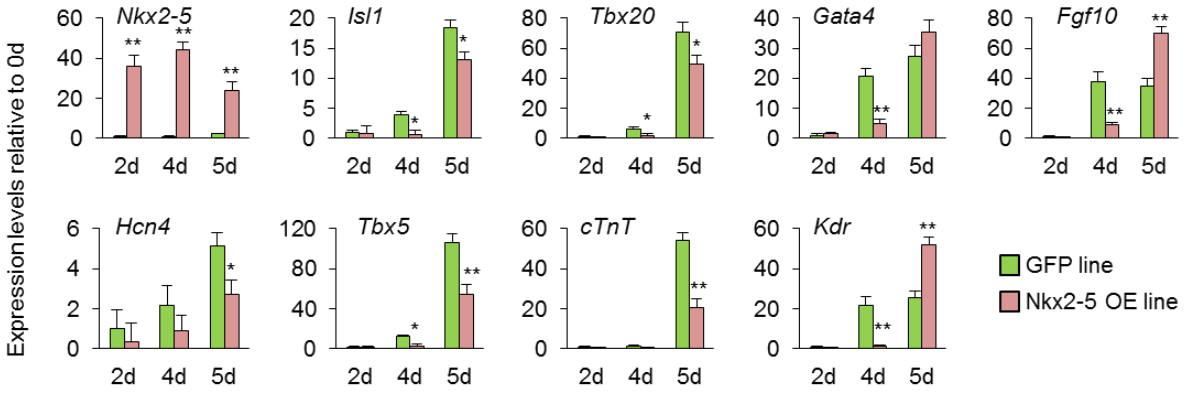

Figure 12: Delayed expression of early cardiac progenitor markers during differentiation of Nkx2-5 OE ESCs.
Gene expression analysis of early cardiac progenitor markers in GFP control (green) and Nkx2-5 OE (red) cells at 2, 4 and 5 days of spontaneous EB differentiation. Data are means ± SEM from three independent experiments. * = p-value <0.05 and ** = p-value <0.01 vs. GFP at the same time point. Adapted from Dorn, Goedel et al. 2015.

Kdr, a marker for a common progenitor population of hematopoietic, cardiomyocytic and endothelial/smooth muscle cell lineage, was upregulated at day 5 in Nkx2-5 overexpressing EBs. To test whether cardiac differentiation potential was impaired due to a shift towards the hematopoietic or endothelial/smooth muscle cell lineage, expression of hematopoietic (*Cd34* and *Gata1*) and endothelial markers (*Pecam-1*, *Tie2*, *Cdh5*) as well as the smooth muscle gene *Acta2*, was analyzed. These transcripts were downregulated in Nkx2-5 overexpressing cells, indicating a general inhibition of early mesoderm specification by Nkx2-5 (Fig. 13).

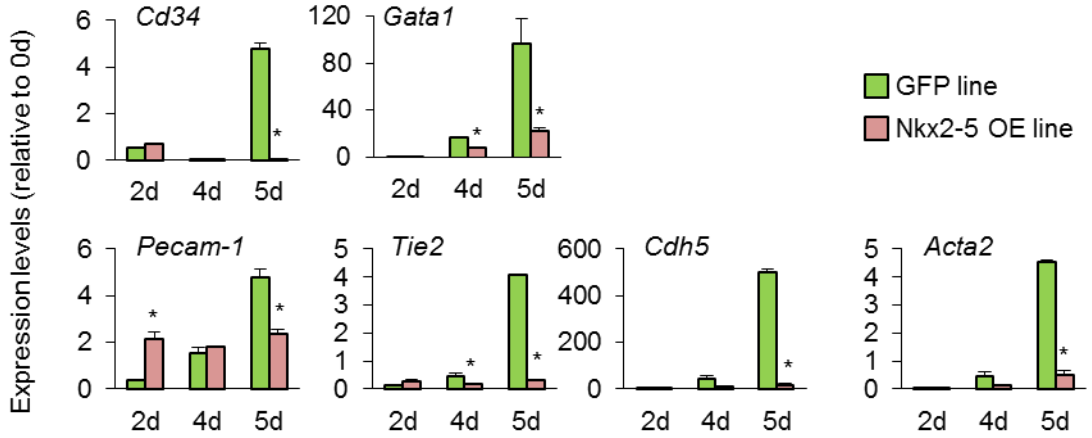

Figure 13: Downregulation of hemangioblast lineage markers during differentiation of Nkx2-5 OE ESCs.
qRT-PCR analysis of smooth muscle (*Acta2*) and endothelial/hematopoietic genes (*Pecam-1*, *Tie2*, *Cdh5*, *Cd34* and *Gata1*) in GFP control (green) and Nkx2-5 OE (red) cells at 2, 4 and 5 days of spontaneous EB differentiation. Data are means ± SEM from three independent experiments. * = p-value <0.05 and ** = p-value <0.01 vs. GFP at the same time point. Adapted from Dorn, Goedel et al. 2015.

3.1.2 Nkx2-5 negatively regulates cardiac progenitor specification by direct inhibition of *Isl1* transcription

To investigate whether Nkx2-5 overexpression was leading to an inhibition of the cardiac specification program due to the dysregulation of the *Isl1* expression, an Isl1 OE ESC line was generated and its cardiac differentiation potential was compared to that of the Nkx2-5 OE ESCs. Isl1 was overexpressed in the *Isl1-nlacZ* knock-in ESC line with a similar strategy as in the case of the Nkx2-5 OE line, using a lentiviral plasmid carrying Isl1 cDNA (Fig. 14a). Western blot analysis confirmed overexpression of Isl1 at the protein level in undifferentiated Isl1 OE ESCs (Fig. 14b). The number of ß-gal expressing cells per EB was used for evaluation of Isl1 progenitor specification. Quantification of ß-gal$^+$ cells showed that Isl1 progenitor specification was enhanced in Isl1 OE line in comparison to the GFP control, contrary to the Nkx2-5 OE line, which exhibited reduced Isl1 progenitor specification (Fig. 14c).

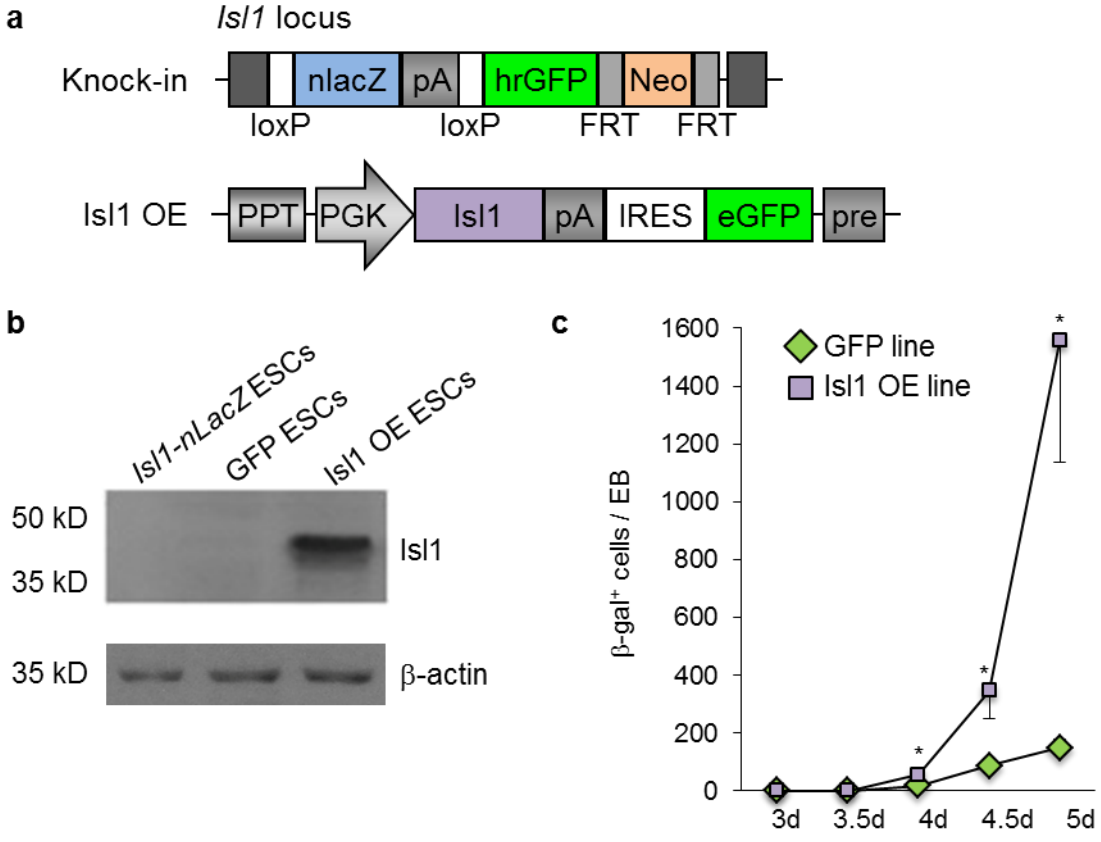

Figure 14: Enhanced cardiac progenitor specification in Isl1 OE ESC line.
a) Knock-in of floxed nlacZ with a polyadenylation sequence followed by hrGFP and a FRT-flanked neo cassette in the *Isl1* locus of embryonic stem cells. Isl1 OE cells were generated by lentiviral-mediated overexpression of Isl1 in the *Isl1-nlacZ* ESC line. eGFP = enhanced green fluorescent protein, FRT = flippase recognition target, hrGFP = humanized renilla reniformis green fluorescent protein, IRES = internal ribosome entry site, Neo = neomycin cassette, nlacZ = nuclear location signal lacZ, pA = polyadenylation sequence, PGK = phosphoglycerate kinase, PPT = polypurine tract, pre = posttranscriptional regulatory element. b) Western blot analysis of Isl1 protein expression in undifferentiated embryonic stem cells of *Isl1-nlacZ*, GFP and Isl1 OE line. ß-

actin served as loading control. c) Quantification of ß-gal expressing cells per EB in GFP control (green diamonds) and Isl1 OE (purple squares) cell lines at indicated time points of spontaneous EB differentiation. Data are mean values ± SEM from three different experiments. * = p-value <0.05 and ** = p-value <0.01 vs. GFP at the same time point. Adapted from Dorn, Goedel et al. 2015.

In addition, gene expression of the early cardiac progenitors markers was analyzed similarly to the Nkx2-5 OE line. Isl1 OE cells revealed an increased expression of SHF (*Tbx20*, *Gata4*, *Fgf10* and *Kdr*) and FHF markers (*Hcn4* and *Tbx5*) indicating opposed effects of Isl1 and Nkx2-5 on cardiac specification. Interestingly, *Nkx2-5* expression was significantly upregulated in day 4 Isl1 OE cells compared to the GFP control, which could represent a possible compensatory upregulation as a consequence of forced Isl1 expression (Fig. 15).

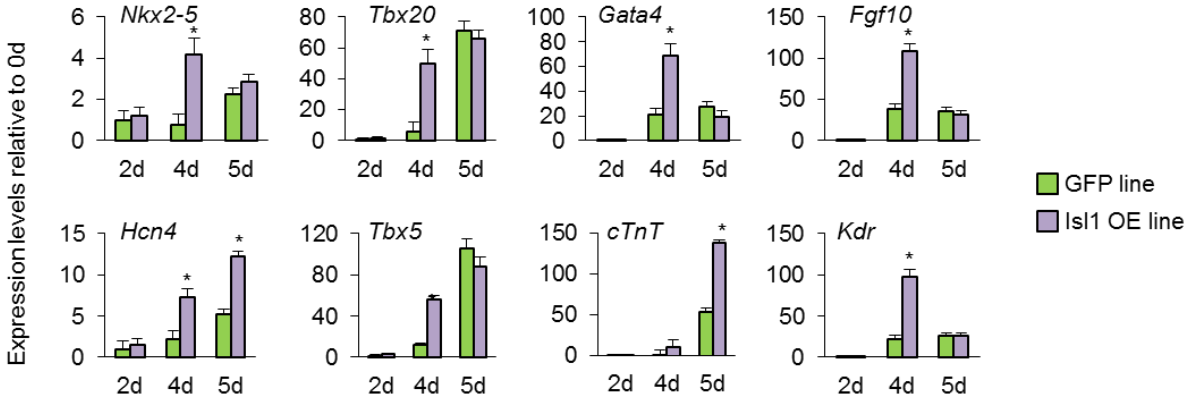

Figure 15: Upregulation of early cardiac progenitor markers during differentiation of Isl1 OE ESCs. Gene expression analysis of early cardiac progenitor markers in GFP control (green) and Isl1 OE (purple) cells at 2, 4 and 5 days of EB differentiation. Data are means ± SEM from three independent experiments. * = p-value <0.05 and ** = p-value <0.01 vs. GFP at the same time point. Adapted from Dorn, Goedel et al. 2015.

Differences in expression levels of cardiac differentiation markers and numbers of Isl1 expressing progenitors detected in Isl1 OE and Nkx2-5 OE lines could be attributed to aberrant specification or proliferation of cardiac precursors. To address the contribution of specification, proliferation was blocked first. The cells were treated with Mitomycin C to inhibit mitosis and then the number of β-gal$^+$ progenitors was quantified. Inhibition of proliferation in 3-day old EBs resulted in dramatic decrease of β-gal expressing cells in the GFP and Isl1 OE line (Fig. 16a). In contrast to the GFP control, Isl1 OE line displayed a higher number of β-gal$^+$ cells at day 4, which did not increase further at day 5, indicating that more cells were able to turn on and complete faster the cardiac specification program (Fig. 16a). Nkx2-5 OE cells were inhibited in switching on *Isl1* expression, which resulted in very few ß-gal$^+$ cells (Fig. 16a). In the next step, the proliferation rate of Isl1$^+$ cardiac progenitor from GFP, Isl1 OE and Nkx2-5 OE lines was analyzed. LacZ$^+$ cells were isolated from 5-day old EBs of all three lines by FACS after labeling with the β-gal substrate $F_{12}DG$. Sorted FDG$^+$ cells exhibited a very high purity (Fig. 16b) and increased *Isl1* transcript as compared to the FDG$^-$ fraction

(Fig. 16c). Proliferation capacity was tested by flow cytometry analysis of proliferation marker Ki67. Isl1$^+$/β-gal$^+$ progenitors revealed similar proliferation rates in all transgenic lines, suggesting that differences in the number of Isl1$^+$ precursors in Isl1 OE and Nkx2-5 OE lines were not due to differences in proliferation but arose from opposed regulation of Isl1 progenitor specification in the Isl1 OE and Nkx2-5 OE cells (Fig. 16d+e).

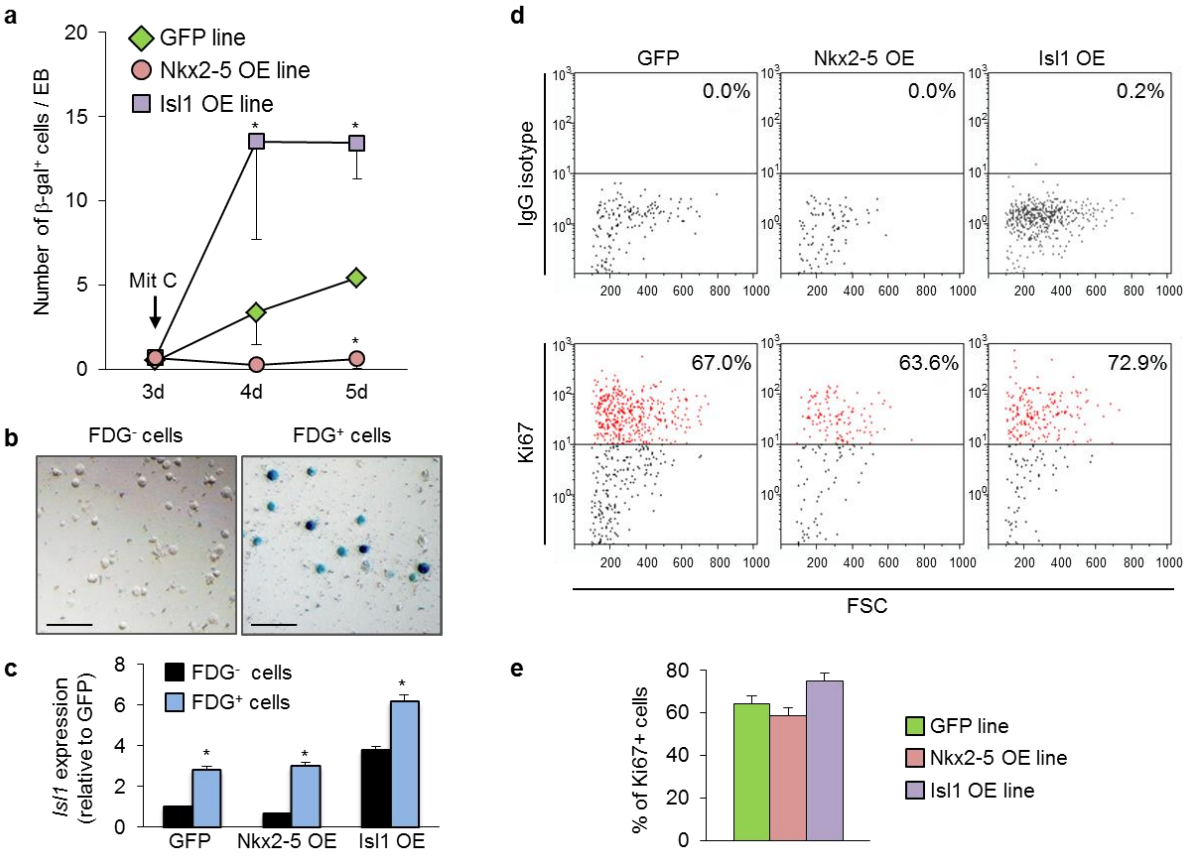

Figure 16: Lack of Isl1 progenitor specification in Nkx2-5 OE cells not due to differences in proliferation. a) Quantification of ß-gal$^+$ cells per EB in Isl1 OE (purple), GFP control (green), Nkx2-5 OE (red) lines at indicated time points of spontaneous EB differentiation after inhibition of proliferation by Mitomycin C at day 3 of differentiation. Data are mean values ± SEM from three different experiments. * = p-value <0.05 vs. GFP. b) Representative images of FACS-sorted FDG$^-$ (left panel) and FDG$^+$ (right panel) cells after x-Gal staining. Scale bars = 150 µm. c) Gene expression analysis of *Isl1* in FDG$^-$ (black) and FDG$^+$ (blue) fraction after FACS sorting of GFP control, Nkx2-5 OE and Isl1 OE cells from 4-day old EBs. Values are relative to GFP control and presented as mean ± SEM from three experiments. d+e) Flow cytometry analysis for proliferation marker Ki67 (lower panels) and IgG isotype control (upper panels) of FDG$^+$-sorted cells from 5-day old EBs of all three cell lines (d). Percentage of Ki67$^+$ cells in GFP control (green), Nkx2-5 OE (red) and Isl1 OE (purple) EBs. Data are mean values ± SEM from three different experiments (e). FSC = forward side scatter. Adapted from Dorn, Goedel et al. 2015.

To further characterize the role of Nkx2-5 in the regulation of Isl1 transcriptional program, a ChIP analysis on 4-day old *Isl1-nlacZ* EBs was performed to identify direct Isl1 target genes. Several of the identified Isl1 target genes, which play an important role in heart development, were selected and their expression was analyzed in Isl1 OE and Nkx2-5 OE differentiated cells. These were genes controlling known cardiac signaling pathways (*Bmpr1b*, *Dlk1*, *Wif1*),

and regulating cell growth, differentiation and migration (*Ret*, *Odz1*, *Robo2*), or transcription (*Snf1lk*) or being itself cardiac transcription factor (*Sox6*), progenitor marker (*Igfbp5*) or muscle genes (*Tnnt2*, *Dscr1/1*). All of the selected genes were enriched in the precipitated compared to the input DNA (Fig. 17a).

To test if the delay in cardiac progenitor specification in Nkx2-5 OE differentiating cells was mediated by direct inhibition of *Isl1*, expression of *Isl1* and its selected direct target genes was compared in FACS-sorted $FDG^{+}/Isl1^{+}$ progenitors from 5-day old EBs between GFP control, Isl1 OE and Nkx2-5 OE lines (Fig. 17b). Indeed, *Isl1* transcript was significantly reduced in Nkx2-5 OE cells, which led to a dysregulation of the selected Isl1 downstream target genes in opposite direction in Isl1 and Nkx2-5 OE EBs, strongly suggesting Nkx2-5 as a negative regulator of *Isl1* transcription causing a delay in cardiac progenitor specification. The reduction of *Isl1* transcript in the Nkx2-5 OE line was also seen in other experiments (Fig. 11+12), confirming the hypothesis of an Isl1-Nkx2-5 regulatory relationship.

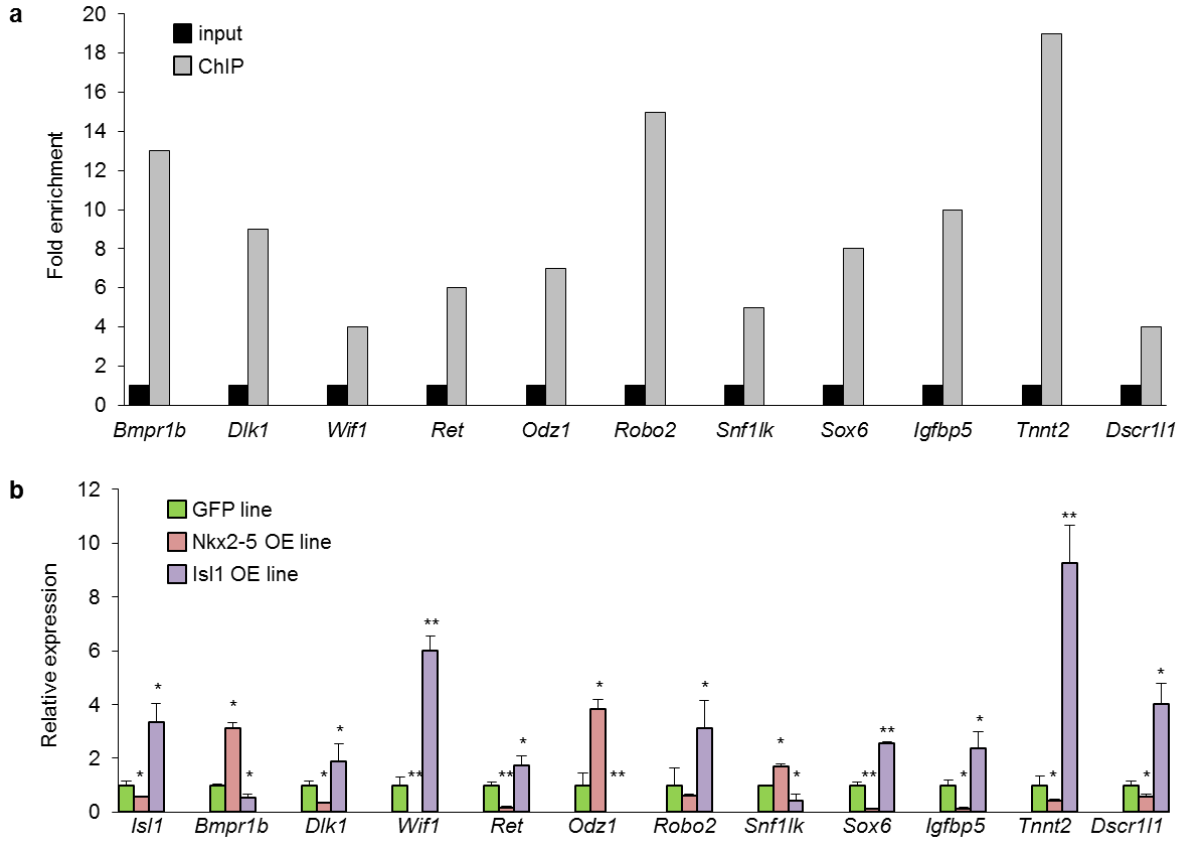

Figure 17: Opposite regulation of ChIP-identified Isl1 target genes in Nkx2-5 OE and Isl1 OEcells.
a) Fold enrichment of selected Isl1 downstream target genes in ChIP precipitated (grey) versus total input DNA (black) as analyzed by q-PCR. b) Gene expression analysis of downstream Isl1 target genes in FDG^{+} FACS-sorted fraction of 5-day old EBs from GFP control (green), Nkx2-5 OE (red) and Isl1 OE (purple) cell lines. Data are means ± SEM from three independent experiments. * = p-value <0.05 and ** = p-value <0.01 vs. GFP. Adapted from Dorn, Goedel et al. 2015.

To verify if this phenomenon relied on a direct inhibition of *Isl1* transcription by Nkx2-5, the presence of potential Nkx2-5 binding sites, with the sequence 5'-TYAAGTG-3', was investigated in the regions within ± 10 kbp of the *Isl1* transcription start site (TSS). Indeed, three putative Nkx2-5 DNA-binding motifs in the evolutionarily conserved region 4.5 – 8.0 kb upstream of the TSS were found (Fig. 18a). While one of the identified sites is evolutionarily conserved within the Placentalia infraclass, including the orders Rodentia, Primates and Carnivora (rat, human and dog), the other two sites display conservation even within the Mammalian class, including opossum, additionally, the representative of the Marsupialia infraclass. These sites are located at -8004, -7198 and -4554 bp upstream of the Isl1-TSS. To test if these identified regions could be regulated by Nkx2-5, a luciferase transactivation assay was performed. The regulatory regions were inserted upstream of the luciferase gene in the pGL4.24 vector (pGL4.24/Isl1). This resulted in a higher basal luminescence measured in relative light units (RLU) compared to the same vector driven by a minimal promoter. When GFP was added as a control reaction, no significant changes in the light emission were detected. However, addition of Nkx2-5 protein strongly decreased the luminescence compared to the GFP control (Fig. 18b). This result indicated Nkx2-5-mediated repression of the activity of the "*Isl1* enhancer" region, demonstrating biological functionality of the Nkx2-5 binding region identified *in silico* (Fig. 18b). Moreover, EMSA revealed specific binding of Nkx2-5 protein to each of the three identified binding sites (Fig. 18c). Biotin-labeled probes containing 27-29 bp of each identified Nkx2-5 binding site sequence were incubated with nuclear extract of HEK293T cells overexpressing Nkx2-5. After blotting and incubation with Streptavidin Horseradish Peroxidase Conjugate and luminol solution, biotin-labeled probes could be visualized. Binding of Nkx2-5 protein to the labeled probes resulted in a shift of the band (Fig. 18c). Non-labeled oligos were used as competitors and showed specific binding to the Nkx2-5 protein by the decrease of the shift signal. Mutated oligos did not bind to Nkx2-5 protein, proved by the lack of a shift when incubated with the mutated labeled probes, and absence of the competitive action when incubated with mutated non-labeled DNA.

These results together revealed that the negative regulation observed in cardiac progenitor specification was mediated through direct inhibition of *Isl1* transcription by Nkx2-5.

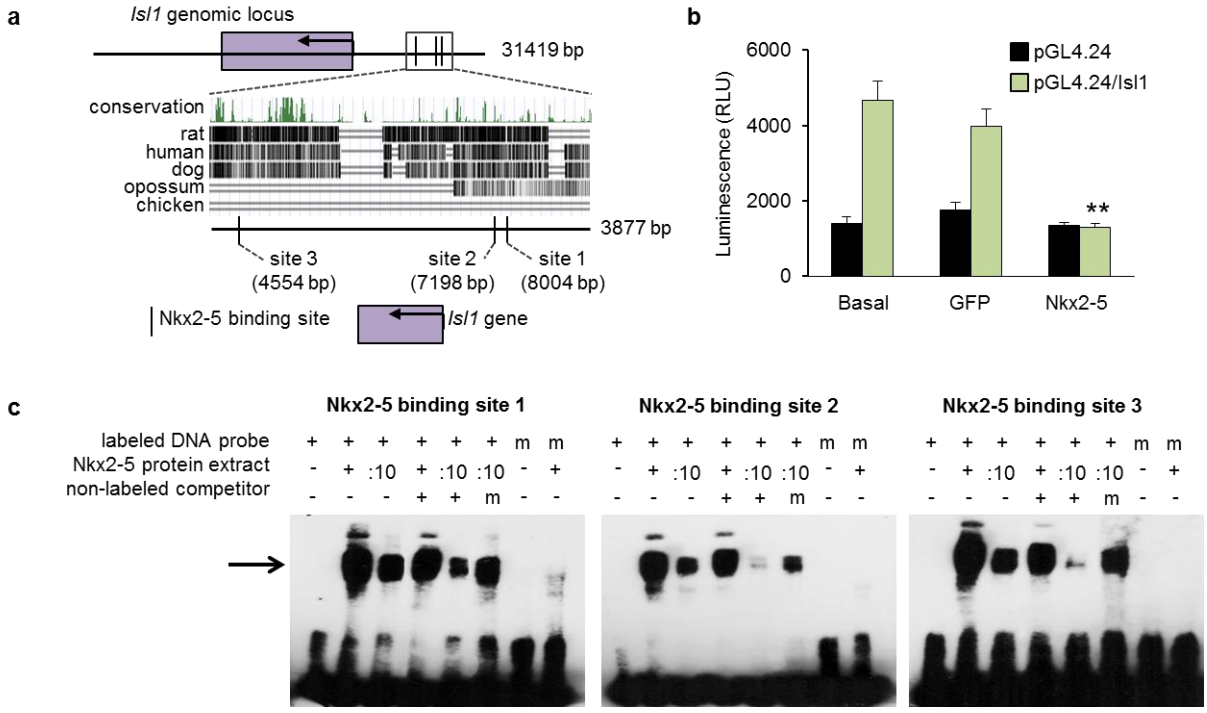

Figure 18: Specific binding of Nkx2-5 to *in silico* identified Nkx2-5 binding sites in the *Isl1* locus.
a) Visualization of the *Isl1* genomic locus (purple square) with 10 kb up- and 10 kb downstream of the *Isl1* transcription start site. The boxed region contains three putative highly conserved Nkx2-5 binding sites, as shown in a cross-species sequence comparison. b) Luciferase assay quantification of luminescence in relative light units (RLU). C3H 10T1/2 cells were transfected with either an empty vector (black) or a vector containing the upstream region with the three potential binding sites boxed in panel a (green). Cotransfection with an empty vector (basal), GFP or Nkx2-5. Data are means ± SEM from eight experiments. ** = p-value <0.01 vs. GFP. c) EMSA using biotin-labeled DNA probe of each Nkx2-5 binding site (+) and nuclear extract of HEK293T cells overexpressing Nkx2-5. Mutated labeled DNA probes (m) were used as a negative control. Non-labeled competitor DNA probes and mutated non-labeled competitor DNA probes (m) were used to test specificity of the binding. :10 = nuclear extract diluted 1 to 10 for improvement of visualization. Adapted from Dorn, Goedel et al. 2015.

3.1.3 Nkx2-5-mediated downregulation of *Isl1* occurs during normal SHF progenitor differentiation *in vivo*

To further investigate the function of Nkx2-5-mediated *Isl1* downregulation during cardiac development *in vivo*, *Isl1*$^{Cre/+}$ mice were crossed to *Nxk2-5*$^{fl/fl}$ mice, which allowed Cre recombinase mediated excision of Nkx2-5 in all cells expressing Isl1 (Fig. 19a). Whole-mount RNA *in situ* hybridization (ISH) showed efficient Cre-mediated deletion of Nkx2-5 in Isl1 expressing cells at E9.5 (Fig. 19b). Interestingly, no Nkx2-5 expression could be detected throughout the heart in the mutant embryos, suggesting Isl1 as a pan-cardiac marker. *Isl1*$^{cre/+}$*;Nkx2-5*$^{fl/fl}$ embryos exhibited severe SHF defects around E9.5, manifesting in truncated OFT and loss of right ventricle as well as a defect in the looping process, leading to embryonic lethality at E10.5 one day later. Malformations observed in the mutant embryos were similar to those detected in the global Nkx2-5 KO mice, indicating that Isl1 could be a pan-cardiac marker. Detailed ISH analysis with *Tbx5* and *Wnt11* probes for ventricular tissue and OFT marker, respectively, confirmed the identity of these malformed tissues (Fig. 19b).

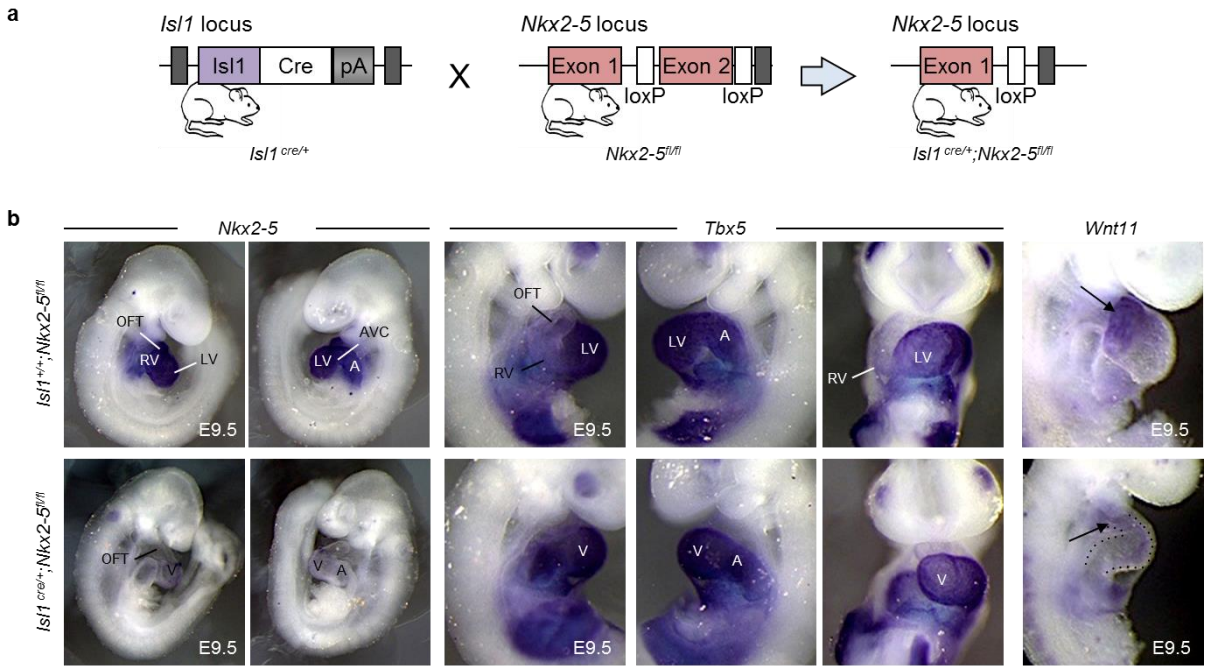

Figure 19: Malformation of the OFT and loss of right ventricle in the *Isl1$^{Cre/+}$;Nkx2-5$^{fl/fl}$* mice.
a) Crossing of *Isl1$^{Cre/+}$* mice with *Nkx2-5$^{fl/fl}$* (floxed Nkx2-5 alleles) allowed for deletion of Nkx2-5 in all *Isl1* expressing cells. b) Whole mount RNA *in situ* hybridization for *Nkx2-5*, *Tbx5* and *Wnt11* in control (*Isl1$^{+/+}$;Nkx2-5$^{fl/fl}$*, upper panels) and Nkx2-5 mutant *(Isl1$^{Cre/+}$;Nkx2-5$^{fl/fl}$*, lower panels) embryos at E9.5. Black arrows indicate outflow tract in the control and foreshortened OFT in the mutant embryo. The dotted line marks the ventricle and OFT in the mutant embryo. A = atria, AVC = atrioventricular canal, LV = left ventricle, OFT = outflow tract, RV = right ventricle, V = ventricle. Adapted from Dorn, Goedel et al. 2015.

Importantly, whole mount RNA ISH demonstrated downregulation of *Isl1* expression in the OFT, the ventricles and the atria in the control embryo at E9.0, whereas *Isl1* expression persisted in the ventricles and atria in the absence of the Nkx2-5 (Fig. 20a). For detailed immunohistochemical analysis transverse sections at three different positions of the hearts at E9.25 were stained for Isl1 and cTnT (Fig. 20b). Consistent with the persistence of *Isl1* transcript in the mutant heart, also Isl1 protein was maintained in the whole heart of the *Isl1$^{Cre/+}$;Nkx2-5$^{fl/fl}$* embryos as detected by immunostaining (Fig. 20b). Taken together, deletion of Nkx2-5 in Isl1 expressing cells resulted in sustained Isl1 expression in differentiated cTnT^{+} cardiomyocytes of the whole heart tube in *Isl1$^{Cre/+}$;Nxk2-5$^{fl/fl}$* embryos, confirming a negative regulation of Isl1 by Nkx2-5 *in vivo*. In comparison, in control embryos Isl1 expression stayed on only in invading cardiomyocytes of both ends of the heart tube, the OFT and the sinus venosus (origin of pacemaker cells).

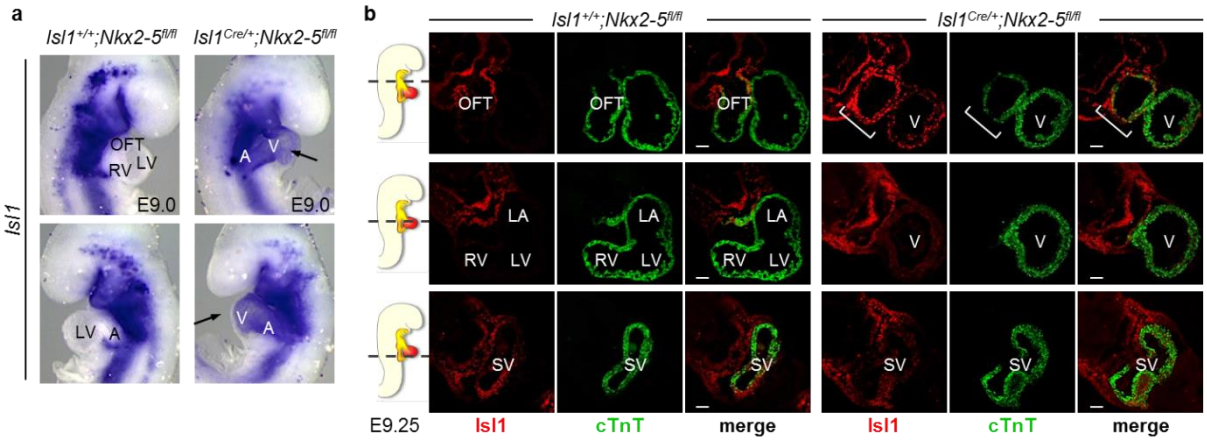

Figure 20: Persistent Isl1 expression in Nkx2-5 deficient myocytes of the forming heart.
a) Whole mount RNA *in situ* hybridization of *Isl1* in control (*Isl1*$^{+/+}$;*Nkx2-5*$^{fl/fl}$, left panels) and Nkx2-5 mutant (*Isl1*$^{Cre/+}$;*Nkx2-5*$^{fl/fl}$, right panels) embryos at E9.0. b) Perforated lines indicate positions of the transverse sections through control (left panels) and *Nkx2-5* mutant (right panels) embryos at E9.25. Immunostaining of Isl1 (red) and cTnT (green) of these sections at different positions through the embryo heart. Scale bars = 50 µm. Images are representative of three embryos per genotype. White brackets mark malformed OFT in the Nkx2-5 mutant heart. A = atria, LA = left atrium, LV = left ventricle, OFT = outflow tract, RV = right ventricle, SV = sinus venosus, V = ventricle. Adapted from Dorn, Goedel et al. 2015.

SHF progenitors of *Isl1*$^{Cre/+}$;*Nkx2-5*$^{fl/fl}$ mutants displayed lower *Isl1* transcript signal compared to control as detected by whole mount RNA ISH. This could be due to a reduced number of Isl1 expressing cells or decreased *Isl1* expression. Co-immunostaining of Isl1 and proliferation marker phosphohistone 3 (PHH3) of the transverse sections of control and *Nkx2-5* mutant embryos at E9.25 allowed detailed quantification and comparison of Isl1^{+}/PHH3^{+} cells in the foregut endoderm and SHF population (Fig. 21). This allowed evaluation whether diminished *Isl1* transcript level was due to differences in proliferation of Isl1^{+} cells. No significant differences in neither number of Isl1^{+} progenitors nor the percentage of proliferating cells (PHH3^{+} cells) within the Isl1^{+} population were observed, indicating that decreased *Isl1* transcript was probably due to reduction of *Isl1* expression in heterozygous *Isl1*$^{Cre/+}$ mice rather than to defects in proliferation (Fig. 21).

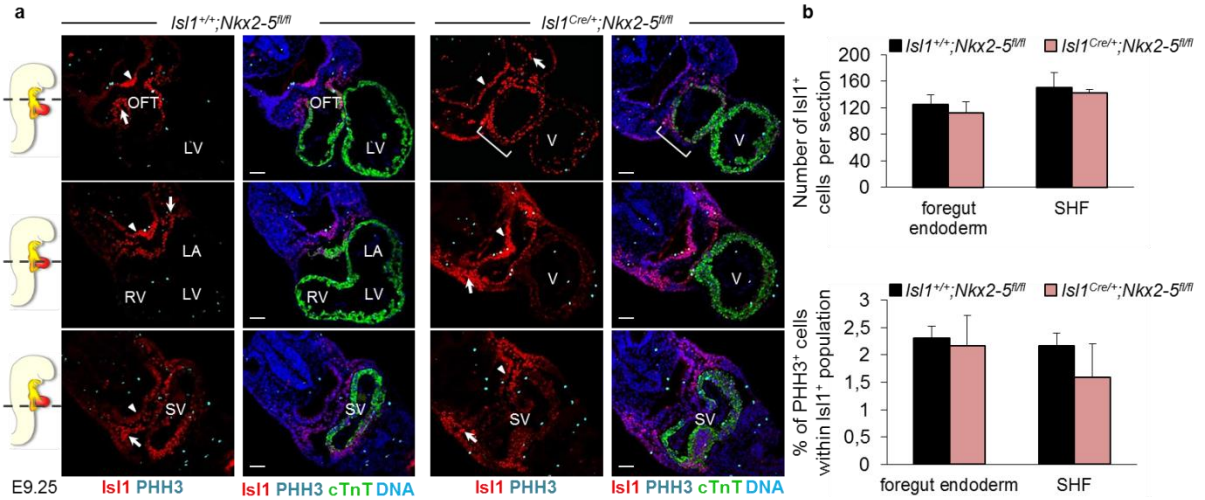

Figure 21: Unchanged proliferation of Isl1^{+} cells in the splanchnic mesoderm and foregut endoderm in *Isl1$^{Cre/+}$;Nkx2-5$^{fl/fl}$* mutants.
a) Perforated lines indicate positions of the transverse sections through control (left panels) and *Nkx2-5* mutant (right panels) embryos at E9.25. Immunostaining of Isl1 (red), phosphohistone 3 (PHH3, cyan), cTnT (green) and DNA (blue) of these sections at different positions through the embryo heart. Scale bars = 50 µm. Images are representative of three embryos per genotype. Arrows indicate splanchnic mesoderm, arrowheads indicate foregut endoderm. LA = left atrium, LV = left ventricle, OFT = outflow tract, RV = right ventricle, SV = sinus venosus, V = ventricle. b) Quantification of Isl1^{+} and Isl1^{+}/PHH3^{+} cells per section located in the foregut endoderm and SHF in control and *Nkx2-5* mutant embryos. Adapted from Dorn, Goedel et al. 2015.

Indeed, *in situ* hybridization of *Isl1$^{Cre/+}$;Nkx2-5$^{fl/fl}$* mutant and control E9.0 embryos carrying different combinations of *Isl1* and *Nkx2-5* alleles revealed that decreased *Isl1* transcript resulted from 50% reduction of *Isl1* expression in heterozygous *Isl1$^{Cre/+}$* compared to *Isl1$^{+/+}$* mice. *Isl1$^{+/+}$;Nkx2-5$^{fl/fl}$* embryos exhibited strong *Isl1* expression in the SHF population dorsally of the heart (Fig. 22). In line with that, *Isl1$^{Cre/+}$;Nkx2-5$^{+/+}$* embryos heterozygous for *Isl1* with full dosis of Nkx2-5 showed 50% reduction of *Isl1* expression in the SHF population. Heterozygous Nkx2-5 expression was enough to downregulate *Isl1* expression in the heart (*Isl1$^{Cre/+}$;Nkx2-5$^{fl/+}$*). *Isl1* expression persisted in the heart of *Isl1$^{Cre/+}$;Nkx2-5$^{fl/fl}$* mutant embryos, with lower intensity in the SHF population compared to the *Isl1$^{+/+}$;Nkx2-5$^{fl/fl}$* mice (Fig. 22).

In summary, the experiments showed that Nkx2-5-mediated negative regulation of *Isl1* transcription takes also place *in vivo*.

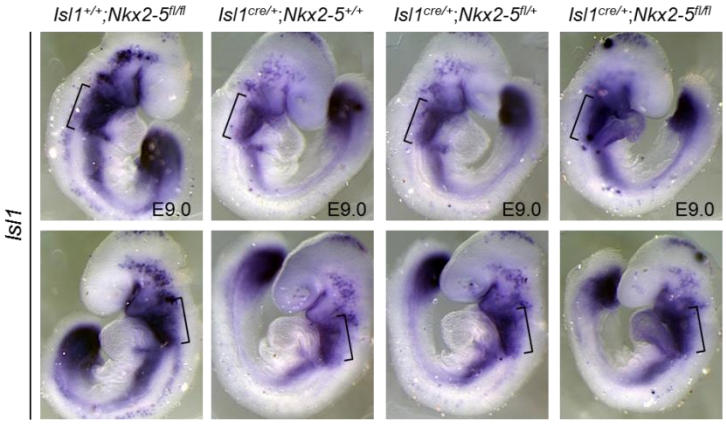

Figure 22: Isl1 dosage in mutant embryos at E9.0.
Whole mount *in situ* analysis for *Isl1* expression in E9.0 embryos in *Isl1$^{Cre/+}$;Nkx2-5$^{fl/fl}$* mutants and controls with different combinations of the genotype for *Isl1* and *Nkx2-5*. Isl1^{+} SHF progenitor population is marked by brackets. Upper panels show right; lower panels show left view of the embryos. Adapted from Dorn, Goedel et al. 2015.

3.1.4 Isl1 promotes specification of the sinoatrial node cells at the expense of the ventricular lineage

The question arose if downregulation of *Isl1* by Nkx2-5 was required for differentiation of cardiac progenitors into fully functional cardiomyocytes. To address this point, cardiac differentiation of Isl1 OE ESCs was analyzed. Functionality of cardiomyocytes was determined by appearance of spontaneous beating areas. Over time quantification of wells in

which beating areas occurred revealed not only functionality of Isl1 OE cardiomyocytes but actually earlier beating compared to the GFP control cardiomyocytes (Fig. 23a). Immunostaining of whole EBs for cTnT demonstrated even larger $cTnT^+$ areas in the Isl1 OE line compared to the GFP control line at 14 days of differentiation (Fig. 23b). Immunofluorescence analysis in cardiomyocytes from dissociated EBs showed normal striated pattern of sarcomeric proteins alpha-actinin, which marks the Z-disk and cTnT, labeling the A-band (Fig. 23c+d). Quantification of $cTnT^+$ cells per EB confirmed significantly more $cTnT^+$ cells in the Isl1 OE line than in the GFP control line, probably due to the enhanced Isl1 progenitor specification (Fig. 23e). Interestingly, a significantly higher beating frequency was detected in Isl1 OE cardiomyocytes compared to GFP control, which is typical for nodal cells, a subtype of cardiomyocytes besides cells of the working myocardium (Fig. 23f). This finding is in accordance with the upregulation of *Hcn4* a nodal specific ion channel gene shown by gene expression analysis (Fig. 15).

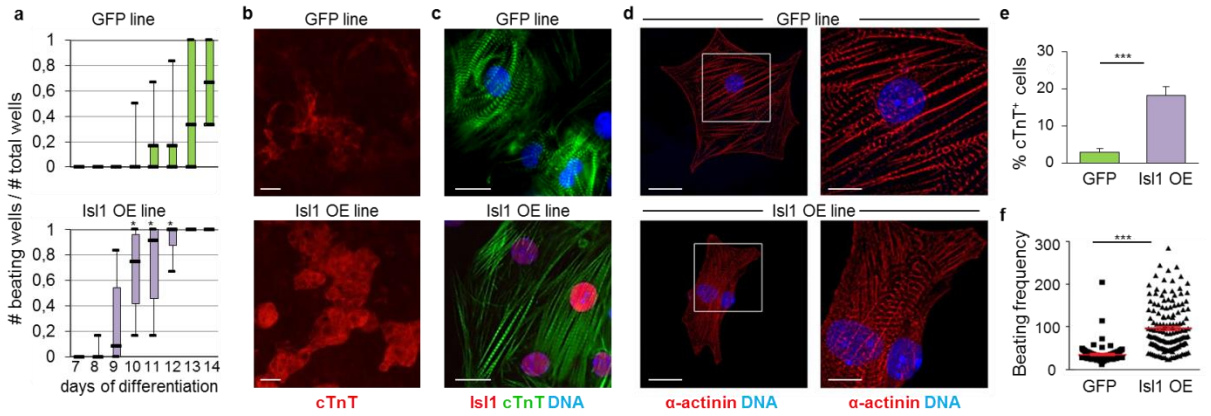

Figure 23: Isl1 overexpression does not prevent differentiation into functional cardiomyocytes.
a) Quantification of beating, functional cardiomyocytes between 7 and 14 days of EB differentiation of GFP control (green) and Isl1 OE (purple) ESC line. Mean values, first and third quartiles, minimal and maximal values are shown of five experiments. * = p-value <0.05 vs. GFP line. b) GFP control (upper panel) and Isl1 OE (lower panel) 14-day old EBs stained for cTnT (red). Scale bars = 100 µm. c) Immunostaining of Isl1 (red), cTnT (green) and DNA (blue) in GFP and Isl1 OE cardiomyocytes. Scale bars = 15 µm. d) Immunostaining of sarcomeric proteins alpha-actinin and cTnT (red) and DNA (blue) in GFP control (upper panels) and Isl1 OE (lower panels) single cardiomyocytes. Scale bars = 25 µm. The boxed region is shown in higher magnification on the right side. Scale bars = 10 µm. e) FACS-based quantification of $cTnT^+$ cells in GFP control (green) and Isl1 OE (purple) cells after 14 days of differentiation. Mean values ± SEM from eight experiments. *** = p-value <0.001 vs. GFP. f) Analysis of beating frequency in GFP control (squares) and Isl1 OE (triangles) 14-day old EBs. Mean values ± SEM from six to seven experiments. n = 170 (GFP) and n = 150 (Isl1 OE). *** = p-value <0.001 vs. GFP. Adapted from Dorn, Goedel et al. 2015.

To test if Isl1 regulates cardiomyocyte subtype specification, several myocyte subtype-specific genes encoding ion channel subunits and transcription factors in nodal and working myocardium were analyzed in GFP control and Isl1 OE cardiomyocytes at different maturation stages (14 and 21 days) by qRT-PCR analysis (Fig. 24). Interestingly, many genes important for development and function of SAN cells were significantly upregulated in the Isl1 OE cells in comparison to the GFP control. These encompassed genes encoding

channel subunits generating pacemaker-specific currents, such as the hyperpolarization-activated cyclic nucleotide-gated channels *Hcn1* and *Hcn4* (Shi, Wymore et al. 1999, Schram, Pourrier et al. 2002), the T-Type Ca^{2+} channel subunit Cav3.1 (*Cacna1g*) (Bohn, Moosmang et al. 2000) as well as the transcription factor Tbx2, crucial for the sinus atrial node (SAN) formation (Habets, Moorman et al. 2002, Christoffels, Hoogaars et al. 2004). Gap junction proteins play an important role in transmission of electrical impulses in the heart. Isl1 OE cells showed elevated levels of Cx45 (*Gjc1*) and Cx29 (*Gjd3*), which are transmembrane proteins belonging to the connexin family, forming gap junctions specifically in the SAN and AVN (atrioventricular node) pacemaker cells. At the same time, Isl1 OE cells failed to upregulate working myocardium markers, such as ventricular specific isoform of myosin light chain 2 (*Myl2*) (O'Brien, Lee et al. 1993, Ng, Wong et al. 2010), transcription factors regulating chamber specification (*Hey1*, *Hey2*, *Irx4*, *Nppa*) (Bao, Bruneau et al. 1999, Houweling, van Borren et al. 2005, Kokubo, Tomita-Miyagawa et al. 2007) and working myocardium specific connexins Cx43 (*Gja1*) (Jansen, van Veen et al. 2010) and Cx40 (*Gja5*) (Jansen, van Veen et al. 2010). Additionally, the cardiac sodium channel Nav1.5 (*Scn5a*) was also downregulated, which is expressed in working myocardium and conduction tissue, but not in SAN and AVN cells. Interestingly, the atrial isoform of myosin light chain 2 (*Myl7*), which is generally expressed in the heart during early embryonic development (Gittenberger-de Groot, Mahtab et al. 2007), was upregulated in Isl1 OE cells. At later embryonic stages, *Myl7* gets specifically expressed in atrial and SAN myocytes (Gittenberger-de Groot, Mahtab et al. 2007), suggesting further that maintained *Isl1* expression might shift differentiation of cardiac progenitors into the nodal fate at the expense of the working myocardium.

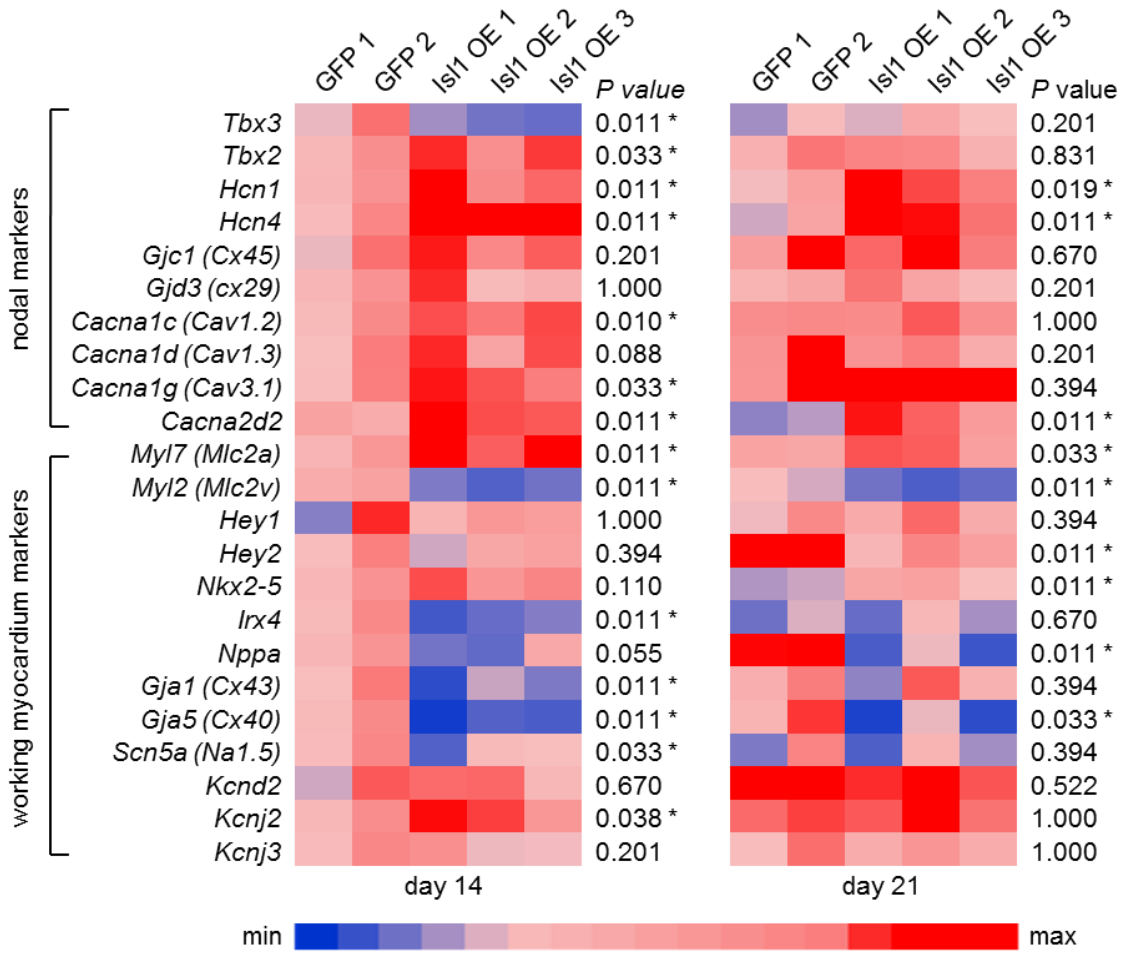

Figure 24: Isl1 overexpression promotes expression of nodal markers at the expense of the working myocardium markers.
qRT-PCR analysis of nodal and working myocardium markers in GFP control and Isl1 OE EBs at day 14 and day 21. All values were normalized to *Gapdh* and relative to the mean expression level of GFP control cells from both experiments at day 14. p-values were calculated using the Mann-Whitney test. Two to three independent experiments. * = p-value <0.05 vs. GFP. Minimum (min) and maximum (max) values were used as reference for heat map representation. Adapted from Dorn, Goedel et al. 2015.

Furthermore, to test if also on protein level, a shift from working myocardial cells such as ventricular and atrial cardiomyocytes towards the nodal lineage could be detected, immunofluorescence analysis of 1-month old cardiomyocytes generated *via* EB differentiation using antibodies against ventricular (Mlc2v), atrial (Mlc2a) and nodal (Hcn4) specific proteins was performed (Fig. 25).

In control conditions cells expressing Mlc2a (40±4%) and Mlc2v (43±3%) were observed at similar percentages (Fig. 25a+b). A smaller population of immature, ventricular myocytes expressed both markers (17±2%) (Fig. 25a+b). In controls, a population of 14±2% within the Mlc2a$^+$ cells also expressed Hcn4, representing the nodal subtype. Hcn4 was never found to be co-expressed with Mlc2v. In Isl1 OE cardiomyocytes, a radical reduction of the Mlc2v$^+$ and Mlc2a$^+$/2v$^+$ populations (both 6±1%) compared to the GFP control line (43±3% and 17±2%,

respectively) was detected. Interestingly, a significant increase of Mlc2a-expressing cells (88±2% in Isl1 OE cells versus 40±4% in control), as well as of $Hcn4^+$ myocytes within the $Mlc2a^+$ subpopulation (38±2% in Isl1 OE versus 14±2% in control cells) was determined in the Isl1 OE line. These results were consistent with those obtained with qRT-PCR analysis and indicated a shift in specification from the working myocardium towards the nodal lineage, suggesting a possible function of Isl1 in controlling myocardial subtype specification by repressing the ventricular and promoting the nodal gene program.

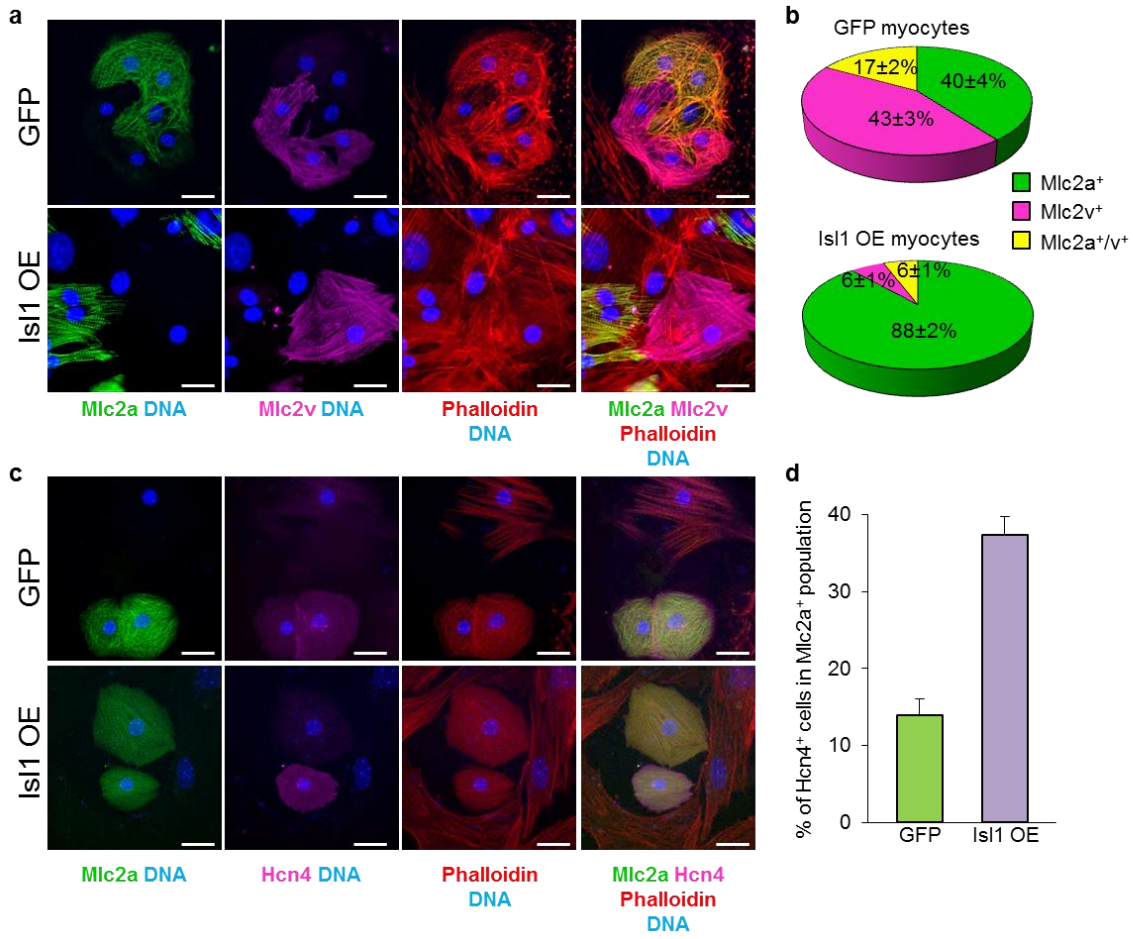

Figure 25: Isl1 overexpression favors specification into $Mlc2a^+/Hcn4^+$ nodal cardiomyocyte subtype.
a) Representative images of GFP control (upper panels) and Isl1 OE (lower panels) single cardiomyocytes at 1-month of differentiation after immunostaining for atrial (Mlc2a, green) and ventricular (Mlc2v, magenta) specific isoforms of myosin light chain 2 (Mlc2), F-actin visualized by Phalloidin (red) and DNA (blue). Scale bars = 25 µm. b) Quantification of Mlc2a (green), Mlc2v (magenta) and Mlc2a/v (yellow) positive myocytes. Mean values ± SEM. n = 189 (GFP) and n = 535 (Isl1 OE) from five to six independent experiments. c) Immunofluorescence analysis of Mlc2a (green), Hcn4 (magenta) and F-actin visualized by Phalloidin (red) in single cardiomyocytes at 1-month of differentiation. Scale bars = 25 µm. d) Quantification of $Hcn4^+$ cells within the $Mlc2a^+$ fraction from GFP control and Isl1 OE myocytes. Mean values ± SEM. n = 86 (GFP) and n = 83 (Isl1 OE) from two to three independent experiments. Adapted from Dorn, Goedel et al. 2015.

Moreover, this observation was further confirmed by the analysis of the electrophysiological properties of Isl1 OE and GFP control myocytes. Cardiomyocyte subtypes can be distinguished by characteristic electrophysiological properties, due to subtype specific channel expression. A high throughput technique with a voltage sensitive fluorescent probe

di8-ANEPPS, which allows optical imaging of APs, was used (Fig. 26a). APs of ventricular cells show a typical long plateau phase (Wobus, Rohwedel et al. 1995). To the contrary, APs of atrial cells have a more triangular shape (Wobus, Rohwedel et al. 1995). Measuring the AP duration at 50% (APD50) and 90% (APD90) of repolarization allowed for distinguishing atrial and ventricular APs based on the APD90/50 ratio. APs with an APD90/50 ratio 1.2 to 1.9 were classified as ventricular-like; APs with a value of more than 2.5 were categorized as atrial-like. The special characteristic of pacemaker cells is the lack of a stable resting potential during diastole and the transient positive inward potassium and sodium current (funny current) mediated through Hcn4 channels during diastolic depolarization (Wobus, Rohwedel et al. 1995). Blocking the Hcn4-channels with 30 µM ivabradine (Bucchi, Tognati et al. 2006) helped to determine SAN APs (Fig. 26b).

Using these parameters it was possible to identify 53±2% ventricular, 20±5% nodal, 7±2% atrial, and 20±5% intermediate cells with a ventricular-atrial mixed AP shape in 1-month old spontaneously beating GFP control cardiomyocytes (Fig. 26c). Importantly, a strong reduction in cells showing ventricular-like APs was detected in Isl1 OE cardiomyocytes (14±3% in Isl1 OE vs. 53±2% in control myocytes), whereas similar percentages of atrial-like APs and “intermediate” APs were recorded (11±2% and 20±6%, respectively). In 55±7% of the cells the pacemaker current was blocked completely by 30 µM ivabradine, supporting the hypothesis of enhanced differentiation into the nodal lineage by Isl1 overexpression. An Isl1-mediated upregulation of Hcn channels could be excluded by comparison of the amount of funny current in control and Isl1 OE pacemaker cells after blocking 60% of funny current channels, by analyzing the changes in the slope of the diastolic depolarization and beating frequency, indicating a similar amount of Hcn channels in the nodal cells of both lines (Fig. 26d) (Baruscotti, Barbuti et al. 2010).

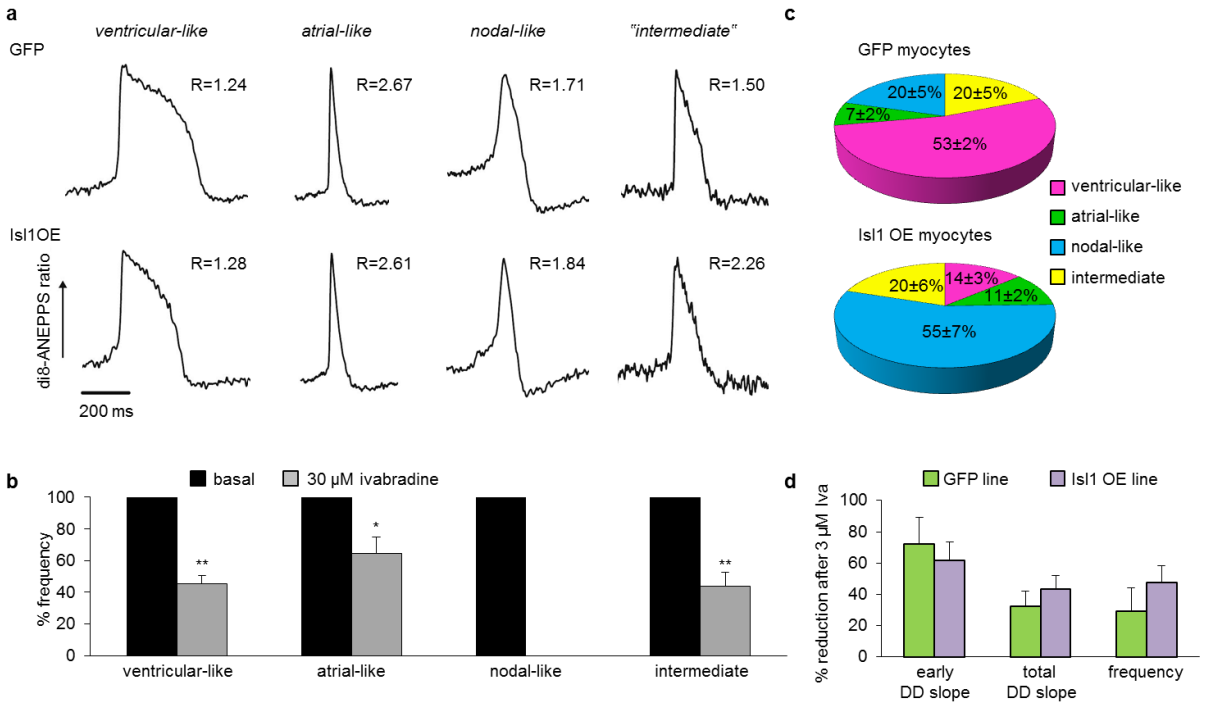

Figure 26: Isl1 overexpression directs cardiomyocyte subtype specification into electrophysiologically functional pacemaker cells.
a) Representative traces of action potentials (APs) and corresponding APD90/50 ratios (R) of 1-month old ventricular- atrial-, nodal-like and intermediate GFP control and Isl1 OE cardiomyocytes, as determined by optical action potential imaging using di8-ANEPPS. b) Quantification of AP frequency of cardiomyocyte subtypes before (basal) and after treatment with 30 µM of selective Hcn channel blocker ivabradine. * = p-value <0.05 and ** = p-value <0.01 vs. basal value. c) Quantification of 1-month old ventricular-, atrial-, nodal-like and intermediate cardiomyocytes from GFP control and Isl1 OE line based on the AP traces identified by optical imaging and the response to ivabradine treatment. Mean values ± SEM. n = 122 (GFP) and n = 65 (Isl1 OE) from three independent experiments. d) Percentage of reduction of early and total DD slope as well as AP frequency in nodal cardiomyocytes of 1-month old myocytes from GFP control and Isl1 OE cell line after treatment with 3 µM ivabradine. DD = diastolic depolarization, Iva = ivabradine. Adapted from Dorn, Goedel et al. 2015.

Taken together, overexpression experiments *in vitro* suggested that Isl1 was negatively regulated by Nkx2-5. This regulation was mediated through direct binding of Nkx2-5 to the *Isl1* enhancer. Embryos lacking Nkx2-5 in Isl1-expressing cells failed to downregulate Isl1 in cardiomyocytes of the developing heart, demonstrating biological significance of Nkx2-5-mediated Isl1 repression *in vivo*. *Isl1* overexpression *in vitro* did not inhibit cardiomyocyte differentiation. Contrariwise, maintained Isl1 expression enhanced progenitor specification. Furthermore, Isl1 regulation was required for cardiomyocyte subtype specification, since Isl1 OE cells exhibited increased specification potential into the nodal cardiomyocyte subtype on the RNA, protein and functional level.

In summary, these data revealed an Nkx2-5-mediated mechanism regulating Isl1 expression, which is critical during SHF lineage specification and acquisition of cardiomyocyte subtype identity.

3.2 Common developmental origin of cardiac myocytes and epicardial fat

Investigation of the developmental origin of EAT was challenging so far, since mice and other experimental traceable animals were thought to not have this tissue. The adipose tissue seen in rodents was thought to be non-cardiac, thoracic (paracardial) fat only, which therefore, has sometimes been mischaracterized as EAT (Yamaguchi, Cavallero et al. 2015). Recent studies identified the fat tissue between the atrium and ventricle, in the so called atrioventricular groove (AV groove), as epicardial fat in the mouse (Fig. 27). This tissue appears 2 weeks after birth and increases with age (Chau, Bandiera et al. 2014, Liu, Huang et al. 2014, Yamaguchi, Cavallero et al. 2015).

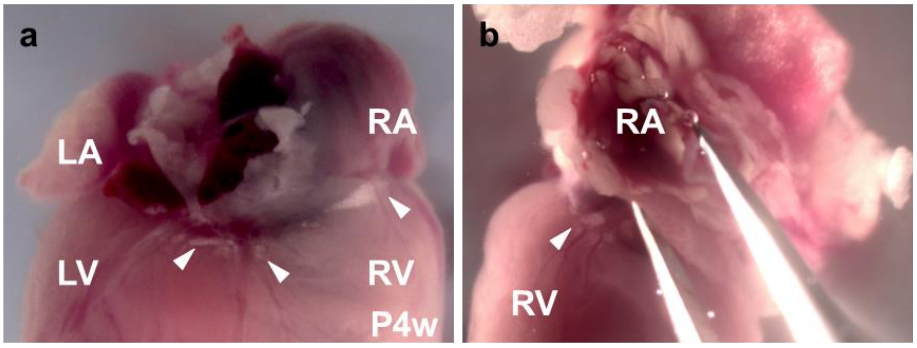

Figure 27: EAT in the AV groove of a 4-week old adult mouse.
a) The dorsal surface of the heart. Cardiac fat is limited in the atrioventricular groove in close proximity to the coronary vessels. b) Fat depot underneath the right atrium. Arrows indicate EAT, LA = left atrium, LV = left ventricle, RA = right atrium, RV = right ventricle, P4w = 4 weeks postnatally.

In the human heart, additional to the AV groove, the epicardial fat is located sub-epicardially in the free walls of the atria. As soon as the amount of fat tissue increases, it progressively fills the space between the ventricles, sometimes covering the entire epicardial surface.

The ratio of fat to myocardium weight for the right ventricle is more than three times that of the left ventricle (Iacobellis, Corradi et al. 2005). This imbalance of fat distribution in the right and left ventricle is also seen in diseased hearts of arrhythmogenic right ventricular cardiomyopathy (ARVC) patients, which is characterized by fibro-fatty replacement mainly of the right ventricle. So far, the cause of the predominant involvement of right ventricle myocytes, the mechanism responsible for their substitution by adipocytes and the cellular source of these pathological adipocytes are unknown (Lombardi, Dong et al. 2009). They can either differentiate from progenitors, which favor the adipocytic lineage in the diseased setting or transdifferentiate from already existing mature cells such as cardiomyocytes. In both settings a close developmental relationship seems to facilitate the differentiation into

adipocytes. Based on the finding of intracytoplasmatic lipid-droplets in cardiomyocytes in an ARVC patient a possible transdifferentiation of adult cardiomyocytes into adipocytes was proposed (d'Amati, di Gioia et al. 2000). Another study performing genetic fate mapping for Nkx2-5, an early and pan-specific cardiogenic marker, and Mef2C, a SHF specific marker, suggests SHF progenitors as a source of excess adipocytes in ARVC (Lombardi, Dong et al. 2009). These observations led to an assumption that a SHF progenitor forming mainly the right ventricle could be a candidate for a possible common precursor of right ventricle myocytes and epicardial adipocytes.

3.2.1 Cardiac muscle and fat derive from Isl1^{+} progenitors *in vivo*

The right ventricle myocytes derive from SHF progenitors, expressing the LIM homeodomain transcription factor Isl1. To investigate whether cardiac fat derives from a SHF progenitor, Isl1 lineage tracing was performed. Therefore, mice expressing heterozygous Cre recombinase under the *Isl1* promoter were crossed with reporter mice homozygous for a double fluorescence cassette in the *Rosa26* locus. In the offspring, the ubiquitous N-terminal membrane-tagged, tandem dimer Tomato (mT)-mediated red fluorescence switches into N-terminal membrane-tagged, EGFP (mG)-mediated green fluorescence after expression of Cre recombinase (Fig. 28). The recombined cells and their derivatives are marked irreversibly by mG, thus allowing for tracing Isl1 expressing cells (Muzumdar, Tasic et al. 2007).

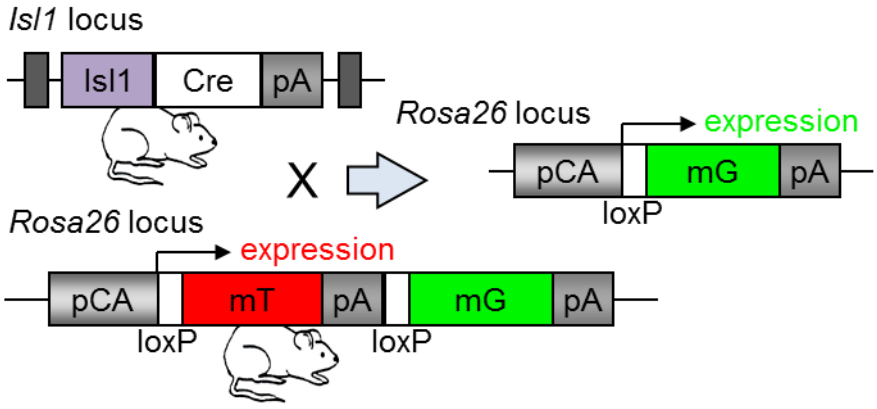

Figure 28: Schematic diagram of the crossing strategy.
Isl1-Cre mice were intercrossed with double fluorescent mTmG reporter mice. The mTmG construct is expressed in the *Rosa26* locus and consists of a chicken ß-actin core promotor with a CMV enhancer (pCA) driving a loxP-flanked coding sequence of N-terminal membrane-tagged, tandem dimer Tomato (mT). Expression of Cre recombinase excises the mT sequence to irreversibly activate N-terminal membrane-tagged, enhanced green fluorescent protein (mG) expression. pA = polyadenylation sequence.

Mice at 4 weeks of age show an adequate amount of cardiac fat tissue that can be examined. Sections of *Isl1*$^{Cre/+}$;*R26*$^{mTmG/+}$ mouse hearts displayed, highly efficient mG marking of myocytes of the right ventricle and a proportion of myocytes of the left ventricle and atria (Fig. 29). AV groove adipocytes were analyzed using the marker perilipin1 (Plin1), a protein present in lipid vacuoles of mature adipocytes. Inspection of the AV groove adipocytes revealed nearly complete co-localization of Plin1^{+} cells with the lineage marker (Fig. 29), indicating that Isl1^{+} precursors give rise to EAT.

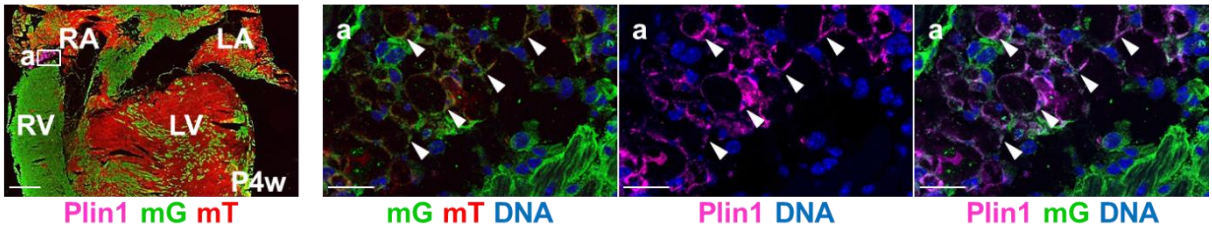

Figure 29: Isl1-Cre mediated mG marking of the adult mouse heart and EAT.
Immunohistological staining of heart sections of *Isl1*$^{Cre/+}$;*R26*$^{mTmG/+}$mice at 4 weeks show Isl1-Cre mediated mG (green) marking of the right ventricle and parts of the left ventricle and both atria. Perilipin1 (Plin1) marks adipocytes of the EAT between the right atrium and the right ventricle. LA = left atrium, LV = left ventricle, RA = right atrium, RV = right ventricle, P4w = 4 weeks postnatally. Scale bar = 500 µm. a) Higher magnification of the boxed region. Recombined mG positive cells do not express mT anymore. Plin1 marks lipid vacuoles of mature adipocytes of the EAT. The merge shows that membranes of Plin1^{+} adipocytes are labeled by mG. Arrows indicate Plin1^{+}/mG^{+} adipocytes. DNA (blue). Scale bars = 25 µm. Adapted from Dorn, Kornherr et al. 2018.

3.2.2 Isl1^{+}/Wt1^{+} proepicardial precursors exist at E8

Recent studies demonstrated that epicardial fat originates from the Wt1 and Tbx18 expressing embryonic epicardial progenitors (Chau, Bandiera et al. 2014, Liu, Huang et al. 2014, Yamaguchi, Cavallero et al. 2015). These cells arise from a transient structure, the so called PEO between E9.5 and E10.5 of mouse development. This organ merges at the caudal side of the heart and dissolves within the next day due to migration of the epicardial progenitors over the forming heart. While it is known that Wt1^{+} PEO cells give rise to epicardial fat, it is still controversial if cardiomyocytes can also originate from proepicardial cells (Wessels, van den Hoff et al. 2012). Isl1^{+} progenitors, which can differentiate into cardiomyocytes, arise early in development between E6 and E9 (Sun, Liang et al. 2007). A study performing Isl1 lineage tracing with *R26*^{fsLacZ}, a robustly recombining reporter, identified a subpopulation of Isl1^{+} SHF progenitors contributing to the Wt1 expressing PEO in addition to large parts of the myocardium including the left ventricle (Zhou, von Gise et al. 2008). Confirming these results, *Isl1*$^{Cre/+}$;*R26*$^{mTmG/+}$ embryos at E9.5 showed mG marking of the PEO (Fig. 30a+b). Detailed immunofluorescence analysis for Isl1 and Wt1 in the PEO of the Isl1-Cre lineage traced embryos at E9.5 showed expression of the lineage marker mG in a significant proportion of Wt1^{+} cells and a complete absence of Isl1 expression throughout the

tissue, demonstrating that a subset of Wt1^{+} proepicardial cells arises from Isl1^{+} progenitors, which turn off Isl1 expression at the stage of the PEO (Fig. 30c-e).

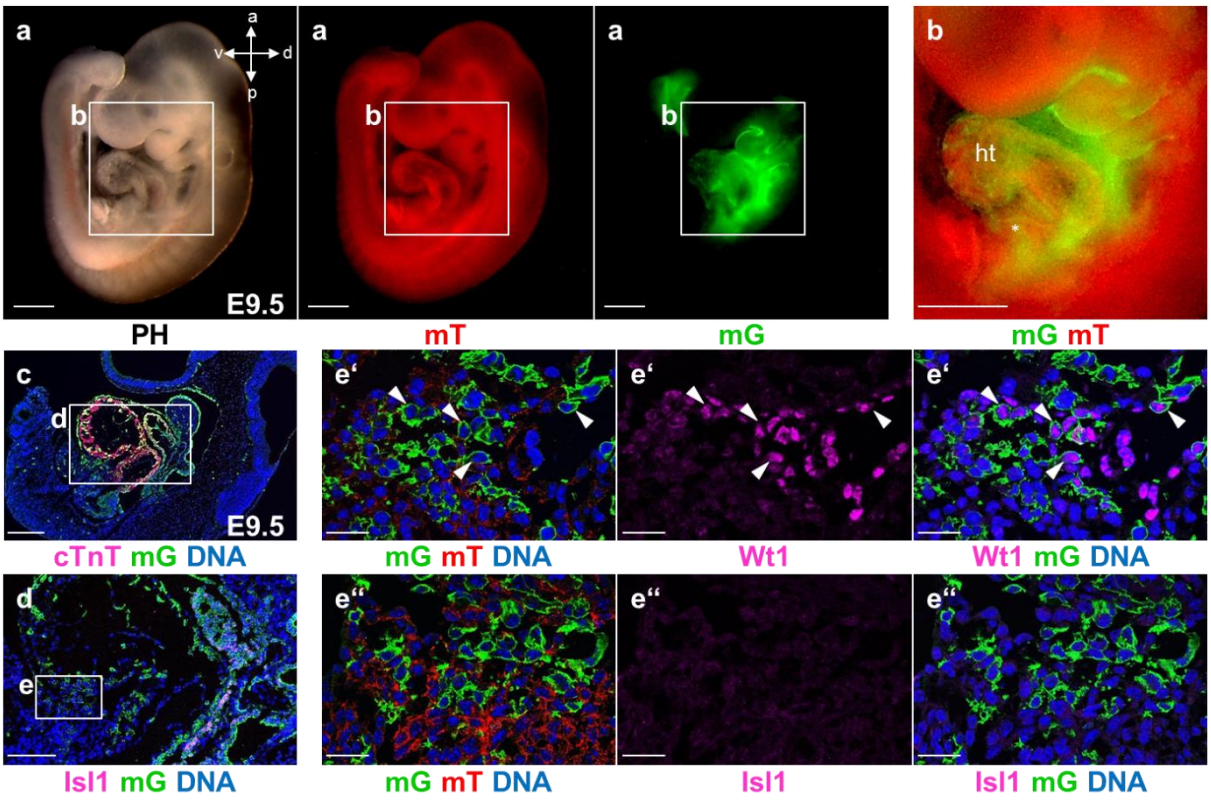

Figure 30: Proepicardium arises from Isl1^{+} progenitors.
a) Left view of an *Isl1*$^{Cre/+}$;*R26*$^{mTmG/+}$ embryo at E9.5 in phase-contrast (PH) and fluorescent microscopy. mT (red) expression is substituted through mG (green) expression in recombined cells. b) Magnified view of the boxed region in a. Proepicardium (asterix) is partially marked by mG (green) expression. ht = heart. Scale bars = 1 mm. c-e) Immunofluorescence staining of sagital sections of an E9.5 embryo. c) Cardiac Troponin T (cTnT, magenta) marks cardiomyocytes of the forming heart. Isl1 derivatives are marked by mG. The PEO is located at the caudal base in the atrioventricular junction of the developing heart. The boxed region is shown in higher magnification in d. Scale bar = 250 µm. d) Immunofluorescence staining showing absence of Isl1 in the PEO, which is boxed and labeled with e. Scale bar = 150 µm. e') Higher magnification of the region boxed in d. Wt1^{+} epicardial progenitors in the PEO are marked by mG. e'') Higher magnification of d shows complete absence of Isl1 trough out the tissue. Scale bars = 25 µm. Adapted from Dorn, Kornherr et al. 2018.

Analysis of the expression pattern of Isl1 and Wt1 at developmental stages preceding the PEO, led us to identification of an Isl1^{+}/Wt1^{+} cell population at E8.

This population is very transient and small in number of cells and is located at the anterior lateral mesoderm, on the caudal side of the forming heart (Fig. 31).

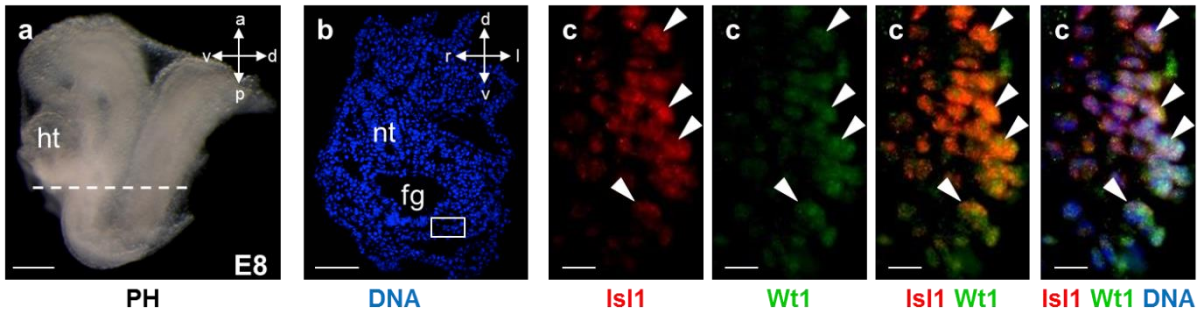

Figure 31: Isl1^{+}/Wt1^{+} progenitors at E8.
a) Left view of an E8 wildtype embryo in phase-contrast (PH) microscopy. Dashed line indicates position of the following transverse sections (b+c). Isl1^{+}/Wt1^{+} in mouse embryo at E8 are located at the caudal site of the heart (ht). ht = heart. Scale bar = 1 mm. b) Framed region defines the localization of proepicardial precursors at the lateral, anterior region of the embryo. nt = neural tube, fg = foregut. Scale bar = 200 µm. c) Magnified view of the white box in b of immunostaining of Isl1 (red), Wt1 (green) and DNA (blue) shows co-expression of Isl1^{+}/Wt1^{+} (white arrows). Scale bars = 10 µm. Adapted from Dorn, Kornherr et al. 2018.

To trace this transient population temporal-specific lineage tracing was performed using inducible *Isl1*$^{MerCreMer/+}$ and *Wt1*$^{CreERT2/+}$*;R26*$^{mTmG/+}$ mice, in which Cre recombinase is expressed as a fusion protein with mutated estrogen receptors. The mutated estrogen receptors prevent Cre delivery to the nucleus by binding to chaperones in the cytoplasm. A single tamoxifen injection allows disruption of this binding and translocation of the protein into the nucleus and thus activation of Cre.

The half-life of tamoxifen in the serum of mice is 11.9 hours (Robinson, Langan-Fahey et al. 1991). Therefore, tamoxifen was injected at E7.5, in both *Isl1*$^{MerCreMer/+}$ and *Wt1*$^{CreERT2/+}$ pregnant mothers to track the Isl1^{+}/Wt1^{+} population at E8. It was shown that tamoxifen activity, measured by Cre translocation into the nucleus, persists over a time period of 24 h, depending on the concentration (Hayashi and McMahon 2002). Since tamoxifen is toxic to early embryos, a low concentration (75 mg/kg bodyweight) was used to induce Cre activity. Few cells only were marked in the *Isl1*$^{MerCreMer/+}$*;R26*$^{mTmG/+}$ and *Wt1*$^{CreERT2/+}$*;R26*$^{mTmG/+}$ inducible lines. Tamoxifen injection in *Isl1*$^{MerCreMer/+}$*;R26*$^{mTmG/+}$ embryos at E7.5 resulted in mG labeling of epicardial cells arising from migrating proepicardial precursors (Fig. 32a+b). Immunohistochemical analysis of *Wt1*$^{CreERT2/+}$*;R26*$^{mTmG/+}$ embryos at E9.5 demonstrated that a subset of the Wt1^{+} cells in the PEO expressed the lineage tracing marker mG, when tamoxifen was injected at E7.5 (Fig. 32c+d).

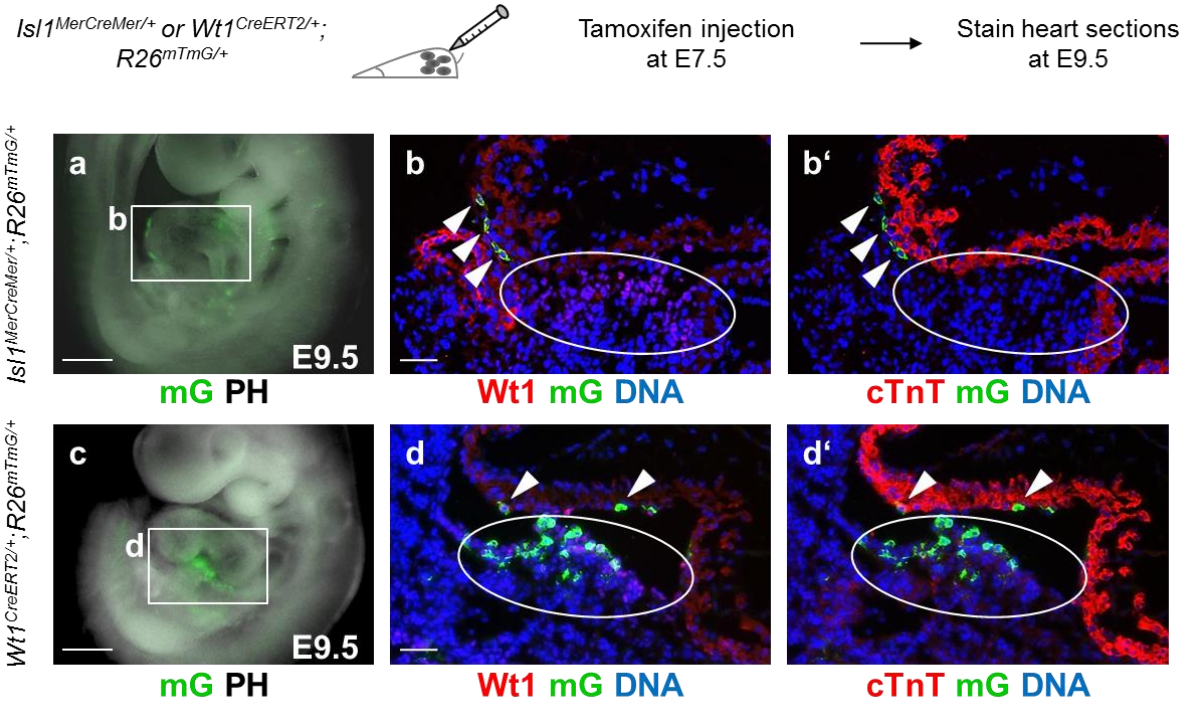

Figure 32: Inducible lineage tracing of Isl1 and Wt1 progenitors at E7.5.
An experimental scheme of labeling of Isl1^{+} and Wt1^{+} progenitors and their derivatives at E7.5 using tamoxifen-inducible *Isl1*$^{MerCreMer/+}$;*R26*$^{mTmG/+}$ and *Wt1*$^{CreERT2/+}$;*R26*$^{mTmG/+}$ mouse lines and their analysis at E9.5. Left view of an *Isl1*$^{MerCreMer/+}$;*R26*$^{mTmG/+}$ (a) and a *Wt1*$^{CreERT2/+}$;*R26*$^{mTmG/+}$ (c) embryo at E9.5. Merged image of mG (green) and phase contrast (PH). Region of the PEO is shown in the box b and d. Scale bars = 1 mm. b and d) Sagittal section of the region boxed in a and c. Immunostaining of Wt1 (red) or cTnT (red), mG (green) and DNA (blue) in sections of an *Isl1*$^{Cre/+}$;*R26*$^{mTmG/+}$ (a+b) and *Wt1*$^{CreERT2/+}$;*R26*$^{mTmG/+}$ (c+d) mouse embryo at E9.5 with tamoxifen treatment at E7.5. Expression of mG was observed in epicardial cells of both lineage traced embryos (arrows). Wt1 expression marks the PEO (white circle). Scale bars = 50 µm.

Comparison of mG marking in *Isl1*$^{Cre/+}$;*R26*$^{mTmG/+}$ (Fig. 30) and *Isl1*$^{MerCreMer/+}$;*R26*$^{mTmG/+}$ embryos at E9.5, in which tamoxifen was injected at E7.5 (Fig. 32a+b), a time point where most of SHF Isl1^{+} progenitors exist, pointed to different recombination efficiencies in the constitutive and inducible mouse lines. *Isl1*$^{MerCreMer/+}$;*R26*$^{mTmG/+}$ embryos revealed very rare recombination events (Fig. 32a+b). Confirming these findings, only few mG^{+} cells clusters, predominantly localized in the right ventricle, could be found in the hearts of inducible *Isl1*$^{MerCreMer/+}$;*R26*$^{mTmG/+}$ mice at the adult stage, indicating a nearly clonal mG marking (Fig. 33 left panel). In contrast, constitutive *Isl1*$^{Cre/+}$;*R26*$^{mTmG/+}$ mice demonstrated efficient mG labeling of Isl1 expressing progenitors and their derivatives at embryonic and adult stages (Fig. 30+33 right panel).

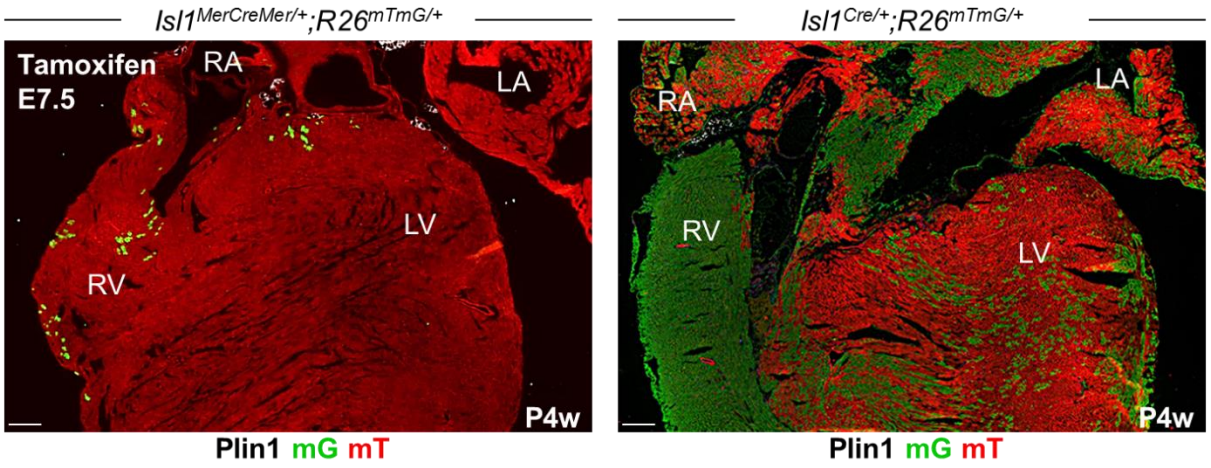

Figure 33: Low recombination efficiency reveals nearly clonal mG marking in adult mouse hearts of inducible lineage traced mice.
Comparison of inducible Isl1-MerCreMer and constitutive Isl1-Cre mediated recombination efficiency demonstrated very low mG marking with tamoxifen induction at E7.5, although most of Isl1 expressing progenitors exist at this developmental stage. Immunostaining of Plin1 (white), mG (green) and mT (red). Labeling of the heart chambers: RA = right atrium, RV = right ventricle, LA = left atrium, LV = left ventricle. P4w = 4 weeks postnatally. Scale bars = 300 µm. Adapted from Dorn, Kornherr et al. 2018.

Immunohistological analysis of the hearts of *Isl1*$^{MerCreMer/+}$;*R26*$^{mTmG/+}$ and *Wt1*$^{CreERT2/+}$;*R26*$^{mTmG/+}$ adult mice, tamoxifen-induced at E7.5, demonstrated mG marking of both, cTnT^{+} cardiomyocytes and Plin1^{+} epicardial adipocytes (Fig. 34). There were less mG^{+} cell clusters of cardiomyocytes per heart in the *Wt1*$^{CreERT2/+}$;*R26*$^{mTmG/+}$ than in the *Isl1*$^{MerCreMer/+}$;*R26*$^{mTmG/+}$ lineage, whereas the amount of mG^{+} adipocytes was higher in the *Wt1*$^{CreERT2/+}$;*R26*$^{mTmG/+}$ reporter line. As stated above, the low recombination efficiency in the inducible lines allowed a nearly clonal analysis, and the finding that cardiomyocytes at the same time as adipocytes were marked with this approach strengthens the hypothesis of a common Isl1 and Wt1 expressing proepicardial precursor at E8.

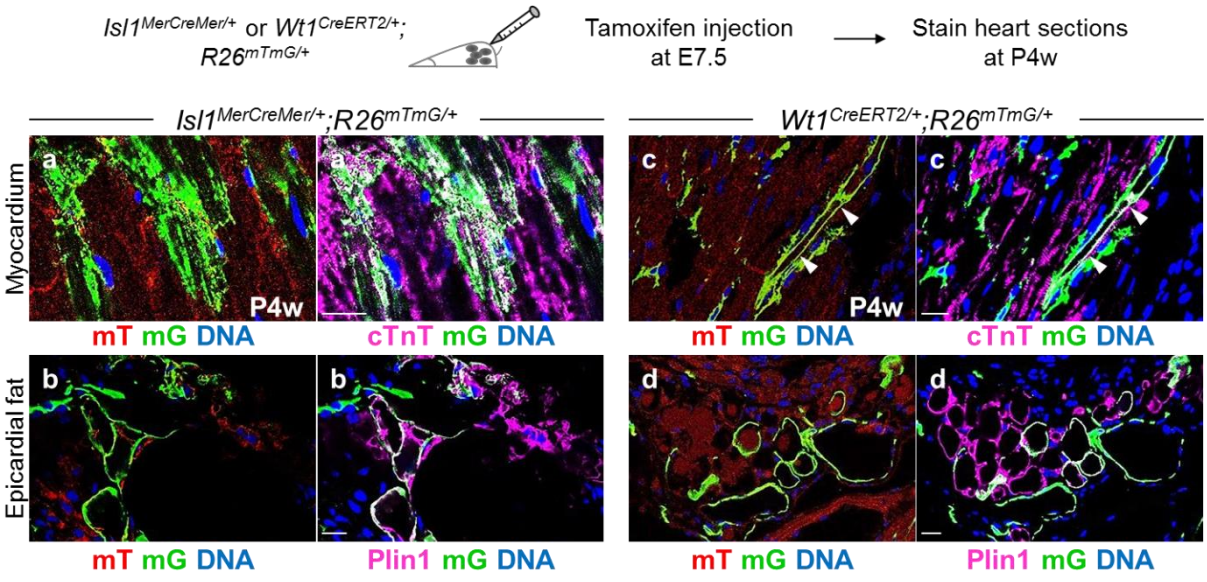

Figure 34: Isl1 and Wt1 inducible lineage tracing at E7.5 marks cardiomyocytes and adipocytes in the adult mouse.
An experimental scheme of labeling of Isl1^{+} and Wt1^{+} progenitors and their derivatives at E7.5 using tamoxifen-inducible *Isl1*$^{MerCreMer/+}$;*R26*$^{mTmG/+}$ and *Wt1*$^{CreERT2/+}$;*R26*$^{mTmG/+}$ mouse lines and their analysis at P4w. a-d) Immunostaining of cTnT (magenta) or Plin1 (magenta), mG (green), mT (red) and DNA (blue) in sections of an *Isl1*$^{Cre/+}$;*R26*$^{mTmG/+}$ (a+b) and *Wt1*$^{CreERT2/+}$;*R26*$^{mTmG/+}$ (c+d) adult mouse at P4w with tamoxifen treatment at E7.5. Expression of mG was observed in cardiomyocytes marked by cTnT (a+c) and epicardial adipocytes positive for Plin1 (b+d). Arrows indicate cTnT^{+}/mG^{+} cardiomyocytes. Scale bars = 25 µm. Adapted from Dorn, Kornherr et al. 2018.

As mentioned before, the Wt1^{+} PEO cell population gives rise to the epicardium (Moore, McInnes et al. 1999). During development a subpopulation of epicardial cells undergoes EMT and contributes to coronary smooth muscle cells and intramyocardial fibroblasts (Katz, Singh et al. 2012). Co-expression with mG, alpha-smooth muscle actin or vimentin confirmed that with tamoxifen injection at E7.5 true Wt1^{+} proepicardial precursors prior to the development of the PEO were marked, giving rise to smooth muscle cells and fibroblasts, respectively (Fig. 35).

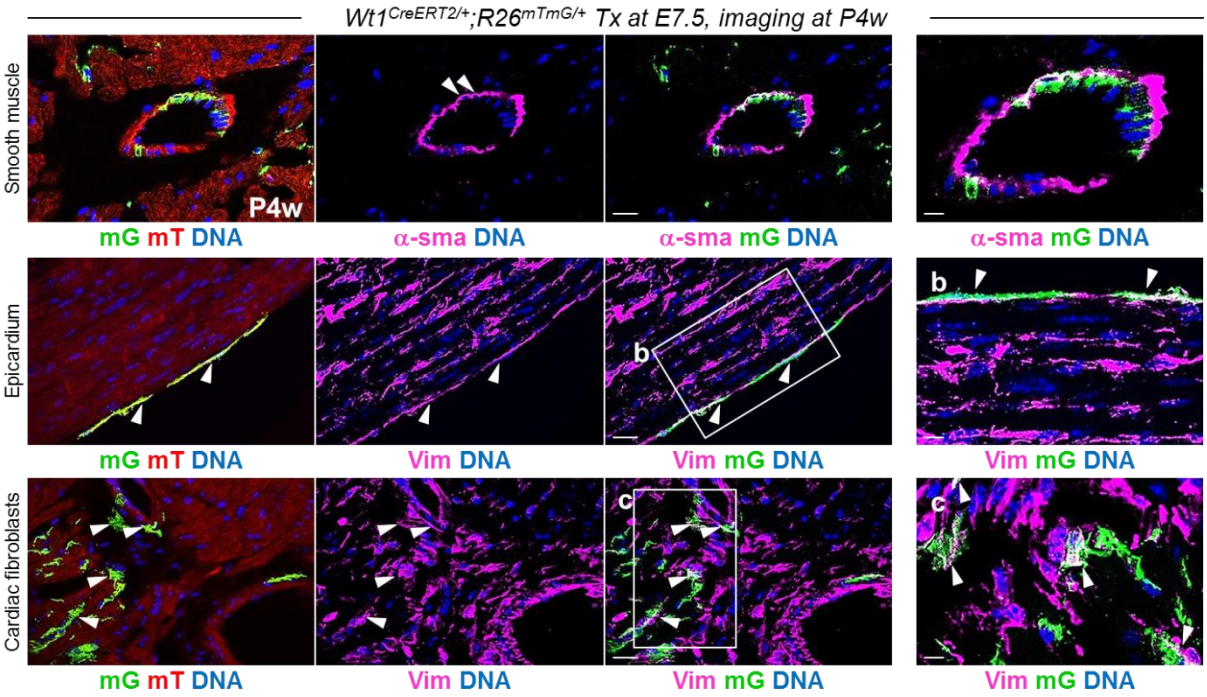

Figure 35: Epicardial-derived lineages arise from early Wt1 expressing progenitors.
Immunostaining of alpha-smooth muscle actin (α-sma, magenta), vimentin (Vim, magenta), mG (green), mT (red) and DNA (blue) in sections of an *Wt1*$^{CreERT2/+}$;*R26*$^{mTmG/+}$ adult mouse at P4w with tamoxifen treatment at E7.5. Expression of mG was observed in epicardial-derived lineages (smooth muscle, epicardium and cardiac fibroblasts) marked by α-sma (upper panels) and Vim (lower panels). White arrows indicate α-sma^{+}/mG^{+} smooth muscle cells or Vim^{+}/mG^{+} fibroblasts. Scale bars = 25 µm. The boxed regions are shown in higher magnification (right panels). Scale bars = 10µm. Adapted from Dorn, Kornherr et al. 2018.

No recombination throughout the embryo and the adult mouse hearts was observed when oil only was injected (Fig. 36+37).

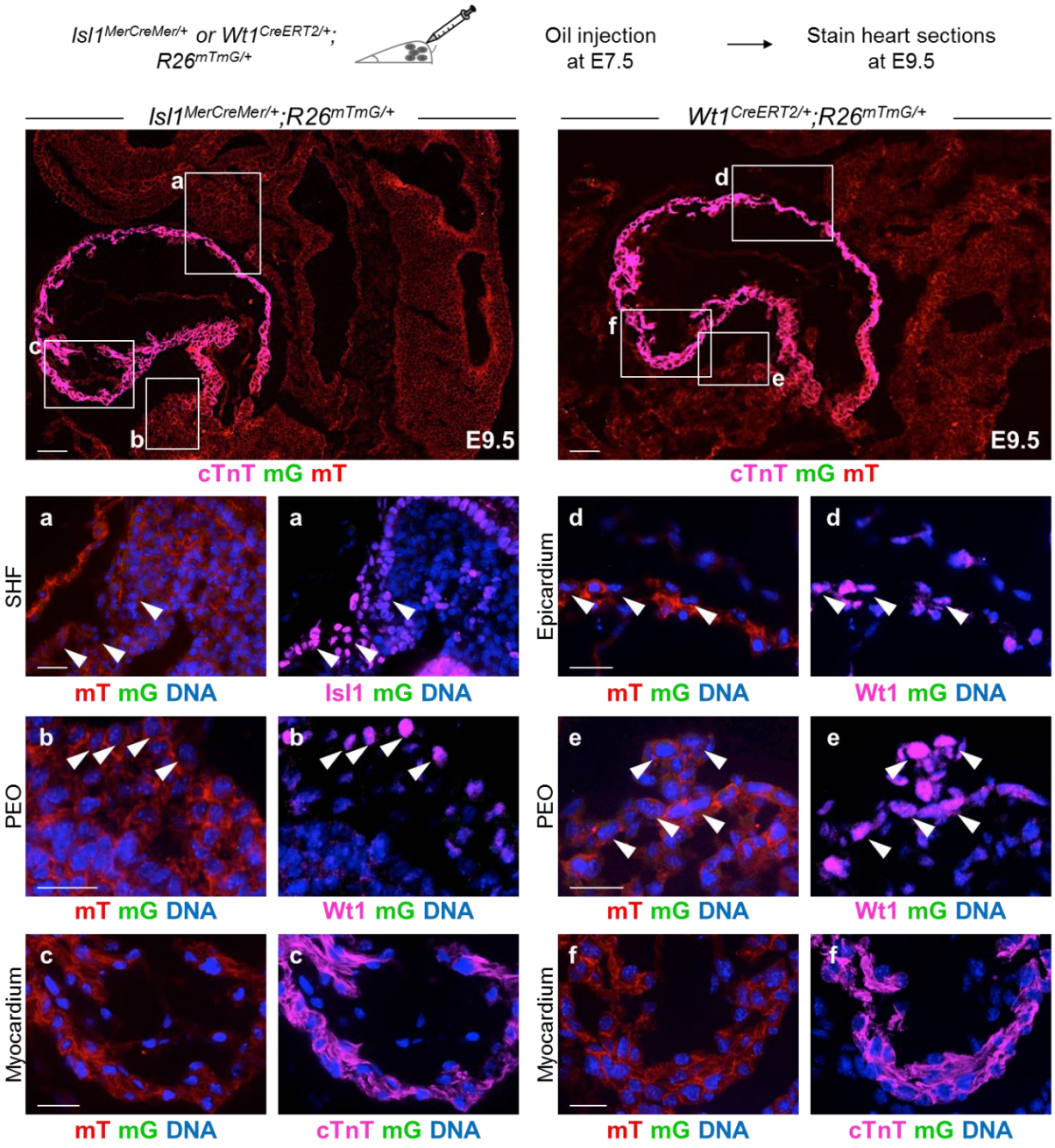

Figure 36: No activation of Cre in the absence of tamoxifen in embryos at E9.5.
Schematic representation of control experimental setup with oil injection in *Isl1*$^{MerCreMer/+}$ or *Wt1*$^{CreERT2/+}$;*R26*$^{mTmG/+}$ mice at E7.5 and their analysis at E9.5. Immunostaining of cardiac troponin T (cTNT, magenta), mG (green) and mT (red) show no mG signal throughout the embryo. Scale bars = 100 µm. Boxed areas are shown in higher magnifications (a-f). a**,** Representative area of Isl1^{+} (magenta) SHF progenitors of *Isl1*$^{MerCreMer/+}$;*R26*$^{mTmG/+}$ (a-c) embryos. d, Representative area of Wt1^{+} (magenta) epicardial cells of *Wt1*$^{CreERT2/+}$;*R26*$^{mTmG/+}$ (d-f). b+e, Wt1^{+} (magenta) PEO. c+f, cTnT^{+} (magenta) cardiomyocytes. DNA (blue). Arrowheads indicate cells of interest (Isl1^{+} SHF progenitors, Wt1^{+} epicardial and proepicardial cells).Scale bars = 25 µm. Adapted from Dorn, Kornherr et al. 2018.

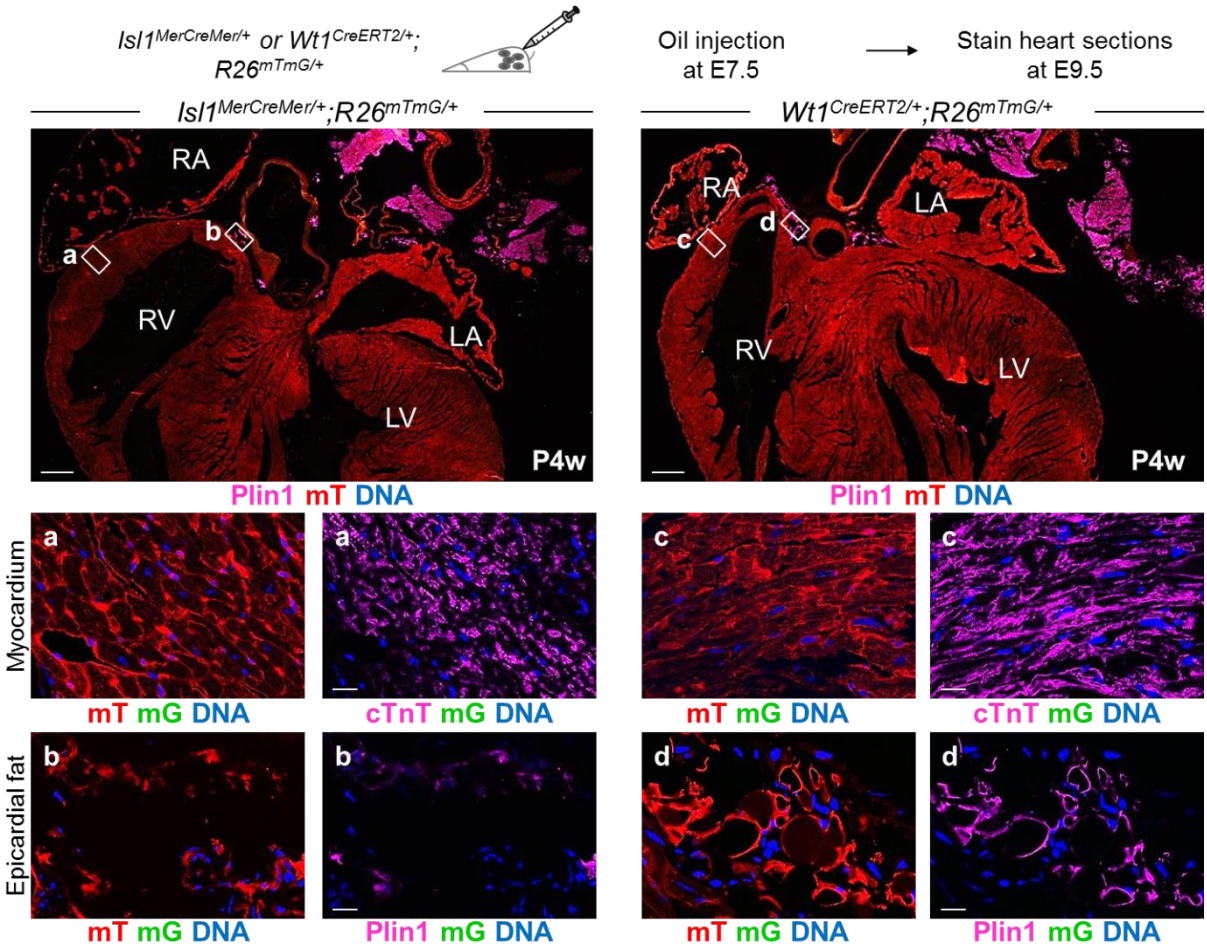

Figure 37: No activation of Cre in the absence of tamoxifen in the adult heart.
Schematic representation of control experimental setup with oil injection in *Isl1*$^{MerCreMer/+}$ or *Wt1*$^{CreERT2/+}$;*R26*$^{mTmG/+}$ mice at E7.5 and their analysis at P4w. Immunostaining of Plin1 (magenta), cTnT (magenta), mG (green), mT (red) and DNA (blue) show no mG signal throughout the whole heart. Labeling of the heart chambers: RA = right atrium, RV = right ventricle, LA = left atrium, LV = left ventricle. P4w = 4 weeks postnatally. Scale bars = 400 µm. Boxed areas are shown in higher magnifications (a-d). a and c**,** Representative areas of cTnT^{+} (magenta) cardiomyocytes; b and d, of Plin1^{+} (magenta) epicardial adipocytes of *Isl1*$^{MerCreMer/+}$;*R26*$^{mTmG/+}$ (a+b) and *Wt1*$^{CreERT2/+}$;*R26*$^{mTmG/+}$ (c+d) hearts. Scale bars = 25 µm. Adapted from Dorn, Kornherr et al. 2018.

In conclusion, the finding of the Isl1^{+}/Wt1^{+} progenitor pool at E8 and the results obtained with the lineage tracing of inducible *Isl1*$^{MerCreMer/+}$;*R26*$^{mTmG/+}$ and *Wt1*$^{CreERT2/+}$;*R26*$^{mTmG/+}$ reporter lines suggest an existence of a bi-potent precursor giving rise to both cardiomyocytes and epicardial fat.

3.2.3 A single Isl1^{+}/Wt1^{+} precursor has bi-differentiation potential

Since the Isl1^{+}/Wt1^{+} population at E8 in the mouse embryo is very transient and small in number, an ESC system was used to identify and isolate these progenitors and assess their differentiation potential clonally. Therefore, an ESC line was generated from blastocysts of an *Isl1*$^{Cre/+}$;*R26*$^{YFP/+}$ mouse line, in which yellow fluorescent protein (YFP) is irreversibly

expressed from the *Rosa26* gene locus upon Isl1-Cre-mediated recombination (Fig. 38). During EB differentiation, Isl1$^+$ progenitors emerged within 4 to 5 days (Fig. 38), as demonstrated by YFP expression (Fig. 39a) and *Isl1* transcript (Fig. 39b).

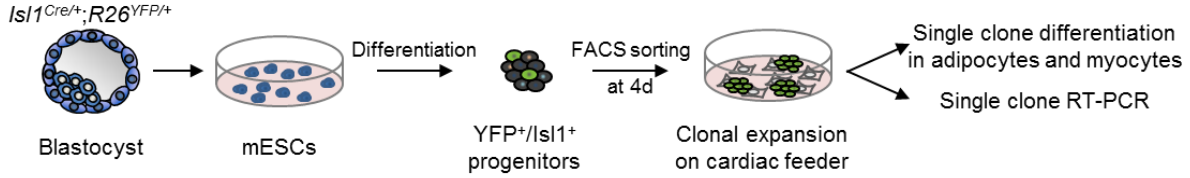

Figure 38: Experimental setup for *in vitro* bi-differentiation analysis of single Isl1$^+$ progenitors.
Schematic representation of the mouse ESC derivation from *Isl1*$^{Cre/+}$;*R26*$^{YFP/+}$ blastocysts, their specification into Isl1$^+$ progenitors, the subsequent clonal expansion and differentiation as well as gene expression analysis. Adapted from Dorn, Kornherr et al. 2018.

This was accompanied by upregulation of other key markers of early cardiac progenitors such as *Nkx2*-5 (Zhang, Nomura-Kitabayashi et al. 2014) and *Gata4* (Fig. 39b). Fluorescent-activated cell sorting (FACS) of YFP$^+$ cells from 4-day old EBs allowed isolation of Isl1$^+$ progenitors (Fig. 39c), which showed elevated expression level of *Isl1*, *Nkx2*-5 and *Gata4* compared to YFP$^-$ cells (Fig. 39d).

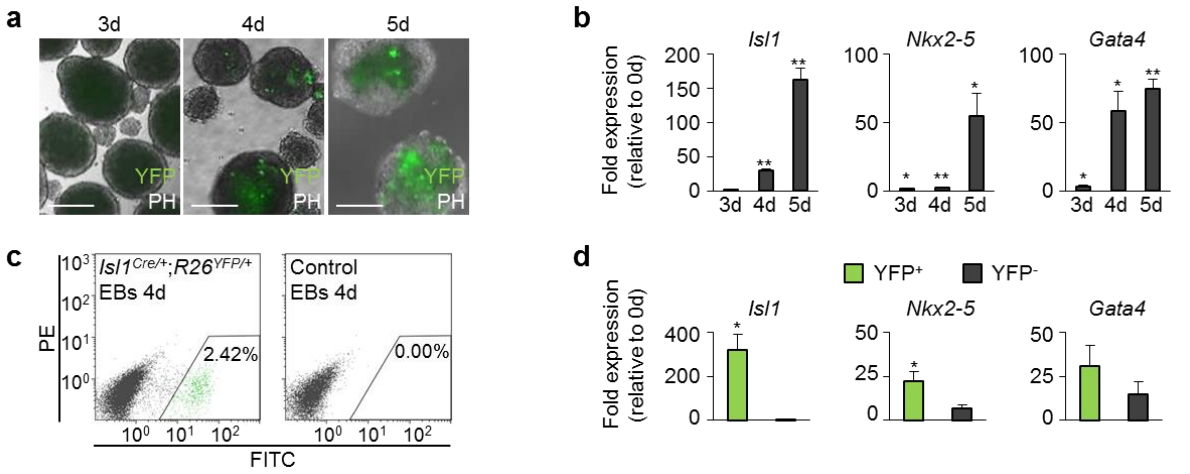

Figure 39: Upregulation of early cardiac progenitor genes during EB differentiation.
a) YFP (green) starts to be expressed at 4 days of EB differentiation of *Isl1*$^{Cre/+}$;*R26*$^{YFP/+}$ ESCs. PH = Phase-contrast microscopy. Scale bars = 200 µm. b) Gene expression analysis of early cardiac progenitor genes *Isl1*, *Nkx2-5* and *Gata4* at 3 to 5 days of EB differentiation. Data are means ± SEM from 4 independent experiments. *P<0.05, **P<0.01 vs. d0. c) Representative flow cytometry analysis of YFP expression in 4-day old *Isl1*$^{Cre/+}$;*R26*$^{YFP/+}$ and control EBs. FITC = fluorescein isothiocyanate, PE = phycoerythrin. d) qRT-PCR analysis of cardiac progenitor markers *Isl1*, *Nkx2-5* and *Gata4* in YFP$^+$ and YFP$^-$ cells sorted from 4-day old *Isl1*$^{Cre/+}$;*R26*$^{YFP/+}$ EBs. Data are means ± SEM from 3 independent experiments. *P<0.05 vs. YFP$^-$. Adapted from Dorn, Kornherr et al. 2018.

The isolated YFP$^+$ cells were subjected to pro-myogenic or pro-adipogenic culture conditions and demonstrated a potential to efficiently differentiate into both beating cardiomyocytes and lipid-droplet filled adipocytes, as detected by immunostaining for cTnT, a protein marking the

A-band of a cardiomyocyte sarcomere, and Pparγ, a key regulator of adipogenesis, in conjuction with fluorescent lipid-droplet marker BODIPY (Fig. 40).

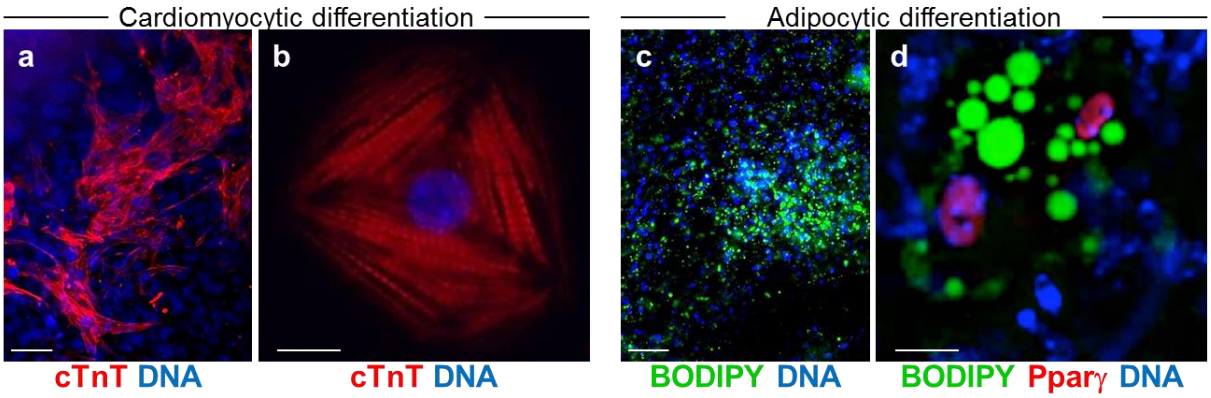

Figure 40: Bi-differentiation potential of Isl1$^+$ progenitors into cardiomyocytes and adipocytes.
a) Immunofluorescence anaysis of differentiated FACS sorted Isl1$^+$ progenitors into cTnT$^+$ (red) cardiomyocytes. Scale bar = 50 µm. b) High magnification of a well-organized cardiomyocyte. Scale bar = 25 µm. c) Overview of adipocytic differentiation. Lipid-droplets are stained with BODIPY (green). Scale bar = 50 µm. d) High magnification of lipid-droplets containing cells expressing adipocyte key transcription factor Pparγ (red). Scale bar = 25 µm. DNA (blue). Adapted from Dorn, Kornherr et al. 2018.

To access if a single precursor is able to differentiate into both lineages, a culture system was used, which allows clonal amplification of Isl1$^+$ progenitors. Therefore, single FACS-sorted YFP$^+$/Isl1$^+$ progenitors were seeded onto cardiac mesenchymal feeder cells and grown clonally. Immunofluorescence analysis confirmed persistence of Isl1 as well as YFP expression in the clones after 6 days of culture. Furthermore, Wt1 was co-expressed in 50% of the emerging clones (Fig. 41a). Each of the arising clones (n=119, in three independent experiments) was differentiated in both, myogenic and adipogenic culture conditions. Immunofluorescence analysis was used to determine differentiation capacity into cardiomyocytes and adipocytes. 42±10% of all analyzed clones were able to differentiate into both lineages. For 10 clones gene expression analysis for *Isl1*, *Wt1* and *Nkx2-5* was performed on one part of each clone before differentiation (Fig. 41b). Expression of *Isl1* was present in all tested clones, confirming the maintenance of their progenitor state. *Wt1* was co-expressed in 60% of the tested clones, which all had potential to differentiate into both lineages. In the remaining 40% of Isl1$^+$/Wt1$^-$ clones three fourth were Isl1$^+$/Wt1$^-$/Nkx2-5$^+$, representing the cardiomyocytic progenitor, and one fourth Isl1$^+$/Wt1$^-$/Nkx2-5$^-$ (Fig. 41c). This suggests that the molecular signature of Isl1$^+$/Wt1$^+$ defines a cardiac “myo-adipo progenitor cell” *in vitro*, which is distinct from Isl1$^+$/Nkx2-5$^+$ myocytic progenitor.

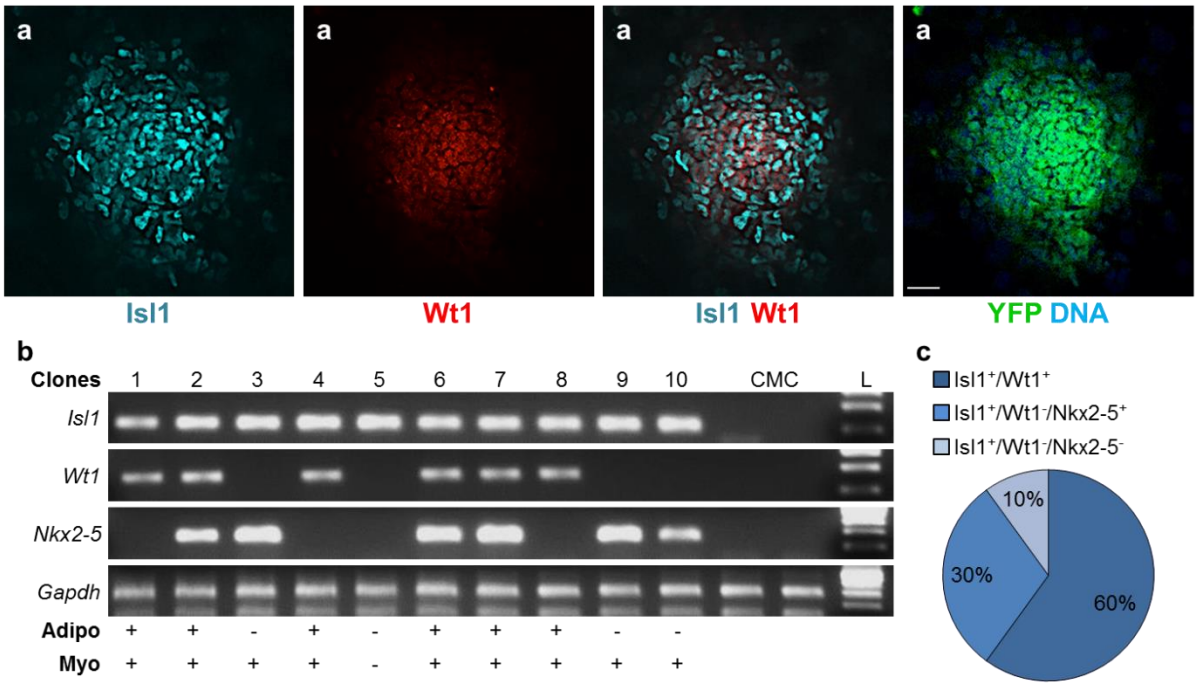

Figure 41: A single Isl1$^+$/Wt1$^+$ progenitor can differentiate into cardiomyocytes and adipocytes.
a) Immunostaining of Isl1 (cyan), Wt1 (red), YFP (green) and DNA (blue) on a representative clone of a single Isl1$^+$ progenitor cell expanded on cardiac mesenchymal feeder cells (CMC) for 6 days. Scale bar = 100 µm. b) RT-PCR profile of 10 representative clones after expansion on CMCs for 6 days show, retrospectively, Isl1$^+$/Wt1$^+$ clones differentiating into both adipocytic and myocytic lineage (clones 1, 2, 4, 6, 7 and 8), whereas Isl1$^+$/Nkx2-5$^+$/Wt1$^-$ clones differentiating into myocytic lineage only (clones 3, 9 and 10). CDNA of CMCs serves as negative control. CMC = cardiac feeder cells, L = ladder, Adipo = clone differentiating into adipocytes, Myo = clone differentiating into myocytes. c) Diagram showing relative distribution of clones with different molecular signature obtained during clonal expansion of Isl1$^+$ progenitors on CMCs. Adapted from Dorn, Kornherr et al. 2018.

Taken together, these results demonstrate that a single Isl1$^+$/Wt1$^+$ progenitor cell, which resembles the Isl1$^+$/Wt1$^+$ proepicardial precursor at E8 in the developing mouse, is able to give rise to both cardiomyocytes and adipocytes. The finding that these cells have bi-potent differentiation capacity strengthens the hypothesis of the existence of a common developmental origin of these two lineages.

4. Discussion

The field of lineage specification and differentiation is still, due to its complexity, in the process of getting understood. The discovery of Isl1 expressing progenitors revealed many insights in cell lineage diversification during cardiogenesis (Moretti, Caron et al. 2006). The findings presented in this thesis showed that Isl1 is not only an important factor for cardiomyocyte differentiation and subtype specification, but is also expressed in progenitors giving rise to epicardial adipocytes, proving Isl1 again as a key transcriptional regulator. This raises the question, which factors are able to regulate *Isl1* expression. Several activators of *Isl1* are known, such as Fgf8, Tbx1, Forkhead proteins, Gata4, Oct1 and Shox2 (Park, Ogden et al. 2006, Liao, Aggarwal et al. 2008, Kang, Nathan et al. 2009, Kappen and Salbaum 2009, Liu, Li et al. 2011, Hoffmann, Berger et al. 2013). Little evidence only exists about factors negatively regulating *Isl1*. Tbx20 was identified to directly repress *Isl1*; however the function of this negative regulation still needs to be assessed, since upregulation of *Isl1* expression did not account for the cardiac phenotype detected in the *Tbx20* null mice (Cai, Zhou et al. 2005). Isl1 and Nkx2-5 are co-expressed in both FHF and SHF and play essential roles for proper cardiac progenitor specification (Ma, Zhou et al. 2008). There is a reciprocal relationship between expression levels of these two factors; to detail, Isl1 is downregulated, while Nkx2-5 expression is maintained and even increases in differentiating progenitors (Moretti, Caron et al. 2006). Moreover, *Nkx2-5* knockout mice and zebrafish embryos exhibited elevated expression of *Isl1* and other SHF markers in differentiating myocytes (Prall, Menon et al. 2007, Witzel, Jungblut et al. 2012), suggesting an inhibitory regulation of Isl1 program through Nkx2-5.

Our study revealed that Nkx2-5 can directly regulate *Isl1* transcription, thus mediating cardiac subtype specification (Dorn, Goedel et al. 2015).

Additionally, *in vivo* fate mapping and clonal analysis of Isl1 expressing progenitors demonstrated that $Isl1^{+}/Wt1^{+}$ progenitors represent a common developmental origin of cardiac muscle and fat, suggesting related mechanisms of determination between the two lineages.

Discussion

4.1 *Isl1* expression is directly downregulated by Nkx2-5

Direct repression of *Isl1* by Nkx2-5 was demonstrated by 1) constitutive Nkx2-5 overexpression in a mouse ESC system, which resulted in downregulation of Isl1 transcriptional program (Fig. 12), 2) finding of a conserved region within the *Isl1* enhancer with three functional Nkx2-5 binding sites (Fig. 18) and 3) conditional knockout of *Nkx2-5* in Isl1 expressing cells *in vivo* leading to persistent expression of Isl1 in the developing heart tube (Fig. 20). Moreover, a recent study showed that Isl1 and Nkx2-5 have an opposing regulatory effect on *Fgf10* cardiac element harboring overlapping binding sites for Isl1 and Nkx2-5, which they compete for, making target gene expression dependent on the expression ratio of these two factors. Fgf10 is expressed in the anterior SHF and promotes proliferation of cardiac progenitors that form the arterial pole. Isl1 principally activates, and Nkx2-5 represses transcription of *Fgf10* (Watanabe, Zaffran et al. 2012). Thus, a similar interplay between Nkx2-5 and Isl1 could be also true for Isl1 downstream targets that displayed opposite expression levels in cardiac progenitors overexpressing either Isl1 or Nkx2-5. Interestingly, a very recent study investigating the potential crosstalk between Isl1 and Nkx2-5 during heart development in the context of hypoxia determined that Isl1 recruits histone deacetylases to repress *Nkx2-5* expression and prevent precocious myocyte specification in cardiac progenitors. When migrating into the hypoxic heart tube $Isl1^{+}$ cells silence *Isl1* expression leading to activation of *Nkx2-5* transcription, thus, promoting myocytic specification (Yuan, Qi et al. 2017). It could be possible that hypoxia may be the initial step in the process of switching off *Isl1*, thus abrogating Isl1-dependent repression of *Nkx2-5*, which in turn negatively regulates *Isl1* to secure stable cardiomyocyte differentiation.

Overexpression of Nkx2-5 in differentiating ESCs inhibited cardiac specification confirming previous work reporting negative regulation of cardiac precursor gene expression by Nkx2-5 (Prall, Menon et al. 2007). *Nkx2-5* knockout mutants showed upregulated expression of cardiac progenitor genes *Igfbp5*, *Pdgfrα*, and *Isl1* resulting in the enhanced precursor specification (Prall, Menon et al. 2007). Interestingly, contrary results were reported from a previous study showing that ectopic expression of human NKX2-5 in mouse ESCs driven by a CMV promoter enhanced cardiogenesis and promoted differentiation of ventricular cardiomyocytes (David, Stieber et al. 2009). Specification and differentiation is a very complex process and requires tight temporal and spatial control, which is mediated by the fine tuning of interlaced genetic networks (Laugwitz, Moretti et al. 2008, Brade, Pane et al. 2013). Thus, phenotypic discrepancies between these studies might be attributed to differences in Nkx2-5 dosage during ESC differentiation based on the usage of different promoters. For example, CMV promoter drives the transgene expression less efficient in

undifferentiated ESCs than the PGK promoter used in our study, which exhibits a strong activity in ESC-derivatives as well (Wang, Liang et al. 2008).

In contrast to Nkx2-5, Isl1 overexpression increased cardiac progenitor specification corroborating former work on *Isl1* knockout mutants, which fail to develop SHF derivatives (Cai, Liang et al. 2003) demonstrating the positive regulatory role of Isl1 in cardiogenesis. Lineage tracing experiments revealed extensive contribution of Isl1 expressing cells to the right ventricle, OFT and atria, suggesting Isl1 as a SHF marker (Cai, Liang et al. 2003). Intriguingly, Isl1 expression was found also in the intra-embryonic coelomic lining at E7.5, which contains progenitors of both heart fields (Prall, Menon et al. 2007). Additional studies with an improved Cre-based approach demonstrated that Isl1 is expressed in the FHF as well (Ma, Zhou et al. 2008). Further evidence that Isl1 is likely to be a pan cardiac marker is provided by two results of this study: Isl1 overexpression activated both FHF and SHF (Fig. 15) and conditional ablation of *Nkx2-5* in Isl1 expressing cells resulted in the absence of Nkx2-5 in almost all cells of the heart and not only in the SHF derivatives (Fig. 19) (Dorn, Goedel et al. 2015).

4.2 Isl1 regulates subtype specification

As soon as cardiac progenitors differentiate, they lose *Isl1* and increase *Nkx2-5* expression, which is crucial for stopping progenitor proliferation in favor of promoting their differentiation (Moretti, Caron et al. 2006). Our results suggest that Nkx2-5 may be directly repressing *Isl1* transcription restricting it to cardiac precursors.

Previous work showed, consistent with the results of our study, that late overexpression of Isl1 leads to enhanced cardiomyocyte differentiation (Kwon, Qian et al. 2009, Bondue, Tannler et al. 2011). However, the effects of constitutive overexpression and, thus, the biological significance of Isl1 downregulation in differentiating cardiomyocytes were not investigated until now. Our results revealed that sustained expression of Isl1 *in vitro* and *in vivo* does not prevent cardiomyocyte differentiation. In contrast, overexpression of Isl1 led to enhanced specification of cardiac progenitors and increased numbers of myocytes. Importantly, failed downregulation of Isl1 during cardiac differentiation repressed ventricular and promoted nodal myocyte lineage (Fig. 24+25). This highlights complex regulatory feedback between Isl1 and Nkx2-5 in cardiac progenitor specification and differentiation. The role of these transcription factors in regulating cardiac progenitor proliferation and differentiation continues to be a point of investigation (Galdos, Guo et al. 2017). Experiments

involving Isl1 overexpression in *Xenopus laevis* (Dorn, Goedel et al. 2015) revealed that Isl1 overexpression did not inhibit cardiac differentiation, corroborating our results on Isl1 OE mouse ESC line (Fig. 23). Moreover, microinjection of *Xenopus isl1* RNA resulted in upregulation of Isl1 downstream targets, while not affecting cardiomyocyte differentiation. Isl1 gain-of-function embryos demonstrated faster heart beating frequency, which is indicative of nodal myocytes (Dorn, Goedel et al. 2015). Using gene and protein expression analysis (Fig. 24+25), as wells as functional AP phenotyping, maintained Isl1 expression enhanced SAN myocyte specification at the expense of working myocardium could be shown (Fig. 26) (Dorn, Goedel et al. 2015). Shortly after the results of this work have been published, the Evans group demonstrated the role of Isl1 to be essential for pacemaker development (Liang, Zhang et al. 2015). Using mice harboring a SAN-specific *Isl1* deletion, the authors demonstrated that Isl1 is required for early embryonic survival and expression of genes, which are critical for SAN function (Liang, Zhang et al. 2015). In addition, they performed ChIP for Isl1 in SAN-purified cells and identified Isl1 downstream targets important for SAN including subunits of the L-type calcium channel and Tbx3 (Liang, Zhang et al. 2015).

Pluripotent stem cell-derived cardiomyocytes, although immature, can be functionally phenotyped according to their APs based on the specific composition of the ion channels on their membrane (Hescheler, Fleischmann et al. 1997). Early *in vitro* differentiated myocytes however, just start to express channels and their APs are similar to the nodal ones making it difficult to distinguish them from each other. Analyzing myocytes at different maturation stages and applying ivabradine, a drug specifically blocking the pacemaker Hcn4 channels, allowed for clearly segregating nodal from working myocardium myocytes. It is unlikely that aberrant myocyte subtype specification detected in Isl1 overexpressing cells attributes to delayed maturation, since even at 21 days of differentiation, representing the terminally differentiated state, Isl1 overexpressing cells exhibited high expression levels of nodal markers and failed to upregulate working-myocardium genes. Reinforcing this, Isl1 overexpressing cells started to beat earlier than control counterparts and displayed well-organized sarcomeres.

Isl1 expressing cells are localized in three regions of the adult heart: clusters of parasympathetic neurons in the interatrial septum and around the pulmonary veins, scattered smooth muscle cells within the wall of the great vessels and cardiomyocytes of the OFT and a strictly delimited cluster of pacemaker cells of the SAN (Weinberger, Mehrkens et al. 2012). Lineage tracing revealed that pacemaker cells derive from Isl1 expressing progenitors, suggesting a stable expression of Isl1 from embryonic stage into adulthood (Mommersteeg, Dominguez et al. 2010, Liang, Wang et al. 2013). Recent studies in mouse and zebrafish delineating the requirement of Isl1 for functional pacemaker cells (de Pater, Clijsters et al.

2009, Tessadori, van Weerd et al. 2012, Hoffmann, Berger et al. 2013, Liang, Zhang et al. 2015) indicate a conserved role of Isl1 in the SAN lineage among different species.

Generation of biological pacemakers offers a great opportunity for treatment of sinus node diseases. Further development of these therapies will require a deeper understanding of transcriptional networks in specialized cardiac pacemaker cells (Vedantham 2015). Several approaches using pharmacological compounds to generate SAN cells were described, including EBIO, suramin and anti-NRG-1β (Kleger, Seufferlein et al. 2010, Zhu, Xie et al. 2010, Wiese, Nikolova et al. 2011), which activate Tbx2 and Tbx3, the key regulators of SAN transcriptional networks (Christoffels, Hoogaars et al. 2004, Hoogaars, Tessari et al. 2004). Tbx3 (Hoogaars, Engel et al. 2007, Bakker, Boink et al. 2012) as well as Tbx18 (Kapoor, Liang et al. 2013, Hu, Dawkins et al. 2014) have been shown to convert ventricular and atrial myocytes into pacemaker cells. Tbx2 and Tbx3 have been demonstrated to repress similar working myocardium genes, such as *Nppa* and *Cx40* to promote SAN development (Habets, Moorman et al. 2002, Christoffels, Hoogaars et al. 2004, Hoogaars, Tessari et al. 2004). Results from this work suggest that in Isl1 overexpressing cells high Tbx2 rather than Tbx3 was imposing nodal myocyte function by suppression of working myocardium pathways (Fig. 24).

To conclude, our findings on Nkx2-5 mediated repression of *Isl1* expression determining nodal subtype specification provides further insight in cardiomyocyte lineage decision during development. Investigation of molecular pathways driving cardiac lineage specification is fundamental for achieving knowledge of the complete picture of developmental biology of the heart and moreover for the need to influence diseased pathways.

4.3 Common developmental origin of cardiac myocytes and epicardial fat

The human healthy heart is covered and infiltrated by an extensive layer of fat, so called pericardial fat, which serves as mechanical support, has thermogenic features, and plays important metabolic roles by buffering free fatty acids away from the myocardium and acting as an energy and paracrine source (Samanta, Pouliopoulos et al. 2016, Gaborit, Sengenes et al. 2017). Pericardial fat is the sum of paracardial fat, located on the external surface of the parietal pericardium and epicardial fat, which is named after its position underneath the epicardium. EAT is an ectopic fat depot found between myocardium and the visceral

pericardium with no fascia separating the tissues, allowing local interaction and cellular cross-talk between myocytes and adipocytes (Gaborit, Sengenes et al. 2017). Recently, fate mapping experiments have demonstrated that EAT is derived from epicardial progenitors expressing Tbx18 and Wt1 (Liu, Huang et al. 2014, Yamaguchi, Cavallero et al. 2015).

In our study, lineage tracing for Isl1 progenitors revealed marking of the SHF-derived cardiomyocytes and of the EAT (Fig. 29). Furthermore, a common progenitor expressing Isl1 and Wt1 at E8, which gives rise to both cardiomyocytes and epicardial adipocytes, was identified.

Using an *Isl1*$^{Cre/+}$*;R26*$^{mTmG/+}$ reporter line (Fig. 30) it was shown that the epicardium originates from Isl1 expressing SHF progenitors *via* a transient structure referred to as PEO, confirming previous results (Zhou, von Gise et al. 2008). Isl1 itself, however, has been shown not to be required for the PEO formation, since in *Isl1* knockout mice the PEO formation is not affected (Cai, Liang et al. 2003). The PEO is characterized by the expression of the key epicardial transcription factor Wt1. Proepicardial cells migrate out of the PEO to form the epicardium, maintaining Wt1 expression, which is crucial for EMT prior the differentiation of epicardial cells into various cell types, such as cardiac fibroblasts, smooth muscle cells and epicardial adipocytes.

Lineage tracing of Isl1^{+} progenitors did not mark all of the Wt1^{+} PEO cells when using *R26*^{mTmG} reporter mice, probably due to low recombination efficiency (Fig. 30). Zhou et al. have shown that lineage tracing experiments with the more sensitive *LacZ* reporter mouse resulted in a robust, however, not complete labeling of the Wt1^{+} PEO population (Zhou, von Gise et al. 2008), suggesting that other precursors might exist contributing to the Wt1^{+} cell pool. In addition, marking of the cells within the PEO that do not express Wt1 was detected, confirming former studies (Zhou, von Gise et al. 2008). These Wt1^{-} cells might represent another proepicardial population characterized by the expression of Scx and Sema3D, which gives rise to the coronary endothelium (Katz, Singh et al. 2012).

Analysis of embryos at early stages prior the PEO formation and downregulation of Isl1 in the proepicardial cells identified a transient Isl1 and Wt1 co-expressing population at E8 (Fig. 31), corroborating previous results (Zhou, von Gise et al. 2008). Indeed, lineage tracing for Isl1 and Wt1 induced at E7.5, shortly before the appearance of Isl1^{+}/Wt1^{+} progenitors demonstrated marking of cardiomyocytes and epicardial fat in adult hearts (Fig. 34). When embryos were analyzed at E9.5, the PEO and epicardium were labeled in *Isl1*$^{MerCreMer/+}$*;R26*$^{mTmG/+}$ and *Wt1*$^{CreERT2/+}$*;R26*$^{mTmG/+}$ inducible mouse lines (Fig. 32). Closer inspection revealed that few marked cells in the *Isl1*$^{MerCreMer/+}$*;R26*$^{mTmG/+}$ line started to migrate over the heart tube, and already left the PEO at this stage, while in the epicardium of the

Wt1$^{CreERT2/+}$;*R26*$^{mTmG/+}$ line consistently more cells were labeled additionally to those that could be found in the PEO as well. This could be due to differences in labeling efficiency in the mouse lines or a hint that different Isl1^{+}/Wt1^{+} populations exist, one starting migration earlier than the other.

PEO cells represent quite a heterogeneous population. It is still unknown whether PEO cells are already primed for their cell fate and represent committed progenitors for specific lineages (Mikawa and Gourdie 1996) or if they follow a more plastic fate and fate segregation towards different cell types takes place at the stage of the epicardium (Acharya, Baek et al. 2012) (Maya-Ramos, Cleland et al. 2013). For the development of the epicardium two models have been proposed: a committed and a non-committed model. Using inducible lineage tracing for Tcf21 Acharya et al. demonstrated that epicardial cells are committed to the cardiac fibroblast lineage prior to the initiation of epicardial EMT, suggesting that the committed fate model is more likely (Acharya, Baek et al. 2012). Similar mechanisms could also apply for the specification of the proepicardial cells.

The recombination efficiency observed in the inducible *Isl1*$^{MerCreMer/+}$;*R26*$^{mTmG/+}$ and *Wt1*$^{CreERT2/+}$;*R26*$^{mTmG/+}$ lines in our study was much lower than in the constitutive *Cre* lines (Fig. 33), which has been already reported (Laugwitz, Moretti et al. 2005, Rudat and Kispert 2012). Moreover, the high toxicity effect of tamoxifen when injected at early stages of embryogenesis required administration of low doses for induction of Cre activity. Using *Isl1*$^{MerCreMer/+}$, *Wt1*$^{CreERT2/+}$ and *R26*$^{mTmG/+}$, a less sensitive reporter compared to LacZ (Sun, Liang et al. 2007), in addition to injection of low tamoxifen dose at E7.5 allowed a nearly clonal labeling of Isl1 and Wt1 expressing progenitors in this study (Fig. 32+33). Thus, it was possible to almost clonally mark cardiomyocytes and adipocytes in the *Isl1*$^{MerCreMer/+}$;*R26*$^{mTmG/+}$ and *Wt1*$^{CreERT2/+}$;*R26*$^{mTmG/+}$ adult mice, reinforcing the hypothesis that a single common progenitor expressing Isl1 and Wt1 with cardiomyogenic and adipogenic bi-potential exists at E8.0. To definitely prove the existence of an Isl1^{+}/Wt1^{+} progenitor giving rise to cardiac muscle and fat a lineage tracing analysis of a mouse *R26*$^{mTmG/+}$ reporter line expressing both inducible *Isl1*$^{MerCreMer/+}$ and *Wt1*$^{DreERT2/+}$ will be needed.

In the *Wt1*$^{CreERT2/+}$;*R26*$^{mTmG/+}$ reporter line also smooth muscle cells, epicardium and cardiac fibroblasts were marked, indicating that a true pre-proepicardial progenitor was labeled at E8.0. The number of cardiomyocytes marked in these mice was very low, showing that the Isl1^{+}/Wt1^{+} pre-proepicardial progenitor population has the cardiomyocytic potential but a higher propensity to specify into other epicardial derivatives. Epicardial origin of endothelial cells was long time controversially discussed, since studies in avian species suggested a proepicardial origin for this lineage (Gittenberger-de Groot, Vrancken Peeters et al. 1998, Reese, Mikawa et al. 2002), whereas fate mapping in mice using *Wt1* and *Tbx18* reporter

lines was not able to clearly confirm these data (Cai, Martin et al. 2008, Zhou, Ma et al. 2008). Recent data suggests that most of the endothelial cells derive from a second proepicardial population expressing Scx and Sema3D (Katz, Singh et al. 2012). Consistent with latter data no endothelial cells were labeled in the inducible *Wt1*$^{CreERT2/+}$*;R26*$^{mTmG/+}$ lineage traced mice in this study (data not shown).

An epicardial origin of cardiomyocytes was previously demonstrated, using *Tbx18*$^{Cre/+}$*;R26*^{lacZ}, *Wt1*$^{CreEGFP/+}$ and *Wt1*$^{CreERT2/+}$*;R26*$^{fsLz/+}$*/R26*$^{Z/Red}$ lines when tamoxifen was injected at the epicardial stage E10.5/E11.5 (Cai, Martin et al. 2008, Zhou, Ma et al. 2008). Results of the *Tbx18* reporter line are controversially discussed, since endogenous Tbx18 expression was found in cardiomyocytes of the interventricular septum and the left ventricle (Christoffels, Grieskamp et al. 2009). Also the results of the *Wt1* lineage tracing were under discussion since Rudat and Kispert demonstrated ectopic labeling in the *Wt1*$^{CreEGFP/+}$*;R26*$^{mTmG/+}$ line, which did not faithfully recapitulate endogenous expression of Wt1 at E8.5, E9.5, E12.5 and E18.5 (Rudat and Kispert 2012). In line with that, the group around Zhou found that the choice of Cre-activated reporter is important when using the *Wt1*$^{CreEGFP/+}$ line to avoid ectopic labeling (Zhou and Pu 2012). Moreover, Rudat and Kispert experienced problems with tamoxifen administration at early developmental stages, which resulted in embryonic lethality, and thus, were not able to evaluate lineage tracing before E11.5. With tamoxifen injection after E11.5 no recombination in cardiomyocytes was detected, which they refer to very low recombination efficiency. Due to this, the authors could not confirm epicardial contribution to the cardiomyocytic lineage (Rudat and Kispert 2012).

Since the Isl1^{+}/Wt1^{+} population at E8 is very transient and little in cell number, the ESC system offered the great opportunity to analyze the Isl1^{+}/Wt1^{+} cells for their bi-potential to differentiate into both cardiomyocytes and adipocytes. ESCs isolated from blastocysts of *Isl1*$^{Cre/+}$*;R26*$^{YFP/+}$ mice allowed isolation of Isl1^{+} progenitors by FACS sorting of YFP^{+} cells, which could be grown on cardiac mesenchymal feeders promoting self-renewal of Isl1^{+} progenitors in culture and preventing their differentiation (Laugwitz, Moretti et al. 2005). This system enabled us to divide each clone and take one part for analysis of its transcriptional profile and at the same time to expose the other two parts to adipogenic and cardiomyogenic conditions, allowing for comparing expression profile and the outcome of the differentiation cultures (Moretti, Caron et al. 2006). As expected, all clones expressed Isl1, confirming the maintenance of the Isl1 progenitor state. Isl1^{+} clones that were able to differentiate into both lineages co-expressed Wt1, corroborating the hypothesis that a common progenitor for cardiac adipocytes and myocytes *in vivo* expresses Isl1 and Wt1 early in development (Fig. 41). Thus, clonal *in vitro* experiments gave a hint of differentiation potentials of single

progenitors, which support the findings made *in vivo* in this and other studies (Yamashita, Itoh et al. 2000, Laugwitz, Moretti et al. 2005).

In conclusion, the results of this work provide *in vivo* and *in vitro* evidence that epicardial adipocytes derive from an $Isl1^{+}/Wt1^{+}$ pre-proepicardial progenitor, which has adipocytic as well as cardiomyocytic potential.

4.4 Defective regulation of adipogenic and myogenic programs in ARVC

Previously, a common developmental origin of skeletal muscle and brown fat was demonstrated by the Spiegelman group. Using lineage tracing the authors showed that brown fat cells arise from precursors that express *Myf5*, a gene so far thought to be expressed only in the myogenic lineage (Seale, Bjork et al. 2008). Moreover, they found a transcription factor Prdm16, which regulates a switch *in vitro* between these two lineages. In detail, knockdown of Prdm16 leads to conversion of brown adipocytes into skeletal myocytes and overexpression of Prdm16 in myoblasts induces their differentiation into brown fat cells (Seale, Bjork et al. 2008).

Our work revealed that cardiac muscle and fat also have a common developmental origin, suggesting that by modifying gene expression conversion of cardiac muscle into fat could be induced, similarly to skeletal muscle and brown fat. This cell fate switch could possibly apply in ARVC patients displaying replacement of cardiomyocytes by adipocytes. Indeed, d'Amati et al. group showed that cardiomyocytes of ARVC patients acquire fat droplets and adipocytic marker vimentin, while losing myofibrils and myocytic marker desmin, suggesting a direct transdifferentiation of cardiomyocytes into adipocytes (d'Amati, di Gioia et al. 2000). Lombardi et al. provided first evidence that mature cardiomyocytes could convert into adipocytes using cardiac lineage reporter mice $Myh6^{Cre/+};Dsp^{fl/+};R26^{EYFP/EYFP}$ to ablate desmosomal protein desmoplakin (Dsp) at the stage of adult cardiomyocyte or $Nkx2\text{-}5^{Cre/+};Dsp^{fl/+};R26^{EYFP/EYFP}$ and $Mef2c^{Cre/+};Dsp^{fl/+};R26^{EYFP/EYFP}$ lines to delete Dsp in cardiac progenitors (Lombardi, Dong et al. 2009). Moreover, when desmoplakin was ablated at the stage of cardiac progenitors the overall number of "excess adipocytes" as well as the percentage of adipocytes expressing EYFP was increased, indicating that pathological desmoplakin expression at early stages of cardiogenesis has even more severe effect on

cardiomyocyte-to-adipocyte conversion. This suggests a “priming” for the cardiomyocyte-adipocyte switch, which could occur at the level of a progenitor.

Multiple mouse models have been established to study ARVC *in vivo* (Lodder and Rizzo 2012). Transgenic mice with specific mutations in desmosomal proteins (Pkp2, Pg and Dsp) recapitulated the human phenotype only in terms of the arrhythmogenicity, fibrosis, and calcification; however they did not display any massive fatty infiltration (Lodder and Rizzo 2012). Since ARVC in humans occurs with prevalence in young extreme athletes, whose hearts have to work under tremendous mechanical cues, a research group exposed Plakophilin-2 mutant mice to endurance training, but even in this setting mice did not develop any fat deposition in the heart (Cruz, Sanz-Rosa et al. 2015). The first study demonstrating an ARVC phenotype in mice displaying excessive fat accumulation in the heart, used a transgenic model expressing a dominant-negative Rho-kinase under the muscle specific promoter SM22α, leading to activation of Pparγ inducing an adipogenic program (Ellawindy, Satoh et al. 2015).

Several iPSC-based models of ARVC have reported increased accumulation of lipid droplets and abnormal activation of PPARγ in iPSC-derived cardiomyocytes from ARVC patients upon treatment with adipogenic stimuli (Caspi, Huber et al. 2013, Kim, Wong et al. 2013, Ma, Wei et al. 2013, Dorn, Kornherr et al. 2018). It has been described that Pparγ is potent enough to initiate adipogenesis in myoblasts, and also other cell lineages, such as fibroblasts and osteoblasts (Hu, Tontonoz et al. 1995, Spiegelman, Hu et al. 1997, Kim, Her et al. 2005). In line with that, our study demonstrated that overexpression of Pparγ in cardiomyocytes is driving the conversion of myocytes into adipocytes. Moreover, it was shown that the cardiomyocyte-to-adipocyte cell fate switch is due to defective cell-cell-contact-mediated mechanosensing, which leads to impaired RhoA signaling. Mediating the dynamic control of monomeric and filamentous cytoskeleton actin, RhoA signaling is regulating cytoskeleton rearrangement (Sotiropoulos, Gineitis et al. 1999). Our study revealed that iPSC-derived cardiomyocytes with *PKP2* mutation undergo cytoskeleton rearrangement releasing monomeric G-actin, which binds to myocardin-related transcription factor (MRTF) and regulates its nucleus-cytoplasm shuttling. Following, in the mutated cardiomyocytes, MRTF with its co-regulator serum response factor (SRF) is prevented to act as a transcription factor in the nucleus leading to derepression of PPARγ and thus activation of the adipogenic program (Dorn, Kornherr et al. 2018). These findings corroborate the study of Ellawindy et al., demonstrating that inhibition of the Rho-pathway induces adipogenesis in mouse hearts (Ellawindy, Satoh et al. 2015). Rho-kinase signaling regulates gene expression, proliferation, differentiation, intracellular transport, and organizes cytoskeletal filaments, which supports desmosomal protein complex between cardiomyocytes (Amano, Fukata et al. 2000, Riento

and Ridley 2003). Furthermore, it activates canonical Wnt/β-catenin signaling, which results in inhibition of adipogenesis and activation of myogenesis (Kennell and MacDougald 2005, Schlessinger, Hall et al. 2009). Ellawindy et al. reported that mice overexpressing dominant-negative-Rho-kinase display aberrant Wnt signaling (Kennell and MacDougald 2005, Schlessinger, Hall et al. 2009, Ellawindy, Satoh et al. 2015). In addition, several other studies linked downregulated Wnt signaling with the development of ARVC in mice (Garcia-Gras, Lombardi et al. 2006, Lombardi, Dong et al. 2009, Lombardi, da Graca Cabreira-Hansen et al. 2011).

Our study revealed that inhibition of RhoA signaling could drive the myocyte-adipocyte transdifferentiation when wild type cardiomyocytes were treated with the ROCK inhibitor Y-27632. Interestingly, conversion was observed only in a subset of cardiomyocytes, which was in line with the finding that also in ARVC settings only a certain subpopulation of cardiomyocytes undergo myocyte-adipocyte switch. This suggests that only some cardiomyocytes are primed for this cell fate switch, presumably because of permissive transcriptional or epigenetic states acquired during development. Moreover, our results, demonstrating that a subset of cardiac muscle and epicardial fat cells share a common developmental origin, suggest that cardiomyocytes emerging from $Isl1^{+}/Wt1^{+}$ progenitors could be those more prone to a myocyte-to-adipocyte switch when exposed to adipogenesis-inducing stimuli (Dorn, Kornherr et al. 2018).

Wt1 plays an important role during development and is found cytoplasmatic, mainly localized on cytoskeleton-bound polysomes, in vast majority of cell types including human cardiomyocytes at fetal (Parenti, Perris et al. 2013, Ambu, Vinci et al. 2015) and adult stages (Dorn, Kornherr et al. 2018). Furthermore, its subcellular localization can be regulated by binding to actin (Niksic, Slight et al. 2004, Dudnakova, Spraggon et al. 2010). In the nucleus, Wt1 regulates transcription of numerous genes and functions both as transcriptional activator and as co-activator or as repressor of gene expression (Lee and Haber 2001). In ARVC cardiomyocytes as well as ROCK-inhibitor treated myocytes a nuclear translocation of Wt1 during myocyte-adipocyte conversion was detected, contrary to the wild type cardiomyocytes, in which Wt1 remained cytoplasmatic; suggesting that Wt1 could be involved in the process of myocyte-adipocyte-transdifferentiation. Overexpression of Wt1 alone was not sufficient to induce adipogenesis in human iPSC-derived wild type cardiomyocytes, but in conjunction with Pparγ it promoted the adipogenic program, indicating a cooperative role of Pparγ and Wt1. Interestingly, mouse cardiomyocytes lack expression of Wt1 at both embryonic and adult stages, but it is expressed in the proepicardium and in the fetal and activated adult epicardium (Scholz and Kirschner 2005, van Wijk, Gunst et al.

2012). Its absence in mouse cardiomyocytes might be an additional mechanism why murine ARVC models do not develop a fatty phenotype.

Our results suggest that myocyte-adipocyte cell fate switch could be a possible underlying mechanism of the ARVC pathogenesis. Furthermore, a subset of cardiomyocytes derived from $Isl1^{+}/Wt1^{+}$ progenitors could be more prone to convert into adipocytes, due to their close developmental relationship, when exposed to adipogenesis-inducing stimuli. Our study shows that factors involved in cellular destabilization, like mutant desmosomal proteins, alter the mechanosensing signaling pathway *via* RhoA/ROCK pathway, which has an impact on important adipocyte/cardiomyocyte key regulatory pathways, such as MRTF/SRF transcriptional program. MRTF/SRF sustains cardiac muscle identity and function and inhibits adipogenic commitment (Nobusue, Onishi et al. 2014, Mokalled, Carroll et al. 2015). Results from iPSC-derived cardiomyocytes from an ARVC patient harboring a new *MYH10* mutation identified by the exome sequencing resemble those obtained with PKP2 mutated cells and endorse the involvement of RhoA/ROCK signaling in the disease mechanism by demonstrating reduced accumulation of active RhoA-GTP at the desmosomes and disorganization of actin cytoskeleton (Rex, Gavin et al. 2010) and resulting in cytoplasmic sequestration of MRTF and derepression of Pparγ (Priya, Gomez et al. 2015, Dorn, Kornherr et al. 2018).

Additionally to the hypothesized mechanism of direct cardiomyocyte-adipocyte transdifferentiation, studies reported that ARVC adipocytes might directly derive from SHF- or $c\text{-}kit^{+}/Sca1^{+}$-progenitors or differentiated cell types, such as cardiac mesenchymal stromal cells and epicardial-resident progenitors (Lombardi, Dong et al. 2009, Stadiotti, Catto et al. 2017). Given the fact that epicardial cells might derive from the same $Isl1^{+}/Wt1^{+}$ pre-proepicardial progenitor pool (Kuhn and Wu 2010), these studies might be seen as complementary to our proposed mechanism of myocyte-adipocyte-conversion. It is possible that altered environment from diseased epicardial progenitors and cardiomyocytes could facilitate the adipocytic cell fate switch.

All together, our data show how Isl1 is involved in different aspects of heart development. Our study demonstrate that on the one hand Isl1 together with Nkx2-5 is the key mediator in cardiomyocyte subtype specification decision and on the other Isl1 together with Wt1 marks a common progenitor giving rise to cardiac myocytes and adipocytes (Fig. 42). This study reveals insights into Isl1 biology, which enrich the growing understanding of developmental processes. Fueled by the expectation of using this knowledge for possible future therapies this work will be the base for further investigations.

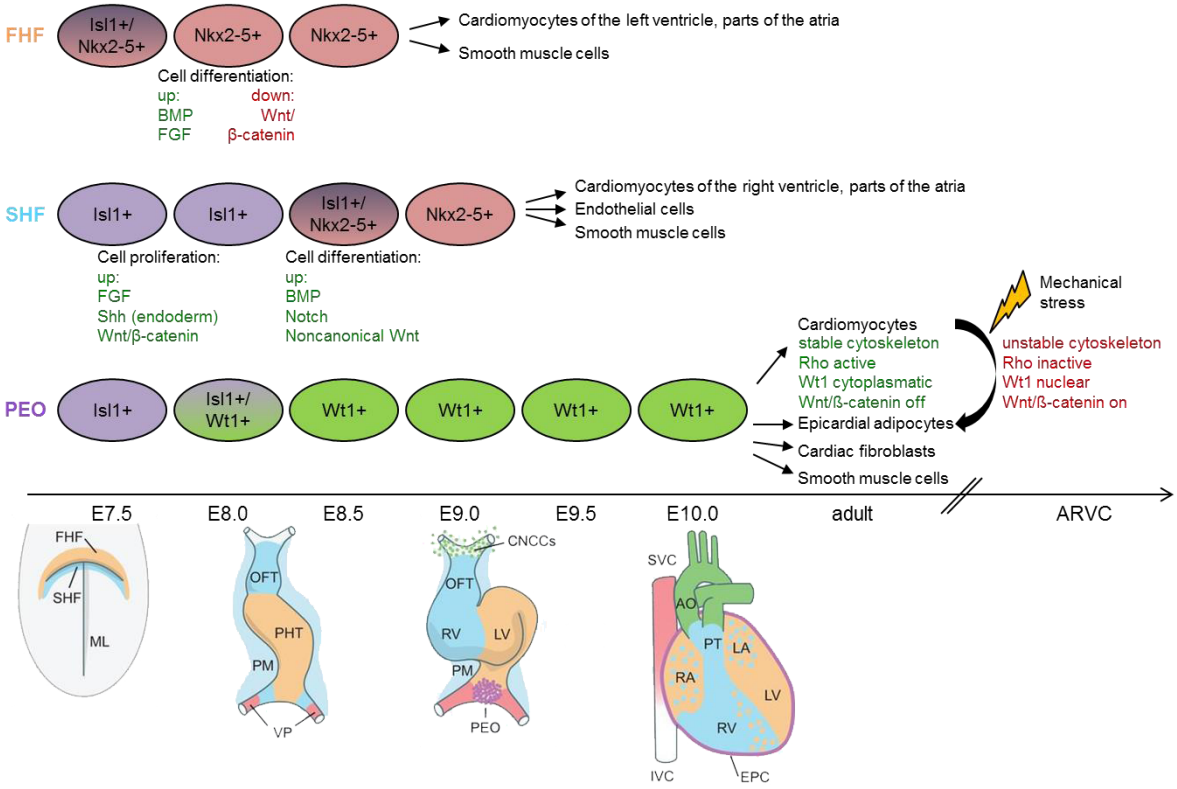

Figure 42: Descendants of Isl1 expressing progenitors in heart development and disease.
Heart development from first Isl1 expressing progenitor at E7.5 to adulthood of mouse development and in ARVC diseased settings. FHF progenitors shut down Isl1 expression earlier than SHF progenitors and subsequently initiate differentiation. Molecules involved in cell proliferation and differentiation are written in green (upregulated) and red (downregulated). $Isl1^+$ pre-proepicardial cells at E8.0 transiently co-express Wt1 before switching off Isl1. Epicardial-derived cardiomyocytes have a stable cytoskeleton and normal myocytic maintaining pathways (green) in wild type settings. In ARVC settings mechanical stress can induce cytoskeleton remodeling and affect different signaling pathways (red) resulting in cardiomyocyte-adipocyte-transdifferentiation. Drafts of the forming heart adapted from Spater, Hansson et al. 2014.
AO= Aorta, CNCCs= Cardiac neural crest cells, EPC= Epicardial cells, FHF= First heart field, IVC= Inferior vena cava, LA= Left atrium, LV= Left ventricle, ML= Midline, OFT= Outflow tract, PEO= Proepicardial organ, PHT= Primitive heart tube, PM= Pharyngeal mesoderm, PT= Pulmonary trunk, RA= Right atrium, RV= Right ventricle, SHF= Second heart field, SVC= Superior vena cava, VP= Venous pole.

5. Outlook

The last decades of research provided tremendous progress in understanding heart development. Studies in mice revealed insights in cell lineage determination processes, some of those being conserved in mammalian organisms. In this study Isl1 and Nkx2-5 were identified to regulate cardiomyocyte subtype specification. Further experiments will be needed to explore which additional factors might play a role in this process. Mimicking embryonic development, embryonic and induced pluripotent stem cell models allow for analyzing cardiac cell lineage specification in the dish. Optimization of differentiation protocols of pluripotent stem cells is a matter of ongoing research. Additionally, the development of 3D-organoids is a future objective to imitate the complex formation of the heart in respect of functional and structural properties *in vitro* (Lou and Leung 2017). The generation of well-characterized progenitors will allow direct examination of the pathways that drive cardiac differentiation. In addition, the opportunity to produce properly fated cells for cell replacement therapy is an exciting challenge of current biomedical research and might help curing degenerative diseases (Bergsmedh, Donohoe et al. 2011).

Using mouse reporter lines in combination with PSCs a common developmental origin of cardiac muscle and fat was discovered. Since it is of large interest to translate the revealed knowledge to the human system, the existence of a common progenitor for cardiac muscle and fat in humans needs to be verified. The identification of the $Isl1^{+}/Wt1^{+}$ progenitors that can give rise to both myocytic and adipocytic lineage suggests that the cardiomyocytes emerging from these precursors could be those that are more prone to myocyte-adipocyte-transdifferentiation in ARVC disease conditions. Future investigation of the $Isl1^{+}/Wt1^{+}$ progenitors and their myocytic derivatives harboring ARVC disease causing mutations is needed to prove their contribution to excess adipocytes in ARVC *in vivo*. Molecular insights of the transdifferentiation of cardiac myocytes and adipocytes might help to develop novel therapeutic approaches to revert this process. The key question aiming to be answered in future is: How is cell lineage choice controlled?

6. Appendix

6.1 References

Acharya, A., S. T. Baek, G. Huang, B. Eskiocak, S. Goetsch, C. Y. Sung, S. Banfi, M. F. Sauer, G. S. Olsen, J. S. Duffield, E. N. Olson and M. D. Tallquist (2012). "The bHLH transcription factor Tcf21 is required for lineage-specific EMT of cardiac fibroblast progenitors." Development **139**(12): 2139-2149.

Amano, M., Y. Fukata and K. Kaibuchi (2000). "Regulation and functions of Rho-associated kinase." Exp Cell Res **261**(1): 44-51.

Ambu, R., L. Vinci, C. Gerosa, D. Fanni, E. Obinu, A. Faa and V. Fanos (2015). "WT1 expression in the human fetus during development." Eur J Histochem **59**(2): 2499.

Awad, M. M., H. Calkins and D. P. Judge (2008). "Mechanisms of disease: molecular genetics of arrhythmogenic right ventricular dysplasia/cardiomyopathy." Nat Clin Pract Cardiovasc Med **5**(5): 258-267.

Bakker, M. L., G. J. Boink, B. J. Boukens, A. O. Verkerk, M. van den Boogaard, A. D. den Haan, W. M. Hoogaars, H. P. Buermans, J. M. de Bakker, J. Seppen, H. L. Tan, A. F. Moorman, P. A. t Hoen and V. M. Christoffels (2012). "T-box transcription factor TBX3 reprogrammes mature cardiac myocytes into pacemaker-like cells." Cardiovasc Res **94**(3): 439-449.

Bao, Z. Z., B. G. Bruneau, J. G. Seidman, C. E. Seidman and C. L. Cepko (1999). "Regulation of chamber-specific gene expression in the developing heart by Irx4." Science **283**(5405): 1161-1164.

Baruscotti, M., A. Barbuti and A. Bucchi (2010). "The cardiac pacemaker current." J Mol Cell Cardiol **48**(1): 55-64.

Basso, C., G. Thiene, D. Corrado, A. Angelini, A. Nava and M. Valente (1996). "Arrhythmogenic right ventricular cardiomyopathy. Dysplasia, dystrophy, or myocarditis?" Circulation **94**(5): 983-991.

Bergsmedh, A., M. E. Donohoe, R. A. Hughes and A. K. Hadjantonakis (2011). "Understanding the molecular circuitry of cell lineage specification in the early mouse embryo." Genes (Basel) **2**(3): 420-448.

Bohn, G., S. Moosmang, H. Conrad, A. Ludwig, F. Hofmann and N. Klugbauer (2000). "Expression of T- and L-type calcium channel mRNA in murine sinoatrial node." FEBS Lett **481**(1): 73-76.

Bondue, A., G. Lapouge, C. Paulissen, C. Semeraro, M. Iacovino, M. Kyba and C. Blanpain (2008). "Mesp1 acts as a master regulator of multipotent cardiovascular progenitor specification." Cell Stem Cell **3**(1): 69-84.

Bondue, A., S. Tannler, G. Chiapparo, S. Chabab, M. Ramialison, C. Paulissen, B. Beck, R. Harvey and C. Blanpain (2011). "Defining the earliest step of cardiovascular progenitor specification during embryonic stem cell differentiation." J Cell Biol **192**(5): 751-765.

Brade, T., L. S. Pane, A. Moretti, K. R. Chien and K. L. Laugwitz (2013). "Embryonic heart progenitors and cardiogenesis." Cold Spring Harb Perspect Med **3**(10): a013847.

Appendix

Bucchi, A., A. Tognati, R. Milanesi, M. Baruscotti and D. DiFrancesco (2006). "Properties of ivabradine-induced block of HCN1 and HCN4 pacemaker channels." J Physiol **572**(Pt 2): 335-346.

Buckingham, M., S. Meilhac and S. Zaffran (2005). "Building the mammalian heart from two sources of myocardial cells." Nat Rev Genet **6**(11): 826-835.

Cai, C. L., X. Liang, Y. Shi, P. H. Chu, S. L. Pfaff, J. Chen and S. Evans (2003). "Isl1 identifies a cardiac progenitor population that proliferates prior to differentiation and contributes a majority of cells to the heart." Dev Cell **5**(6): 877-889.

Cai, C. L., J. C. Martin, Y. Sun, L. Cui, L. Wang, K. Ouyang, L. Yang, L. Bu, X. Liang, X. Zhang, W. B. Stallcup, C. P. Denton, A. McCulloch, J. Chen and S. M. Evans (2008). "A myocardial lineage derives from Tbx18 epicardial cells." Nature **454**(7200): 104-108.

Cai, C. L., W. Zhou, L. Yang, L. Bu, Y. Qyang, X. Zhang, X. Li, M. G. Rosenfeld, J. Chen and S. Evans (2005). "T-box genes coordinate regional rates of proliferation and regional specification during cardiogenesis." Development **132**(10): 2475-2487.

Capecchi, M. R. (2005). "Gene targeting in mice: functional analysis of the mammalian genome for the twenty-first century." Nat Rev Genet **6**(6): 507-512.

Carlson, B. M. (2015). "Establishment of Basic Embryonic Body Plan." Reference Modul in Biomedical Sciences.

Caspi, O., I. Huber, A. Gepstein, G. Arbel, L. Maizels, M. Boulos and L. Gepstein (2013). "Modeling of arrhythmogenic right ventricular cardiomyopathy with human induced pluripotent stem cells." Circ Cardiovasc Genet **6**(6): 557-568.

Chan, S. S., X. Shi, A. Toyama, R. W. Arpke, A. Dandapat, M. Iacovino, J. Kang, G. Le, H. R. Hagen, D. J. Garry and M. Kyba (2013). "Mesp1 patterns mesoderm into cardiac, hematopoietic, or skeletal myogenic progenitors in a context-dependent manner." Cell Stem Cell **12**(5): 587-601.

Chau, Y. Y., R. Bandiera, A. Serrels, O. M. Martinez-Estrada, W. Qing, M. Lee, J. Slight, A. Thornburn, R. Berry, S. McHaffie, R. H. Stimson, B. R. Walker, R. M. Chapuli, A. Schedl and N. Hastie (2014). "Visceral and subcutaneous fat have different origins and evidence supports a mesothelial source." Nat Cell Biol **16**(4): 367-375.

Chen, S. N., P. Gurha, R. Lombardi, A. Ruggiero, J. T. Willerson and A. J. Marian (2014). "The hippo pathway is activated and is a causal mechanism for adipogenesis in arrhythmogenic cardiomyopathy." Circ Res **114**(3): 454-468.

Chen, X., S. Bonne, M. Hatzfeld, F. van Roy and K. J. Green (2002). "Protein binding and functional characterization of plakophilin 2. Evidence for its diverse roles in desmosomes and beta -catenin signaling." J Biol Chem **277**(12): 10512-10522.

Christoffels, V. M., T. Grieskamp, J. Norden, M. T. Mommersteeg, C. Rudat and A. Kispert (2009). "Tbx18 and the fate of epicardial progenitors." Nature **458**(7240): E8-9; discussion E9-10.

Christoffels, V. M., W. M. Hoogaars, A. Tessari, D. E. Clout, A. F. Moorman and M. Campione (2004). "T-box transcription factor Tbx2 represses differentiation and formation of the cardiac chambers." Dev Dyn **229**(4): 763-770.

Corrado, D., C. Basso, G. Thiene, W. J. McKenna, M. J. Davies, F. Fontaliran, A. Nava, F. Silvestri, C. Blomstrom-Lundqvist, E. K. Wlodarska, G. Fontaine and F. Camerini (1997). "Spectrum of clinicopathologic manifestations of arrhythmogenic right ventricular cardiomyopathy/dysplasia: a multicenter study." J Am Coll Cardiol **30**(6): 1512-1520.

Corrado, D., M. S. Link and H. Calkins (2017). "Arrhythmogenic Right Ventricular Cardiomyopathy." N Engl J Med **376**(15): 1489-1490.

Cruz, F. M., D. Sanz-Rosa, M. Roche-Molina, J. Garcia-Prieto, J. M. Garcia-Ruiz, G. Pizarro, L. J. Jimenez-Borreguero, M. Torres, A. Bernad, J. Ruiz-Cabello, V. Fuster, B. Ibanez and J. A. Bernal (2015). "Exercise triggers ARVC phenotype in mice expressing a disease-causing mutated version of human plakophilin-2." J Am Coll Cardiol **65**(14): 1438-1450.

d'Amati, G., C. R. di Gioia, C. Giordano and P. Gallo (2000). "Myocyte transdifferentiation: a possible pathogenetic mechanism for arrhythmogenic right ventricular cardiomyopathy." Arch Pathol Lab Med **124**(2): 287-290.

David, R., J. Stieber, E. Fischer, S. Brunner, C. Brenner, S. Pfeiler, F. Schwarz and W. M. Franz (2009). "Forward programming of pluripotent stem cells towards distinct cardiovascular cell types." Cardiovasc Res **84**(2): 263-272.

de Pater, E., L. Clijsters, S. R. Marques, Y. F. Lin, Z. V. Garavito-Aguilar, D. Yelon and J. Bakkers (2009). "Distinct phases of cardiomyocyte differentiation regulate growth of the zebrafish heart." Development **136**(10): 1633-1641.

Devine, W. P., J. D. Wythe, M. George, K. Koshiba-Takeuchi and B. G. Bruneau (2014). "Early patterning and specification of cardiac progenitors in gastrulating mesoderm." Elife **3**.

Dorn, T., A. Goedel, J. T. Lam, J. Haas, Q. Tian, F. Herrmann, K. Bundschu, G. Dobreva, M. Schiemann, R. Dirschinger, Y. Guo, S. J. Kuhl, D. Sinnecker, P. Lipp, K. L. Laugwitz, M. Kuhl and A. Moretti (2015). "Direct nkx2-5 transcriptional repression of isl1 controls cardiomyocyte subtype identity." Stem Cells **33**(4): 1113-1129.

Dorn, T., J. Kornherr, E. Parrotta, D. Zawada, H. Ayetey, G. Santamaria, L. Iop, E. Mastantuono, D. Sinnecker, A. Goedel, R. Dirschinger, I. My, S. Laue, T. Bozoglu, C. Baarlink, T. Ziegler, E. Graf, R. Hinkel, G. Cuda, S. Kääb, A. Grace, R. Grosse, C. Kupatt, T. Meitinger, A. Smith, K. L. Laugwitz and A. Moretti (2018). "Interplay of cell-cell contacts and RhoA/MRTF-A signaling regulates cardiomyocytic identity." EMBO J **37**(12).

Dudnakova, T., L. Spraggon, J. Slight and N. Hastie (2010). "Actin: a novel interaction partner of WT1 influencing its cell dynamic properties." Oncogene **29**(7): 1085-1092.

Duim, S. N., M. J. Goumans and B. P. T. Kruithof (2016). WT1 in Cardiac Development and Disease. Wilms Tumor. M. M. van den Heuvel-Eibrink. Brisbane (AU).

Eguchi, G. and R. Kodama (1993). "Transdifferentiation." Curr Opin Cell Biol **5**(6): 1023-1028.

El Agha, E., A. Moiseenko, V. Kheirollahi, S. De Langhe, S. Crnkovic, G. Kwapiszewska, D. Kosanovic, F. Schwind, R. T. Schermuly, I. Henneke, B. MacKenzie, J. Quantius, S. Herold, A. Ntokou, K. Ahlbrecht, R. E. Morty, A. Gunther, W. Seeger and S. Bellusci (2017). "Two-Way Conversion between Lipogenic and Myogenic Fibroblastic Phenotypes Marks the Progression and Resolution of Lung Fibrosis." Cell Stem Cell **20**(2): 261-273 e263.

Ellawindy, A., K. Satoh, S. Sunamura, N. Kikuchi, K. Suzuki, T. Minami, S. Ikeda, S. Tanaka, T. Shimizu, B. Enkhjargal, S. Miyata, Y. Taguchi, T. Handoh, K. Kobayashi, K. Kobayashi, K. Nakayama, M. Miura and H. Shimokawa (2015). "Rho-Kinase Inhibition During Early Cardiac Development Causes Arrhythmogenic Right Ventricular Cardiomyopathy in Mice." Arterioscler Thromb Vasc Biol **35**(10): 2172-2184.

Feil, R. (2007). "Conditional somatic mutagenesis in the mouse using site-specific recombinases." Handb Exp Pharmacol(178): 3-28.

Fressart, V., G. Duthoit, E. Donal, V. Probst, J. C. Deharo, P. Chevalier, D. Klug, O. Dubourg, E. Delacretaz, P. Cosnay, P. Scanu, F. Extramiana, D. Keller, F. Hidden-Lucet, F. Simon, V. Bessirard, N. Roux-Buisson, J. L. Hebert, A. Azarine, D. Casset-Senon, F. Rouzet, Y. Lecarpentier, G. Fontaine, C. Coirault, R. Frank, B. Hainque and P. Charron (2010). "Desmosomal gene analysis in arrhythmogenic right ventricular dysplasia/cardiomyopathy: spectrum of mutations and clinical impact in practice." Europace **12**(6): 861-868.

Gaborit, B., C. Sengenes, P. Ancel, A. Jacquier and A. Dutour (2017). "Role of Epicardial Adipose Tissue in Health and Disease: A Matter of Fat?" Compr Physiol **7**(3): 1051-1082.

Galdos, F. X., Y. Guo, S. L. Paige, N. J. VanDusen, S. M. Wu and W. T. Pu (2017). "Cardiac Regeneration: Lessons From Development." Circ Res **120**(6): 941-959.

Garcia-Gras, E., R. Lombardi, M. J. Giocondo, J. T. Willerson, M. D. Schneider, D. S. Khoury and A. J. Marian (2006). "Suppression of canonical Wnt/beta-catenin signaling by nuclear plakoglobin recapitulates phenotype of arrhythmogenic right ventricular cardiomyopathy." J Clin Invest **116**(7): 2012-2021.

Gerull, B., A. Heuser, T. Wichter, M. Paul, C. T. Basson, D. A. McDermott, B. B. Lerman, S. M. Markowitz, P. T. Ellinor, C. A. MacRae, S. Peters, K. S. Grossmann, J. Drenckhahn, B. Michely, S. Sasse-Klaassen, W. Birchmeier, R. Dietz, G. Breithardt, E. Schulze-Bahr and L. Thierfelder (2004). "Mutations in the desmosomal protein plakophilin-2 are common in arrhythmogenic right ventricular cardiomyopathy." Nat Genet **36**(11): 1162-1164.

Gessert, S. and M. Kuhl (2010). "The multiple phases and faces of wnt signaling during cardiac differentiation and development." Circ Res **107**(2): 186-199.

Gestblom, C., J. C. Hoehner, F. Hedborg, B. Sandstedt and S. Pahlman (1997). "In vivo spontaneous neuronal to neuroendocrine lineage conversion in a subset of neuroblastomas." Am J Pathol **150**(1): 107-117.

Gilbert, S. F. (2000). "Lateral Plate Mesoderm." Developmental Biology, Sunderland (MA): Sinauer Associates **6th edition**.

Gittenberger-de Groot, A. C., E. A. Mahtab, N. D. Hahurij, L. J. Wisse, M. C. Deruiter, M. C. Wijffels and R. E. Poelmann (2007). "Nkx2.5-negative myocardium of the posterior heart field and its correlation with podoplanin expression in cells from the developing cardiac pacemaking and conduction system." Anat Rec (Hoboken) **290**(1): 115-122.

Gittenberger-de Groot, A. C., M. P. Vrancken Peeters, M. M. Mentink, R. G. Gourdie and R. E. Poelmann (1998). "Epicardium-derived cells contribute a novel population to the myocardial wall and the atrioventricular cushions." Circ Res **82**(10): 1043-1052.

Habets, P. E., A. F. Moorman, D. E. Clout, M. A. van Roon, M. Lingbeek, M. van Lohuizen, M. Campione and V. M. Christoffels (2002). "Cooperative action of Tbx2 and Nkx2.5 inhibits ANF expression in the atrioventricular canal: implications for cardiac chamber formation." Genes Dev **16**(10): 1234-1246.

Hadjantonakis, A. K., M. E. Dickinson, S. E. Fraser and V. E. Papaioannou (2003). "Technicolour transgenics: imaging tools for functional genomics in the mouse." Nat Rev Genet **4**(8): 613-625.

Hayashi, S. and A. P. McMahon (2002). "Efficient recombination in diverse tissues by a tamoxifen-inducible form of Cre: a tool for temporally regulated gene activation/inactivation in the mouse." Dev Biol **244**(2): 305-318.

Herrmann, F., K. Bundschu, S. J. Kuhl and M. Kuhl (2011). "Tbx5 overexpression favors a first heart field lineage in murine embryonic stem cells and in Xenopus laevis embryos." Dev Dyn **240**(12): 2634-2645.

Hescheler, J., B. K. Fleischmann, S. Lentini, V. A. Maltsev, J. Rohwedel, A. M. Wobus and K. Addicks (1997). "Embryonic stem cells: a model to study structural and functional properties in cardiomyogenesis." Cardiovasc Res **36**(2): 149-162.

Hoffmann, S., I. M. Berger, A. Glaser, C. Bacon, L. Li, N. Gretz, H. Steinbeisser, W. Rottbauer, S. Just and G. Rappold (2013). "Islet1 is a direct transcriptional target of the homeodomain transcription factor Shox2 and rescues the Shox2-mediated bradycardia." Basic Res Cardiol **108**(2): 339.

Hoogaars, W. M., A. Engel, J. F. Brons, A. O. Verkerk, F. J. de Lange, L. Y. Wong, M. L. Bakker, D. E. Clout, V. Wakker, P. Barnett, J. H. Ravesloot, A. F. Moorman, E. E. Verheijck and V. M. Christoffels (2007). "Tbx3 controls the sinoatrial node gene program and imposes pacemaker function on the atria." Genes Dev **21**(9): 1098-1112.

Hoogaars, W. M., A. Tessari, A. F. Moorman, P. A. de Boer, J. Hagoort, A. T. Soufan, M. Campione and V. M. Christoffels (2004). "The transcriptional repressor Tbx3 delineates the developing central conduction system of the heart." Cardiovasc Res **62**(3): 489-499.

Houweling, A. C., M. M. van Borren, A. F. Moorman and V. M. Christoffels (2005). "Expression and regulation of the atrial natriuretic factor encoding gene Nppa during development and disease." Cardiovasc Res **67**(4): 583-593.

Hu, E., P. Tontonoz and B. M. Spiegelman (1995). "Transdifferentiation of myoblasts by the adipogenic transcription factors PPAR gamma and C/EBP alpha." Proc Natl Acad Sci U S A **92**(21): 9856-9860.

Hu, Y. F., J. F. Dawkins, H. C. Cho, E. Marban and E. Cingolani (2014). "Biological pacemaker created by minimally invasive somatic reprogramming in pigs with complete heart block." Sci Transl Med **6**(245): 245ra294.

Iacobellis, G., D. Corradi and A. M. Sharma (2005). "Epicardial adipose tissue: anatomic, biomolecular and clinical relationships with the heart." Nat Clin Pract Cardiovasc Med **2**(10): 536-543.

Indra, A. K., X. Warot, J. Brocard, J. M. Bornert, J. H. Xiao, P. Chambon and D. Metzger (1999). "Temporally-controlled site-specific mutagenesis in the basal layer of the epidermis: comparison of the recombinase activity of the tamoxifen-inducible Cre-ER(T) and Cre-ER(T2) recombinases." Nucleic Acids Res **27**(22): 4324-4327.

Itskovitz-Eldor, J., M. Schuldiner, D. Karsenti, A. Eden, O. Yanuka, M. Amit, H. Soreq and N. Benvenisty (2000). "Differentiation of human embryonic stem cells into embryoid bodies compromising the three embryonic germ layers." Mol Med **6**(2): 88-95.

Jamora, C. and E. Fuchs (2002). "Intercellular adhesion, signalling and the cytoskeleton." Nat Cell Biol **4**(4): E101-108.

Jansen, J. A., T. A. van Veen, J. M. de Bakker and H. V. van Rijen (2010). "Cardiac connexins and impulse propagation." J Mol Cell Cardiol **48**(1): 76-82.

Joyner, A. L. and M. Zervas (2006). "Genetic inducible fate mapping in mouse: establishing genetic lineages and defining genetic neuroanatomy in the nervous system." Dev Dyn **235**(9): 2376-2385.

Kang, J., E. Nathan, S. M. Xu, E. Tzahor and B. L. Black (2009). "Isl1 is a direct transcriptional target of Forkhead transcription factors in second-heart-field-derived mesoderm." Dev Biol **334**(2): 513-522.

Kapoor, N., W. Liang, E. Marban and H. C. Cho (2013). "Direct conversion of quiescent cardiomyocytes to pacemaker cells by expression of Tbx18." Nat Biotechnol **31**(1): 54-62.

Kappen, C. and J. M. Salbaum (2009). "Identification of regulatory elements in the Isl1 gene locus." Int J Dev Biol **53**(7): 935-946.

Katz, T. C., M. K. Singh, K. Degenhardt, J. Rivera-Feliciano, R. L. Johnson, J. A. Epstein and C. J. Tabin (2012). "Distinct compartments of the proepicardial organ give rise to coronary vascular endothelial cells." Dev Cell **22**(3): 639-650.

Kennell, J. A. and O. A. MacDougald (2005). "Wnt signaling inhibits adipogenesis through beta-catenin-dependent and -independent mechanisms." J Biol Chem **280**(25): 24004-24010.

Kim, C., J. Wong, J. Wen, S. Wang, C. Wang, S. Spiering, N. G. Kan, S. Forcales, P. L. Puri, T. C. Leone, J. E. Marine, H. Calkins, D. P. Kelly, D. P. Judge and H. S. Chen (2013). "Studying arrhythmogenic right ventricular dysplasia with patient-specific iPSCs." Nature **494**(7435): 105-110.

Kim, S. W., S. J. Her, S. Y. Kim and C. S. Shin (2005). "Ectopic overexpression of adipogenic transcription factors induces transdifferentiation of MC3T3-E1 osteoblasts." Biochem Biophys Res Commun **327**(3): 811-819.

Kimelman, D. (2006). "Mesoderm induction: from caps to chips." Nat Rev Genet **7**(5): 360-372.

Kispert, A., S. Vainio, L. Shen, D. H. Rowitch and A. P. McMahon (1996). "Proteoglycans are required for maintenance of Wnt-11 expression in the ureter tips." Development **122**(11): 3627-3637.

Kleger, A., T. Seufferlein, D. Malan, M. Tischendorf, A. Storch, A. Wolheim, S. Latz, S. Protze, M. Porzner, C. Proepper, C. Brunner, S. F. Katz, G. Varma Pusapati, L. Bullinger, W. M. Franz, R. Koehntop, K. Giehl, A. Spyrantis, O. Wittekindt, Q. Lin, M. Zenke, B. K. Fleischmann, M. Wartenberg, A. M. Wobus, T. M. Boeckers and S. Liebau (2010). "Modulation of calcium-activated potassium channels induces cardiogenesis of pluripotent stem cells and enrichment of pacemaker-like cells." Circulation **122**(18): 1823-1836.

Kokubo, H., S. Tomita-Miyagawa, Y. Hamada and Y. Saga (2007). "Hesr1 and Hesr2 regulate atrioventricular boundary formation in the developing heart through the repression of Tbx2." Development **134**(4): 747-755.

Kreidberg, J. A., H. Sariola, J. M. Loring, M. Maeda, J. Pelletier, D. Housman and R. Jaenisch (1993). "WT-1 is required for early kidney development." Cell **74**(4): 679-691.

Kretzschmar, K. and F. M. Watt (2012). "Lineage tracing." Cell **148**(1-2): 33-45.

Kuhn, E. N. and S. M. Wu (2010). "Origin of cardiac progenitor cells in the developing and postnatal heart." J Cell Physiol **225**(2): 321-325.

Kwon, C., L. Qian, P. Cheng, V. Nigam, J. Arnold and D. Srivastava (2009). "A regulatory pathway involving Notch1/beta-catenin/Isl1 determines cardiac progenitor cell fate." Nat Cell Biol **11**(8): 951-957.

Laugwitz, K. L., A. Moretti, L. Caron, A. Nakano and K. R. Chien (2008). "Islet1 cardiovascular progenitors: a single source for heart lineages?" Development **135**(2): 193-205.

Laugwitz, K. L., A. Moretti, J. Lam, P. Gruber, Y. Chen, S. Woodard, L. Z. Lin, C. L. Cai, M. M. Lu, M. Reth, O. Platoshyn, J. X. Yuan, S. Evans and K. R. Chien (2005). "Postnatal isl1+ cardioblasts enter fully differentiated cardiomyocyte lineages." Nature **433**(7026): 647-653.

Lee, S. B. and D. A. Haber (2001). "Wilms tumor and the WT1 gene." Exp Cell Res **264**(1): 74-99.

Lescroart, F., S. Chabab, X. Lin, S. Rulands, C. Paulissen, A. Rodolosse, H. Auer, Y. Achouri, C. Dubois, A. Bondue, B. D. Simons and C. Blanpain (2014). "Early lineage restriction in temporally distinct populations of Mesp1 progenitors during mammalian heart development." Nat Cell Biol **16**(9): 829-840.

Liang, X., G. Wang, L. Lin, J. Lowe, Q. Zhang, L. Bu, Y. Chen, J. Chen, Y. Sun and S. M. Evans (2013). "HCN4 dynamically marks the first heart field and conduction system precursors." Circ Res **113**(4): 399-407.

Liang, X., Q. Zhang, P. Cattaneo, S. Zhuang, X. Gong, N. J. Spann, C. Jiang, X. Cao, X. Zhao, X. Zhang, L. Bu, G. Wang, H. S. Chen, T. Zhuang, J. Yan, P. Geng, L. Luo, I. Banerjee, Y. Chen, C. K. Glass, A. C. Zambon, J. Chen, Y. Sun and S. M. Evans (2015). "Transcription factor ISL1 is essential for pacemaker development and function." J Clin Invest **125**(8): 3256-3268.

Liao, J., V. S. Aggarwal, S. Nowotschin, A. Bondarev, S. Lipner and B. E. Morrow (2008). "Identification of downstream genetic pathways of Tbx1 in the second heart field." Dev Biol **316**(2): 524-537.

Lin, L., L. Cui, W. Zhou, D. Dufort, X. Zhang, C. L. Cai, L. Bu, L. Yang, J. Martin, R. Kemler, M. G. Rosenfeld, J. Chen and S. M. Evans (2007). "Beta-catenin directly regulates Islet1 expression in cardiovascular progenitors and is required for multiple aspects of cardiogenesis." Proc Natl Acad Sci U S A **104**(22): 9313-9318.

Lindsley, R. C., J. G. Gill, T. L. Murphy, E. M. Langer, M. Cai, M. Mashayekhi, W. Wang, N. Niwa, J. M. Nerbonne, M. Kyba and K. M. Murphy (2008). "Mesp1 coordinately regulates cardiovascular fate restriction and epithelial-mesenchymal transition in differentiating ESCs." Cell Stem Cell **3**(1): 55-68.

Liu, N. and E. N. Olson (2010). "MicroRNA regulatory networks in cardiovascular development." Dev Cell **18**(4): 510-525.

Liu, Q., X. Huang, J. H. Oh, R. Z. Lin, S. Duan, Y. Yu, R. Yang, J. Qiu, J. M. Melero-Martin, W. T. Pu and B. Zhou (2014). "Epicardium-to-fat transition in injured heart." Cell Res **24**(11): 1367-1369.

Liu, Y., Y. Li, T. Li, H. Lu, Z. Jia, W. Wang, P. Chen, K. Ma and C. Zhou (2011). "POU homeodomain protein OCT1 modulates islet 1 expression during cardiac differentiation of P19CL6 cells." Cell Mol Life Sci **68**(11): 1969-1982.

Liu, Y., J. Suckale, J. Masjkur, M. G. Magro, A. Steffen, K. Anastassiadis and M. Solimena (2010). "Tamoxifen-independent recombination in the RIP-CreER mouse." PLoS One **5**(10): e13533.

Lodder, E. M. and S. Rizzo (2012). "Mouse models in arrhythmogenic right ventricular cardiomyopathy." Front Physiol **3**: 221.

Lombardi, R., S. N. Chen, A. Ruggiero, P. Gurha, G. Z. Czernuszewicz, J. T. Willerson and A. J. Marian (2016). "Cardiac Fibro-Adipocyte Progenitors Express Desmosome Proteins and Preferentially Differentiate to Adipocytes Upon Deletion of the Desmoplakin Gene." Circ Res **119**(1): 41-54.

Lombardi, R., M. da Graca Cabreira-Hansen, A. Bell, R. R. Fromm, J. T. Willerson and A. J. Marian (2011). "Nuclear plakoglobin is essential for differentiation of cardiac progenitor cells to adipocytes in arrhythmogenic right ventricular cardiomyopathy." Circ Res **109**(12): 1342-1353.

Lombardi, R., J. Dong, G. Rodriguez, A. Bell, T. K. Leung, R. J. Schwartz, J. T. Willerson, R. Brugada and A. J. Marian (2009). "Genetic fate mapping identifies second heart field progenitor cells as a source of adipocytes in arrhythmogenic right ventricular cardiomyopathy." Circ Res **104**(9): 1076-1084.

Lou, Y. R. and A. W. Leung (2017). "Next generation organoids for biomedical research and applications." Biotechnol Adv.

Ma, D., H. Wei, J. Lu, S. Ho, G. Zhang, X. Sun, Y. Oh, S. H. Tan, M. L. Ng, W. Shim, P. Wong and R. Liew (2013). "Generation of patient-specific induced pluripotent stem cell-derived cardiomyocytes as a cellular model of arrhythmogenic right ventricular cardiomyopathy." Eur Heart J **34**(15): 1122-1133.

Ma, Q., B. Zhou and W. T. Pu (2008). "Reassessment of Isl1 and Nkx2-5 cardiac fate maps using a Gata4-based reporter of Cre activity." Dev Biol **323**(1): 98-104.

Marcus, F. I., G. H. Fontaine, G. Guiraudon, R. Frank, J. L. Laurenceau, C. Malergue and Y. Grosgogeat (1982). "Right ventricular dysplasia: a report of 24 adult cases." Circulation **65**(2): 384-398.

Martinez-Estrada, O. M., L. A. Lettice, A. Essafi, J. A. Guadix, J. Slight, V. Velecela, E. Hall, J. Reichmann, P. S. Devenney, P. Hohenstein, N. Hosen, R. E. Hill, R. Munoz-Chapuli and N. D. Hastie (2010). "Wt1 is required for cardiovascular progenitor cell formation through transcriptional control of Snail and E-cadherin." Nat Genet **42**(1): 89-93.

Masters, M. and P. R. Riley (2014). "The epicardium signals the way towards heart regeneration." Stem Cell Res **13**(3 Pt B): 683-692.

Maya-Ramos, L., J. Cleland, M. Bressan and T. Mikawa (2013). "Induction of the Proepicardium." J Dev Biol **1**(2): 82-91.

McKoy, G., N. Protonotarios, A. Crosby, A. Tsatsopoulou, A. Anastasakis, A. Coonar, M. Norman, C. Baboonian, S. Jeffery and W. J. McKenna (2000). "Identification of a deletion in plakoglobin in arrhythmogenic right ventricular cardiomyopathy with palmoplantar keratoderma and woolly hair (Naxos disease)." Lancet **355**(9221): 2119-2124.

Mertens, C., C. Kuhn and W. W. Franke (1996). "Plakophilins 2a and 2b: constitutive proteins of dual location in the karyoplasm and the desmosomal plaque." J Cell Biol **135**(4): 1009-1025.

Metzger, D., J. Clifford, H. Chiba and P. Chambon (1995). "Conditional site-specific recombination in mammalian cells using a ligand-dependent chimeric Cre recombinase." Proc Natl Acad Sci U S A **92**(15): 6991-6995.

Mikawa, T. and R. G. Gourdie (1996). "Pericardial mesoderm generates a population of coronary smooth muscle cells migrating into the heart along with ingrowth of the epicardial organ." Dev Biol **174**(2): 221-232.

Mokalled, M. H., K. J. Carroll, B. K. Cenik, B. Chen, N. Liu, E. N. Olson and R. Bassel-Duby (2015). "Myocardin-related transcription factors are required for cardiac development and function." Dev Biol **406**(2): 109-116.

Mommersteeg, M. T., J. N. Dominguez, C. Wiese, J. Norden, C. de Gier-de Vries, J. B. Burch, A. Kispert, N. A. Brown, A. F. Moorman and V. M. Christoffels (2010). "The sinus venosus progenitors separate and diversify from the first and second heart fields early in development." Cardiovasc Res **87**(1): 92-101.

Moore, A. W., L. McInnes, J. Kreidberg, N. D. Hastie and A. Schedl (1999). "YAC complementation shows a requirement for Wt1 in the development of epicardium, adrenal gland and throughout nephrogenesis." Development **126**(9): 1845-1857.

Moretti, A., L. Caron, A. Nakano, J. T. Lam, A. Bernshausen, Y. Chen, Y. Qyang, L. Bu, M. Sasaki, S. Martin-Puig, Y. Sun, S. M. Evans, K. L. Laugwitz and K. R. Chien (2006). "Multipotent embryonic isl1+ progenitor cells lead to cardiac, smooth muscle, and endothelial cell diversification." Cell **127**(6): 1151-1165.

Muzumdar, M. D., B. Tasic, K. Miyamichi, L. Li and L. Luo (2007). "A global double-fluorescent Cre reporter mouse." Genesis **45**(9): 593-605.

Ng, S. Y., C. K. Wong and S. Y. Tsang (2010). "Differential gene expressions in atrial and ventricular myocytes: insights into the road of applying embryonic stem cell-derived cardiomyocytes for future therapies." Am J Physiol Cell Physiol **299**(6): C1234-1249.

Nichols, J., K. Jones, J. M. Phillips, S. A. Newland, M. Roode, W. Mansfield, A. Smith and A. Cooke (2009). "Validated germline-competent embryonic stem cell lines from nonobese diabetic mice." Nat Med **15**(7): 814-818.

Niksic, M., J. Slight, J. R. Sanford, J. F. Caceres and N. D. Hastie (2004). "The Wilms' tumour protein (WT1) shuttles between nucleus and cytoplasm and is present in functional polysomes." Hum Mol Genet **13**(4): 463-471.

Nobusue, H., N. Onishi, T. Shimizu, E. Sugihara, Y. Oki, Y. Sumikawa, T. Chiyoda, K. Akashi, H. Saya and K. Kano (2014). "Regulation of MKL1 via actin cytoskeleton dynamics drives adipocyte differentiation." Nat Commun **5**: 3368.

Noseda, M., T. Peterkin, F. C. Simoes, R. Patient and M. D. Schneider (2011). "Cardiopoietic factors: extracellular signals for cardiac lineage commitment." Circ Res **108**(1): 129-152.

O'Brien, T. X., K. J. Lee and K. R. Chien (1993). "Positional specification of ventricular myosin light chain 2 expression in the primitive murine heart tube." Proc Natl Acad Sci U S A **90**(11): 5157-5161.

Parenti, R., R. Perris, G. M. Vecchio, L. Salvatorelli, A. Torrisi, L. Gravina and G. Magro (2013). "Immunohistochemical expression of Wilms' tumor protein (WT1) in developing human epithelial and mesenchymal tissues." Acta Histochem **115**(1): 70-75.

Park, E. J., L. A. Ogden, A. Talbot, S. Evans, C. L. Cai, B. L. Black, D. U. Frank and A. M. Moon (2006). "Required, tissue-specific roles for Fgf8 in outflow tract formation and remodeling." Development **133**(12): 2419-2433.

Park, K. S., J. M. Wells, A. M. Zorn, S. E. Wert, V. E. Laubach, L. G. Fernandez and J. A. Whitsett (2006). "Transdifferentiation of ciliated cells during repair of the respiratory epithelium." Am J Respir Cell Mol Biol **34**(2): 151-157.

Pashmforoush, M., J. T. Lu, H. Chen, T. S. Amand, R. Kondo, S. Pradervand, S. M. Evans, B. Clark, J. R. Feramisco, W. Giles, S. Y. Ho, D. W. Benson, M. Silberbach, W. Shou and K. R. Chien (2004). "Nkx2-5 pathways and congenital heart disease; loss of ventricular myocyte lineage specification leads to progressive cardiomyopathy and complete heart block." Cell **117**(3): 373-386.

Pilichou, K., A. Nava, C. Basso, G. Beffagna, B. Bauce, A. Lorenzon, G. Frigo, A. Vettori, M. Valente, J. Towbin, G. Thiene, G. A. Danieli and A. Rampazzo (2006). "Mutations in desmoglein-2 gene are associated with arrhythmogenic right ventricular cardiomyopathy." Circulation **113**(9): 1171-1179.

Plikus, M. V., C. F. Guerrero-Juarez, M. Ito, Y. R. Li, P. H. Dedhia, Y. Zheng, M. Shao, D. L. Gay, R. Ramos, T. C. Hsi, J. W. Oh, X. Wang, A. Ramirez, S. E. Konopelski, A. Elzein, A. Wang, R. J. Supapannachart, H. L. Lee, C. H. Lim, A. Nace, A. Guo, E. Treffeisen, T. Andl, R. N. Ramirez, R. Murad, S. Offermanns, D. Metzger, P. Chambon, A. D. Widgerow, T. L. Tuan, A. Mortazavi, R. K. Gupta, B. A. Hamilton, S. E. Millar, P. Seale, W. S. Pear, M. A. Lazar and G. Cotsarelis (2017). "Regeneration of fat cells from myofibroblasts during wound healing." Science **355**(6326): 748-752.

Prall, O. W., M. K. Menon, M. J. Solloway, Y. Watanabe, S. Zaffran, F. Bajolle, C. Biben, J. J. McBride, B. R. Robertson, H. Chaulet, F. A. Stennard, N. Wise, D. Schaft, O. Wolstein, M. B. Furtado, H. Shiratori, K. R. Chien, H. Hamada, B. L. Black, Y. Saga, E. J. Robertson, M. E. Buckingham and R. P. Harvey (2007). "An Nkx2-5/Bmp2/Smad1 negative feedback loop controls heart progenitor specification and proliferation." Cell **128**(5): 947-959.

Priya, R., G. A. Gomez, S. Budnar, S. Verma, H. L. Cox, N. A. Hamilton and A. S. Yap (2015). "Feedback regulation through myosin II confers robustness on RhoA signalling at E-cadherin junctions." Nat Cell Biol **17**(10): 1282-1293.

Rampazzo, A., A. Nava, S. Malacrida, G. Beffagna, B. Bauce, V. Rossi, R. Zimbello, B. Simionati, C. Basso, G. Thiene, J. A. Towbin and G. A. Danieli (2002). "Mutation in human desmoplakin domain binding to plakoglobin causes a dominant form of arrhythmogenic right ventricular cardiomyopathy." Am J Hum Genet **71**(5): 1200-1206.

Reese, D. E., T. Mikawa and D. M. Bader (2002). "Development of the coronary vessel system." Circ Res **91**(9): 761-768.

Rex, C. S., C. F. Gavin, M. D. Rubio, E. A. Kramar, L. Y. Chen, Y. Jia, R. L. Huganir, N. Muzyczka, C. M. Gall, C. A. Miller, G. Lynch and G. Rumbaugh (2010). "Myosin IIb regulates actin dynamics during synaptic plasticity and memory formation." Neuron **67**(4): 603-617.

Riento, K. and A. J. Ridley (2003). "Rocks: multifunctional kinases in cell behaviour." Nat Rev Mol Cell Biol **4**(6): 446-456.

Robinson, S. P., S. M. Langan-Fahey, D. A. Johnson and V. C. Jordan (1991). "Metabolites, pharmacodynamics, and pharmacokinetics of tamoxifen in rats and mice compared to the breast cancer patient." Drug Metab Dispos **19**(1): 36-43.

Ross, S. E., N. Hemati, K. A. Longo, C. N. Bennett, P. C. Lucas, R. L. Erickson and O. A. MacDougald (2000). "Inhibition of adipogenesis by Wnt signaling." Science **289**(5481): 950-953.

Rudat, C. and A. Kispert (2012). "Wt1 and epicardial fate mapping." Circ Res **111**(2): 165-169.

Saga, Y., N. Hata, S. Kobayashi, T. Magnuson, M. F. Seldin and M. M. Taketo (1996). "MesP1: a novel basic helix-loop-helix protein expressed in the nascent mesodermal cells during mouse gastrulation." Development **122**(9): 2769-2778.

Saga, Y., S. Miyagawa-Tomita, A. Takagi, S. Kitajima, J. Miyazaki and T. Inoue (1999). "MesP1 is expressed in the heart precursor cells and required for the formation of a single heart tube." Development **126**(15): 3437-3447.

Samanta, R., J. Pouliopoulos, A. Thiagalingam and P. Kovoor (2016). "Role of adipose tissue in the pathogenesis of cardiac arrhythmias." Heart Rhythm **13**(1): 311-320.

Sauer, B. and N. Henderson (1989). "Cre-stimulated recombination at loxP-containing DNA sequences placed into the mammalian genome." Nucleic Acids Res **17**(1): 147-161.

Schlessinger, K., A. Hall and N. Tolwinski (2009). "Wnt signaling pathways meet Rho GTPases." Genes Dev **23**(3): 265-277.

Scholz, H. and K. M. Kirschner (2005). "A role for the Wilms' tumor protein WT1 in organ development." Physiology (Bethesda) **20**: 54-59.

Schram, G., M. Pourrier, P. Melnyk and S. Nattel (2002). "Differential distribution of cardiac ion channel expression as a basis for regional specialization in electrical function." Circ Res **90**(9): 939-950.

Seale, P., B. Bjork, W. Yang, S. Kajimura, S. Chin, S. Kuang, A. Scime, S. Devarakonda, H. M. Conroe, H. Erdjument-Bromage, P. Tempst, M. A. Rudnicki, D. R. Beier and B. M. Spiegelman (2008). "PRDM16 controls a brown fat/skeletal muscle switch." Nature **454**(7207): 961-967.

Shi, W., R. Wymore, H. Yu, J. Wu, R. T. Wymore, Z. Pan, R. B. Robinson, J. E. Dixon, D. McKinnon and I. S. Cohen (1999). "Distribution and prevalence of hyperpolarization-activated cation channel (HCN) mRNA expression in cardiac tissues." Circ Res **85**(1): e1-6.

Showell, C., O. Binder and F. L. Conlon (2004). "T-box genes in early embryogenesis." Dev Dyn **229**(1): 201-218.

Sohal, D. S., M. Nghiem, M. A. Crackower, S. A. Witt, T. R. Kimball, K. M. Tymitz, J. M. Penninger and J. D. Molkentin (2001). "Temporally regulated and tissue-specific gene manipulations in the adult and embryonic heart using a tamoxifen-inducible Cre protein." Circ Res **89**(1): 20-25.

Sotiropoulos, A., D. Gineitis, J. Copeland and R. Treisman (1999). "Signal-regulated activation of serum response factor is mediated by changes in actin dynamics." Cell **98**(2): 159-169.

Spater, D., E. M. Hansson, L. Zangi and K. R. Chien (2014). "How to make a cardiomyocyte." Development **141**(23): 4418-4431.

Spiegelman, B. M., E. Hu, J. B. Kim and R. Brun (1997). "PPAR gamma and the control of adipogenesis." Biochimie **79**(2-3): 111-112.

Stadiotti, I., V. Catto, M. Casella, C. Tondo, G. Pompilio and E. Sommariva (2017). "Arrhythmogenic Cardiomyopathy: the Guilty Party in Adipogenesis." J Cardiovasc Transl Res **10**(5-6): 446-454.

Sun, Y., X. Liang, N. Najafi, M. Cass, L. Lin, C. L. Cai, J. Chen and S. M. Evans (2007). "Islet 1 is expressed in distinct cardiovascular lineages, including pacemaker and coronary vascular cells." Dev Biol **304**(1): 286-296.

Syrris, P., D. Ward, A. Evans, A. Asimaki, E. Gandjbakhch, S. Sen-Chowdhry and W. J. McKenna (2006). "Arrhythmogenic right ventricular dysplasia/cardiomyopathy associated with mutations in the desmosomal gene desmocollin-2." Am J Hum Genet **79**(5): 978-984.

Tam, P. P. and R. R. Behringer (1997). "Mouse gastrulation: the formation of a mammalian body plan." Mech Dev **68**(1-2): 3-25.

Tessadori, F., J. H. van Weerd, S. B. Burkhard, A. O. Verkerk, E. de Pater, B. J. Boukens, A. Vink, V. M. Christoffels and J. Bakkers (2012). "Identification and functional characterization of cardiac pacemaker cells in zebrafish." PLoS One **7**(10): e47644.

van Wijk, B., Q. D. Gunst, A. F. Moorman and M. J. van den Hoff (2012). "Cardiac regeneration from activated epicardium." PLoS One **7**(9): e44692.

van Wijk, B., G. van den Berg, R. Abu-Issa, P. Barnett, S. van der Velden, M. Schmidt, J. M. Ruijter, M. L. Kirby, A. F. Moorman and M. J. van den Hoff (2009). "Epicardium and myocardium separate from a common precursor pool by crosstalk between bone morphogenetic protein- and fibroblast growth factor-signaling pathways." Circ Res **105**(5): 431-441.

van Wijk, B. and M. van den Hoff (2010). "Epicardium and myocardium originate from a common cardiogenic precursor pool." Trends Cardiovasc Med **20**(1): 1-7.

Vedantham, V. (2015). "New Approaches to Biological Pacemakers: Links to Sinoatrial Node Development." Trends Mol Med **21**(12): 749-761.

Wang, R., J. Liang, H. Jiang, L. J. Qin and H. T. Yang (2008). "Promoter-dependent EGFP expression during embryonic stem cell propagation and differentiation." Stem Cells Dev **17**(2): 279-289.

Watanabe, Y., S. Zaffran, A. Kuroiwa, H. Higuchi, T. Ogura, R. P. Harvey, R. G. Kelly and M. Buckingham (2012). "Fibroblast growth factor 10 gene regulation in the second heart field by Tbx1, Nkx2-5, and Islet1 reveals a genetic switch for down-regulation in the myocardium." Proc Natl Acad Sci U S A **109**(45): 18273-18280.

Weinberger, F., D. Mehrkens, F. W. Friedrich, M. Stubbendorff, X. Hua, J. C. Muller, S. Schrepfer, S. M. Evans, L. Carrier and T. Eschenhagen (2012). "Localization of Islet-1-positive cells in the healthy and infarcted adult murine heart." Circ Res **110**(10): 1303-1310.

Wessels, A., M. J. van den Hoff, R. F. Adamo, A. L. Phelps, M. M. Lockhart, K. Sauls, L. E. Briggs, R. A. Norris, B. van Wijk, J. M. Perez-Pomares, R. W. Dettman and J. B. Burch (2012). "Epicardially derived fibroblasts preferentially contribute to the parietal leaflets of the atrioventricular valves in the murine heart." Dev Biol **366**(2): 111-124.

Wiese, C., T. Nikolova, I. Zahanich, S. Sulzbacher, J. Fuchs, S. Yamanaka, E. Graf, U. Ravens, K. R. Boheler and A. M. Wobus (2011). "Differentiation induction of mouse embryonic stem cells into sinus node-like cells by suramin." Int J Cardiol **147**(1): 95-111.

Witzel, H. R., B. Jungblut, C. P. Choe, J. G. Crump, T. Braun and G. Dobreva (2012). "The LIM protein Ajuba restricts the second heart field progenitor pool by regulating Isl1 activity." Dev Cell **23**(1): 58-70.

Wobus, A. M., J. Rohwedel, V. Maltsev and J. Hescheler (1995). "Development of cardiomyocytes expressing cardiac-specific genes, action potentials, and ionic channels during embryonic stem cell-derived cardiogenesis." Ann N Y Acad Sci **752**: 460-469.

Yamaguchi, Y., S. Cavallero, M. Patterson, H. Shen, J. Xu, S. R. Kumar and H. M. Sucov (2015). "Adipogenesis and epicardial adipose tissue: a novel fate of the epicardium induced by mesenchymal transformation and PPARgamma activation." Proc Natl Acad Sci U S A **112**(7): 2070-2075.

Yamashita, J., H. Itoh, M. Hirashima, M. Ogawa, S. Nishikawa, T. Yurugi, M. Naito, K. Nakao and S. Nishikawa (2000). "Flk1-positive cells derived from embryonic stem cells serve as vascular progenitors." Nature **408**(6808): 92-96.

Yang, L., C. L. Cai, L. Lin, Y. Qyang, C. Chung, R. M. Monteiro, C. L. Mummery, G. I. Fishman, A. Cogen and S. Evans (2006). "Isl1Cre reveals a common Bmp pathway in heart and limb development." Development **133**(8): 1575-1585.

Yoshida, T., P. Vivatbutsiri, G. Morriss-Kay, Y. Saga and S. Iseki (2008). "Cell lineage in mammalian craniofacial mesenchyme." Mech Dev **125**(9-10): 797-808.

Yuan, X., H. Qi, X. Li, F. Wu, J. Fang, E. Bober, G. Dobreva, Y. Zhou and T. Braun (2017). "Disruption of spatiotemporal hypoxic signaling causes congenital heart disease in mice." J Clin Invest **127**(6): 2235-2248.

Zaffran, S., R. G. Kelly, S. M. Meilhac, M. E. Buckingham and N. A. Brown (2004). "Right ventricular myocardium derives from the anterior heart field." Circ Res **95**(3): 261-268.

Zhang, H., W. Pu, Q. Liu, L. He, X. Huang, X. Tian, L. Zhang, Y. Nie, S. Hu, K. O. Lui and B. Zhou (2016). "Endocardium Contributes to Cardiac Fat." Circ Res **118**(2): 254-265.

Zhang, L., A. Nomura-Kitabayashi, N. Sultana, W. Cai, X. Cai, A. M. Moon and C. L. Cai (2014). "Mesodermal Nkx2.5 is necessary and sufficient for early second heart field development." Dev Biol **390**(1): 68-79.

Zhou, B., Q. Ma, S. Rajagopal, S. M. Wu, I. Domian, J. Rivera-Feliciano, D. Jiang, A. von Gise, S. Ikeda, K. R. Chien and W. T. Pu (2008). "Epicardial progenitors contribute to the cardiomyocyte lineage in the developing heart." Nature **454**(7200): 109-113.

Zhou, B. and W. T. Pu (2012). "Genetic Cre-loxP assessment of epicardial cell fate using Wt1-driven Cre alleles." Circ Res **111**(11): e276-280.

Zhou, B., A. von Gise, Q. Ma, J. Rivera-Feliciano and W. T. Pu (2008). "Nkx2-5- and Isl1-expressing cardiac progenitors contribute to proepicardium." Biochem Biophys Res Commun **375**(3): 450-453.

Zhu, W. Z., Y. Xie, K. W. Moyes, J. D. Gold, B. Askari and M. A. Laflamme (2010). "Neuregulin/ErbB signaling regulates cardiac subtype specification in differentiating human embryonic stem cells." Circ Res **107**(6): 776-786.

Zhu, Z. and D. Huangfu (2013). "Human pluripotent stem cells: an emerging model in developmental biology." Development **140**(4): 705-717.

Appendix

6.2 List of figures

Appendix

6.3 List of publications

1. Interplay of cell-cell contacts and RhoA/MRTF-A signaling regulates cardiomyocytic identity.
   Dorn T*, **Kornherr J***, Parrotta E*, Zawada D, Ayetey H Santamaria G, Iop L, Mastantuono E, Sinnecker D, Goedel A, Dirschinger R, My I, Laue S, Bozoglu T, Baarlink C, Ziegler T, Graf E, Hinkel R, Cuda G, Kääb S, Grace A, Grosse R, Kupatt C, Meitinger T, Smith A, Laugwitz KL*, Moretti A*
   EMBO J. 2018 Jun 15;37(12). PMID: 29764980

2. Direct nkx2-5 transcriptional repression of isl1 controls cardiomyocyte subtype identity.
   Dorn T*, Goedel A*, Lam JT*, **Haas J**, Tian Q, Herrmann F, Bundschu K, Dobreva G, Schiemann M, Dirschinger R, Guo Y, Kühl SJ, Sinnecker D, Lipp P, Laugwitz KL, Kühl M, Moretti A.
   Stem Cells. 2015 Apr;33(4):1113-29. PMID: 25524439

3. Functional comparison of induced pluripotent stem cell- and blood-derived GPIIbIIIa deficient platelets.
   Orban M*, Goedel A*, **Haas J**, Sandrock-Lang K, Gärtner F, Jung CB, Zieger B, Parrotta E, Kurnik K, Sinnecker D, Wanner G, Laugwitz KL, Massberg S, Moretti A.
   PLoS One. 2015 Jan 21;10(1). PMID: 25607928

4. Isogenic human pluripotent stem cell pairs reveal the role of a KCNH2 mutation in long-QT syndrome.
   Bellin M, Casini S*, Davis RP*, D'Aniello C*, **Haas J**, Ward-van Oostwaard D, Tertoolen LG, Jung CB, Elliott DA, Welling A, Laugwitz KL, Moretti A, Mummery CL.
   EMBO J. 2013 Dec 11;32(24):3161-75. PMID: 24213244

* Contributed equally

6.4 Acknowledgement

I would like to thank Prof. Dr. Karl-Ludwig Laugwitz and Prof. Dr. Alessandra Moretti for providing me the opportunity to perform my PhD project in their laboratory and offering me a great and broad education under their supervision.

A special thanks goes to Alessandra for preparing me for future work life by teaching me not only how to perform experiments, but also how to present and put down my data in words.

Furthermore, I would like to thank Dr. Thomas Floss for being part of my thesis committee.

A big “thank you” to Dr. Tatjana Dorn for her endless support in the lab and also during the writing process of this thesis.

In addition, I would like to thank all the present and former lab members, who accompanied me during the last years, for their support at any time.

Many thanks go to all the collaborators, whose work allowed to complete this dissertation project.

To my scientific friends I met during my studies from Bachelor to TUM graduate school.
I really appreciated discussing with people going through the same process and I am very thankful that they became close friends.

Many thanks go to all my friends for listening and securing my work life balance.

Finally, I would like to thank my family for their love and that they always want the best for me. A special thanks goes to my parents for teaching me to work hard for reaching my goals and when you can read these lines you know it worked out.